The Role of α- and β-SNAP in Synaptic Vesicle Exocytosis

In partial fulfilment of the requirements
for the degree “Doctor of Philosophy (PhD)”
in the Molecular Biology Program
at the Georg August University Göttingen,
Faculty of Biology

Submitted by
Andrea Burgalossi

Born in
Assisi, Italy

2008

Declaration

This thesis has been written independently and with no other sources and aids than required.

Andrea Burgalossi
March 31st, 2008

Publications

Beccari T., Bibi L., Antuzzi D., Burgalossi A., Costanzi E., Orlacchio A. (2003) “Two novel mutations in the gene for human α-mannosidase that cause α-mannosidosis.” J Inherit Metab Dis. **26**(8): 819-20

Burgalossi A., Meyer G., Varoqueaux F., O’Connor V., Betz H., Brose N. and Rhee J.S. (2008) “α/β-SNAP Levels Determine the Size of the Primed Synaptic Vesicle Pool”. Manuscript in preparation.

Table of Contents

Acknowledgments

This PhD was for me much more than a learning experience in science: it has been a valuable lesson and a constructive experience of life. Particularly, it has been valuable for the relationships I established with the people I met during this time, whom I would like to thank:

Prof. Dr. Nils Brose for his personal support, scientific guidance and constant supervision during all my PhD, and especially for being a wonderful soul, able of managing relationships with wisdom and serenity, which made the lab looking like a joyful, happy and big (italian) family.

Dr. JeongSeop Rhee for the great scientific supervision, for the energy and time he invested to introduce me into the mysteries of electrophysiology, and for his personal and constant help and advices during the time I spent in the lab.

Dr. Guido Meyer for his excellent supervision during the first two years of my PhD, for his critical thinking and his real passion for science which greatly motivated me.

Prof. Wimmer, Prof. Pieler and Dr. Fasshauer for their support as my additional thesis committee members.

Anja Galinski and Thea Hellmann for their excellent technical assistance.

Dr. Wolf Jockusch for assistance and help, and also for teaching me in electrophysiology; Randi Rawson and Dr. Frederique Varoqueaux, for teaching and helping me with morphological experiments.

All other friends and colleagues of the Neurobiology Department for the help they provided me during my PhD and for the friendly atmosphere in the lab, which made it a wonderful place to work.

All friends in Göttingen and in Italy, for having been able to stand me for several years, and most of all for being able to appreciate and understand the meaning and value of real friendship.

The Molecular Biology Coordination Team (Dr. Burkhardt Steffen, Nina McGuinness, Sandra Drube and Ivana Bacakova) for the perfect managing of the MolBio Program, for their invaluable help and for having created a wonderful and supporting environment for graduate students in Göttingen.

The NEUREST for the financial support of the present study, and the Coordination Team (Dr. Bormann Joachim, Eva Strehler, Dr. Alexander Zimek) for their help in administrative matters during my PhD.

My family, *in primis* Mamma, Babbo and Laura, for having been close to me any time, and for having been able to prove, after four years of constant experimentations, a key principle in life: “love can travel unaltered through telephone wires and via mail services, and its intensity does not depend on physical distance”.

Dulcis in fundo, I would like to thank Patricia, with whom I shared all the up and downs of my PhD. Thank you for your great patience and extraordinary support, for being there any moment I needed it, for making everything easy, and for providing me with the energy to make everything possible.

Abstract

Neurotransmitter release is mediated by the neuronal SNARE proteins, which are transmembrane proteins whose assembly into ternary complexes is thought to drive membrane fusion of synaptic vesicles at axonal terminals. After fusion, “spent” SNARE complexes need to be disassembled in order to regenerate fusion-competent “active” SNAREs. This recycling step is performed by a conserved protein machinery consisting of the chaperone NSF and the co-chaperones SNAPs (α- and β-SNAP, but probably not γ-SNAP).

The aim of the present study was to elucidate the functional role of α- and β-SNAP in synaptic vesicle exocytosis at central synapses. The experimental approach consisted of analysing synaptic transmission in glutamatergic hippocampal neurons under conditions of decreased total α/β-SNAP expression levels.

I generated SNAP double mutant mice by crossing β-SNAP deletion mutant with α-SNAP hypomorphic HYH mutant mice. Crossing of the two mutations resulted in a ~70% reduction of total combined α/β-SNAP levels. Electrophysiological analysis of synaptic transmission showed that, while the readily releasable pool of synaptic vesicles (RRP) is only slightly smaller in SNAP double mutant neurons as compared to controls (~25% reduction), total release induced either by strong increases in intracellular Ca^{2+} levels or by 100 Hz stimulation trains is drastically reduced by ~60%. Detailed analysis of neurotransmitter release during stimulus trains showed that this strong reduction mainly arises from changes in the tonic release component, while the phasic release component, much like the RRP, is only slightly decreased.

I propose a two-pool model to describe neurotransmitter release during high-frequency stimulation. According to this model, one pool of primed synaptic vesicles supports slow, tonic release of transmitter, while a second, the RRP, supports fast, phasic release. The two pools operate in a successive fashion with the RRP drawing vesicles from the tonically releasable pool.

My study indicates that α- and β-SNAP are key regulators of the efficacy of central synapses. The levels of α- and β-SNAP are critical in determining the size of the primed synaptic vesicle pool that supports tonic neurotransmitter release during activity trains and feeds the RRP necessary for fast phasic transmitter release.

Abbreviations

AMBA	Acrylamide / N, N'-methylene-bis-Acrylamide
aa	Amino Acid
AP	Action Potential
APS	Ammonium Persulfate
ATP	Adenosine Triphosphate
bp	Base pairs
BSA	Bovine Serum Albumin
C1-Domain	Phorbol Ester/Diacylglycerol Binding Domain
C2-Domain	Ca^{+2} Binding Domain
C. elegans	Caernorhabditis elegans
CNS	Central Nervous System
Ctrl	Control
DAG	Diacylglycerol
DMEM	Dulbecco's Modified Eagle Medium
DMSO	Dimethylsulfoxide
DNA	Deoxyribonucleic Acid
DKO	Double Knock-Out
DMut	Double Mutant
dNTPs	Deoxynucleosides Triphosphate
DTT	Dithiothreitol
E. coli	Escherichia coli
EDTA	Di-sodium-Ethylenediamine-Tetra-Acetate
EGFP	Enhanced Green Fluorescent Protein
g	Gram
GABA	γ-aminobutirric acid
GDP	Guanosine Diphosphate
GFP	Green Fluorescent Protein
GTP	Guanosine Triphosphate
g max	Gravitational acceleration
HFS	High Frequency Stimulation
Hz	Hertz
His	Histidine

HYH	Hydrocephalus with Hop-Gait
EPSC	Excitatory Post Synaptic Current
IPTG	Isopropyl-β-thiogalactopyranoside
kDa	Kilo Dalton
KO	Knock-Out
l	Litre
LB	Luria Broth Medium
LTD	Long Term Depression
LTP	Long Term Potentiation
M	Molar
mA	Milliampere
mEPSC	Miniature EPSC
mg	Milligram
min	Minutes
MNTB	Medial Nucleus of the Trapezoid Body
mRNA	Messenger RNA
NMDA	N-Methyl-D-Aspartate
NSF	N-ethyl-malemide Sensitive Factor
OD	Optical Density
PAGE	Poly Acrylamide Gel Electrophoresis
Pvr	Vesicular Release Probability
KA	Kainate
MK-801	5-methyl-10,11- dihydro-5H-dibenzocyclohepten-5,10-imine maleate
PBS	Phosphate Buffered Salt Solution
PDBU	Phorbol-12, 13-dibutyrate
pH	Negative logarithm of H^+ concentration
PMSF	Phenyl Methyl Sulphonyl Fluoride
PSD	Post Synaptic Density
RNA	Ribonucleic acid
RNase	Ribonuclease
RRP	Readily Releasable vesicle Pool
s	seconds
SEM	Standard Error of the Mean
SDS	Sodium Dodecyl Sulphate

SNAP	Soluble NSF Attachment Factor
SNAP-25	Synaptosome Associated Protein of 25 kDa
SNARE	SNAP Receptor
SV	Synaptic Vesicle
TEMED	N,N,N',N'-Tetramethylethylene diamine
Tris	Tris (hydroxymethyl)-amino methane
UV	Ultra Violet
V	Volt
VCN	Ventral Cochlear Nucleus
vGlut	Vesicular Glutamate Transporter
WT	Wild-Type
X-Gal	5-bromo-4-chloro-3-indoyl-β-D-Galactoside

List of Figures

1 Introduction

1.1 Information Processing in the Brain: The Synapse

The brain is the most complex organ in the living universe. Unlike any other organ, the brain is an information-processing unit, which in response to incoming inputs computes and generates coherent outputs.

The nature of the "information" being processed in the brain is electric. Electrical signals flow through the circuits that compose the brain. These circuits are not simply made of passive conductors, but are assembled from functional "active" units, the neurons, which are electrically excitable postmytotic cells and highly specialized for conducting, computing, and storing (electrical) information. The electric description of local brain networks is extremely complex because information flow is constantly modulated and processed by each "active" element in the circuit. Apart from the contribution of electrotonic passive and active conductile properties of neurons, the major site of information modulation in neural circuits is the point of chemical contact between two neurons. These points of contacts were first described by Charles Sherrington in 1887, who also named them "synapses", from the Greek "συν-" (together) and "απτει" (to clasp).

Chemical synapses are specialised contact structures, where electrical activity is converted into a chemical signal in the form of neurotransmitter release from the presynapse. A prototypical chemical synapse is an asymmetric structure consisting of two elements: (1) the presynaptic bouton, which is the site where neurotransmitter release occurs, and (2) the postsynaptic signal reception apparatus, where the neurotransmitter released is converted into electrical activity into the postsynaptic cell (Garner et al., 2000; Sudhof 2004; Fig. 1). The pre- and postsynaptic apparatus are not contiguous but separated by the ~20 nm wide "synaptic cleft". Chemical transmitters bridge this gap by diffusing from release sites to receptors on the postsynaptic side (Garner et al., 2000; Dresbach et al., 2001).

The expression "synaptic transmission" indicates the sequence of signal-transduction events underlying electrical information transfer at synaptic sites from the pre- to the postsynaptic neuron. Synaptic transmission is initiated when an action potential (AP) triggers neurotransmitter release from a presynaptic nerve terminal (Katz, 1969). An action potential induces the opening of Ca^{2+} channels, and the resulting Ca^{2+} transient stimulates synaptic vesicle exocytosis. Neurotransmitter is

then released into the synaptic cleft and binds to postsynaptic receptors, where the chemical signal is transduced into an electric current in the postsynaptic neuron (Sudhof, 2004).

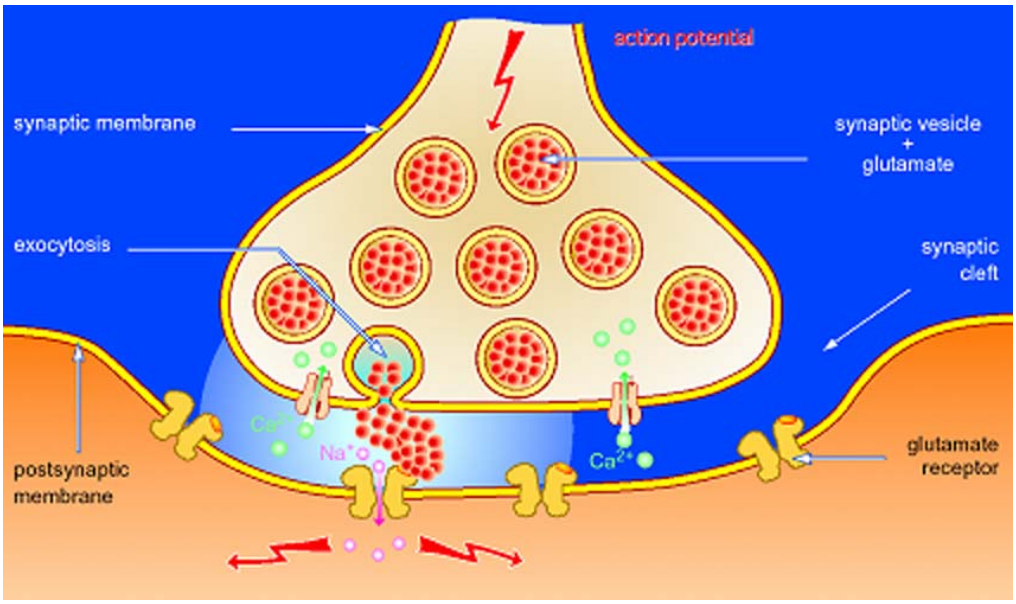

Figure 1 **Schematic Representation of a Prototypical Glutamatergic Synapse.** The synaptic junctions of chemical synapses are asymmetric structures composed of three compartments: the presynaptic bouton (where synaptic vesicle exocytosis occurs), the synaptic cleft (which separates the pre- and post-synaptic compartments), and the postsynaptic signal reception apparatus (where the chemical signal is transduced into an electric current in the postsynaptic neuron). Image from N. Brose and J. Ficner.

In the mammalian brain there are two major types of functionally distinct synapses: excitatory and inhibitory synapses. From the electrophysiological point of view, “excitation” brings the membrane potential of the postsynaptic cell closer to the threshold for action potential generation than under resting conditions, while “inhibition” shifts it further away. Excitation and inhibition are mediated by different neurotransmitters. Glutamate is the major excitatory, while γ-aminobutyric acid (GABA) is the major inhibitory neurotransmitter in the mammalian brain (Kandel et al., 2000).

Furthermore, excitatory and inhibitory synapses also display different ultrastructural features. Excitatory glutamatergic synapses are classified as “type-I” (or “asymmetric”). These synapses mainly occur between an axon and a dendritic spine or dendritic shaft. They involve axons that contain predominantly round or

spherical vesicles and form synapses that are distinguished by a thickened postsynaptic density (Kandel et al., 2000). In contrast, inhibitory GABAergic synapses are “type-II” (or “symmetric”) synapses, which primarily occur on dendritic shafts and neuronal cell bodies. They involve axons that contain clusters of vesicles that are predominantly flattened or elongated in their appearance, and the synapse does not contain a prominent postsynaptic density (Williams et al., 1989).

1.2 The Synaptic Vesicle Cycle

Ca^{2+}-triggered exocytosis of neurotransmitter is a spatially and temporally regulated process, which allows communication between neuronal cells. During evolution this form of regulated exocytosis has been optimised for speed, with fusion occurring in microseconds after an increase in cytosolic Ca^{2+} concentrations (Borst and Sakmann, 1996; Sabatini and Regher, 1996). Speed is of course a crucial parameter in many aspects of nervous system physiology. Rapid information processing by neuronal circuits allows rapid responses to environmental inputs by living animals.

However, many - if not all - of the maturation steps that make a vesicle available for fusion are intrinsically slow. Processes like vesicle biogenesis, translocation, and physical attachment to the active zone release site may require minutes (Sorensen, 2004). To allow for rapid responses to stimulation, neurons generate a pool of vesicles that are fully matured and fusion competent (“primed”), awaiting the Ca^{2+} signal at the release site. Speed is thus achieved by maintaining a stable pool of vesicles in a “primed” ready-to-fuse state (termed Readily Releasable Pool, RRP), which upon stimulation undergoes fusion with a sub-millisecond time delay (Sudhof 1995).

Early functional studies have conceptually envisioned the process of neurotransmitter release at the synaptic active zone as a linear sequence of three processes (Sorensen, 2004; Jahn et al., 2003), (1) docking (2) priming and (3) Ca^{2+} triggering of fusion (Fig. 2). The existence of vesicles in different maturation states has become evident from early physiological experiments at the neuromuscular junction (Elmqvist et al., 1965), but since then this model has been generalised to other cell types (e.g. adrenal chromaffin cells, pancreatic β-cells, pituitary melanotrophs, and neurons) (Bittner et al., 1992; Neher et al., 1993; Runden et al., 1993; Rorsmann et al., 2000; Thomas et al., 1993). However, recent studies have

proposed alternative views of this classical maturation scheme, suggesting that docking and priming may not be functionally separated events but indeed represent different aspects of the same cell-biological process (Wojcik et al., 2007; Gracheva et al., 2006; Weimer et al., 2006).

The docking step has been postulated on the basis of morphological data, showing that only a subset of vesicles are physically contacting the active zone plasma membrane (Sudhof, 1995; Zucker, 1996). The concept of priming has emerged after morphological and physiological studies had shown that synapses can be exhausted or rendered completely secretion-incompetent without any appreciable change in the number of docked vesicles (Sudhof, 1995). Priming, therefore, appears to be the key maturation step required after docking to render a vesicle fusion-competent. The Ca^{2+} triggering step involves sensing of the Ca^{2+} signal and its transduction to execute the fusion reaction (Rosenmund et al., 2003; Sudhof 1995, 2004).

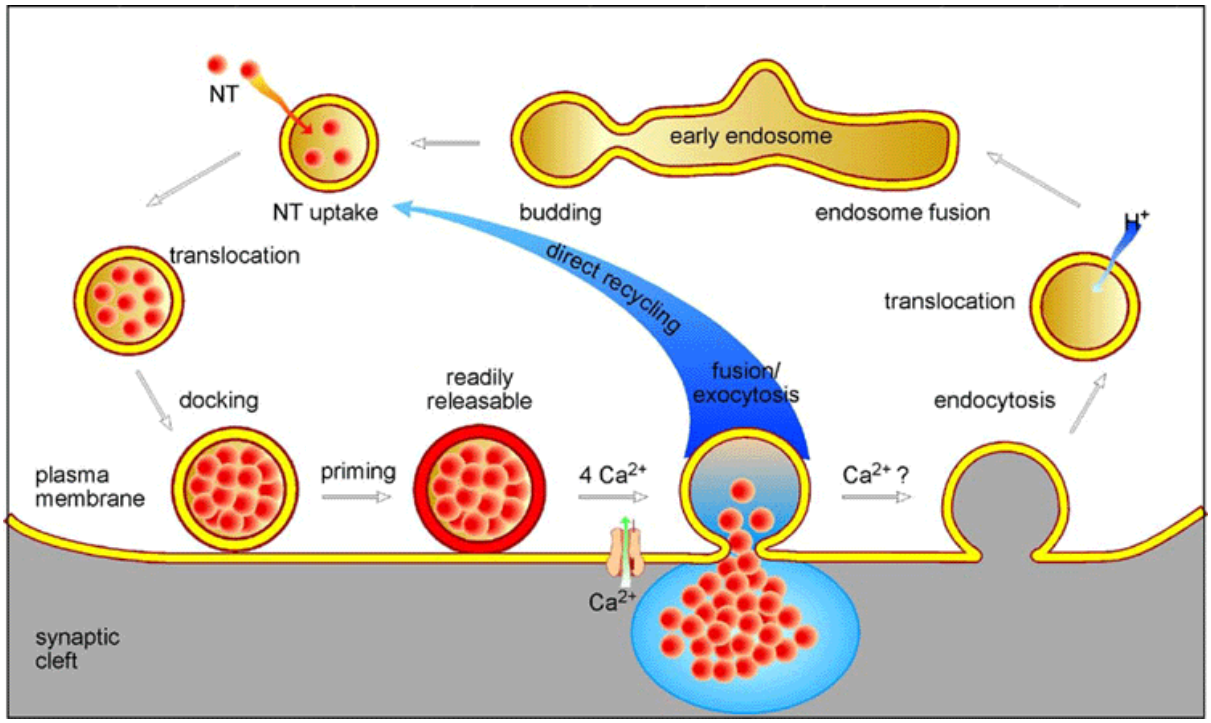

Figure 2 **The Synaptic Vesicle Cycle.** Synaptic vesicles are loaded with neurotransmitter by active transport and targeted to the active zone plasma membrane. Early functional studies have conceptually envisioned the process of neurotransmitter release at the synaptic active zone as a linear sequence of three processes, docking, priming and fusion. After docking, the vesicles undergo a priming reaction that makes them competent for Ca^{+2} triggered fusion (priming). After fusion,

synaptic vesicles undergo endocytosis and can recycle via several routes. Image from Brose et al. (2000).

After exocytosis, synaptic vesicles are recycled via endocytosis. Three alternative pathways have been proposed, which seem to operate under different physiological conditions: (1) local recycling, where vesicles undock and recycle locally; (2) recycling via endocytosis and translocation, where vesicles endocytose via clathrin-coated pits and reacidify and refill with neurotransmitter either directly or after passing through an intermediate endosomal compartment where sorting of components occurs; (3) “kiss-and-stay” recycling, where vesicles are reacidified and refilled with neurotransmitter without undocking from the release site (Farsad and De Camilli, 2002).

1.3 Experimental Models and Electrophysiological Techniques to Study Regulated Exocytosis

In the past few years, several experimental models have been developed to study Ca^{2+} regulated secretion under voltage-clamp conditions: (1) chromaffin cells, to study catecholamine release (Neher, 2006), (2) the calyx of Held, to study neurotransmitter release at a single synapse level (Neher, 2006; Schneggenburger and Neher, 2005), and (3) autaptic cultured hippocampal neurons, to study neurotransmitter release at the single-cell level (Bekkers and Stevens, 1991).

Among the cell models that have provided insight into the molecular machinery underlying exocytosis, the adrenal chromaffin cells have a prominent place. They have been used intensively as a model for neuronal as well as neuroendocrine exocytosis. It is now clear that many proteins that function in neurotransmission, also act in hormone release from adrenal chromaffin cells and indeed may be universal components of the Ca^{2+} regulated exocytotic machinery (Sorensen, 2004). Chromaffin cells secrete the catecholamines adrenaline and noradrenaline as well as a range of proteins and peptides, which are all stored in the same large dense-core secretory granules (Ashery, 2004). Two techniques have been traditionally used for quantitative and qualitative analysis of Ca^{2+}-regulated exocytosis: (1) the patch-clamp technique, to measure the electrical membrane capacitance, and (2) carbon fiber amperometry, to electrochemically detect the released catecholamines (Chow et al., 1992).

The whole-cell membrane capacitance is proportional to the cell surface area, which increases when the vesicular membrane becomes part of the plasma membrane during fusion and catecholamine release. Therefore, as long as exocytosis is fast relative to endocytosis and other forms of membrane retrieval, the membrane capacitance increase is a measure of cumulative exocytosis. In a classical caged Ca^{2+} flash experiment (where the intracellular Ca^{2+} concentration is increased via a light-induced release of Ca^{2+} from a photolabile cage compound loaded into the cell) a so called “exocytotic burst” can be observed upon sudden elevation of the intracellular Ca^{2+} concentration (Neher, 2006). Detailed analysis of the capacitance trace showed that a sum of two exponential functions is necessary to fit the increase in membrane capacitance of the burst component, indicating the presence of two releasable vesicle pools with distinct release kinetics (Sorensen, 2004, 2005). These vesicle pools have been termed Immediately Releasable (IRP) and the Slowly Releasable Pool (SRP). A sustained phase of release, which probably reflects the slower kinetics of docking, priming and fusion after the releasable vesicle pools have been depleted, follows the exocytotic burst. Therefore, by whole-cell capacitance measurements both quantitative (e.g. RRP size) and qualitative (e.g. release kinetics) parameters of the exocytotic process can be analysed with high temporal resolution. Carbon fiber amperometry is used to electrochemically detect catecholamines released from chromaffin cells (Neher, 2006). Amperometric currents from secreting cells arise almost exclusively from oxidation of catecholamines at the electrode surface. Thus, one can accurately monitor the catecholamine release process and directly estimate the number of catecholamine molecules being released.

The calyx of Held is a projection of the globular bushy cells in the Ventral Cochlear Nucleus (VCN) onto principal cells in the Medial Nucleus of the Trapezoid Body (MNTB). Owing to their unusually large size of 10-15 μm, these terminals are accessible to whole-cell patch clamp recordings and capacitance measurements (Scheggenburger and Forsythe, 2006; Schnegenburger and Neher, 2005). This offers the unique advantage of precise and exact control of the voltage in both pre- and post-synaptic compartments. Thus, the presynaptic membrane potential can be measured and controlled by voltage-clamp, and Ca^{2+} currents can be directly recorded from the presynaptic compartment. Neurotransmitter release from the presynaptic compartment of the calyx can be studied in great detail, and the time

course of the exocytotic process can be analysed with great temporal resolution. Interestingly, like for catecholamine release from chromaffin cells, total cumulative release from Calyx terminals also shows two distinct kinetic phases, which indicate the presence of both a rapidly and a slowly releasing pool of vesicles (Sakaba, 2002 and 2006; Schneggenburger et al., 2002).

The autaptic culture system consists of single hippocampal neurons grown on pre-cultured glial microislands (Bekkers and Stevens, 1991). In this isolated configuration, single neurons form synapses with themselves (termed “autapses”). Autaptic transmission provides the enormous advantage that the origin of all synapses onto each given neuron is known, and that a single patch electrode can be used to stimulate a neuron and record from it. Over recent years, this system has proven to be invaluable for the study of presynaptic neurotransmitter release mechanisms at central synapses (Gerber and Sudhof, 2002; Sudhof, 2004). Autaptic responses are usually evoked by a brief somatic depolarisation, which generates an unclamped action potential that triggers neurotransmitter release from presynaptic terminals. This evokes a postsynaptic current response, which can be measured and taken as a readout for the neurotransmitter being released. Therefore, the properties of neurotransmitter release can be studied at the single cell level, where the neuron is at the same time the source of the neurotransmitter and the readout for the release process itself.

In summary, the three experimental models described above have been widely used to characterise the biophysical aspects of the Ca^{2+} regulated exocytotic process.

1.4 The Core Fusion Machinery

The elucidation of the molecular events underlying and regulating the synaptic vesicle cycle has been greatly facilitated by the key discovery and characterisation of the SNARE protein family (Sollner et al, 1993). SNARE proteins have been widely recognized as the molecular engines that drive the membrane fusion reactions - they seem to mediate fusion in all trafficking steps of the secretory pathway (Jahn and Scheller, 2006).

The so-called neuronal SNAREs (plasma membrane-associated Syntaxin-1 and SNAP-25, synaptic vesicle-associated Synaptobrevin) are responsible for synaptic

vesicle fusion. As indicated by several genetic deletion studies, neuronal SNAREs are essential for the fast Ca^{2+} triggered exocytosis that is characteristic for synapses (Deak et al., 2004; Schoch et al., 2001; Washbourne et al., 2002).

The current "zippering" model of SNARE function (Fig. 3) proposes that a preformed Syntaxin-1/SNAP-25 heterodimer would assemble with Synaptobrevin to form an extremely stable trimeric complex (*trans*-SNARE complex) whose assembly provides the driving force for the fusion reaction (Poier et al., 1998; Sutton et al., 1998). The *trans*-SNARE complex formation is a key intermediate in the SNARE and synaptic vesicle cycle. Ample evidence indicates that its formation is the basic biochemical process underlying the priming reaction (Deichter et al., 1998; Schoch et al., 2001; Sweeney et al., 1995; Jahn and Scheller, 2006; Wojcik and Brose, 2007).

After fusion, the *trans*-SNARE complex relaxes into a *cis*-configuration, where all components now reside in the presynaptic plasma membrane. Spent "inactive" *cis*-SNARE complexes need to be recycled, in order to regenerate "free" active SNAREs for subsequent fusion reactions (Lang et al., 2002). This recycling reaction is performed by a conserved protein machinery, consisting of the SNAP co-chaperones and the chaperone NSF (cfr. 1.9), which, through an ordered sequence of molecular interactions, ultimately leads to the ATP-dependent disassembly of the SNARE complex (Hayashi et al., 1995). The activity of this machinery therefore guarantees that free "active" SNAREs are constantly regenerated.

The basic SNARE-mediated membrane fusion reaction was shown to be rather slow *in vitro* (Weber et al., 1998). Only artificial stabilisation of the Syntaxin-1/SNAP-25 heterodimer resulted in a drastic increase in speed and efficacy of SNARE complex formation *in vitro* (Pobbati et al., 2006). Furthermore, *in vitro* experiments have shown that SNAREs assemble rather promiscuously into complexes (Fasshauer et al., 1999; Vang et al., 1999). These findings indicate that the molecular events of the SNARE cycle alone cannot account for the specificity and speed of the synaptic vesicle cycle observed *in vivo*. The existence of additional protein components has been therefore postulated, which would be responsible for defining the spatial specificity, speed, and Ca^{2+} sensitivity of the synaptic release machinery *in vivo*.

1.5 Regulatory Proteins of the Neuronal SNARE Cycle

The neuronal SNARE complex assembly reaction is assisted by several proteins, which have been classified as “early” or “late” regulators, depending on whether their point of action is before or after the formation of *trans*-SNARE complexes (Jahn and Scheller, 2006). In the cascade of events leading to the formation of the SNARE complex, the SM protein family member Munc18 is one of the best characterised early players (Verhage et al., 2000; Wojcik and Brose, 2007). The current model assumes that “free” active SNAREs are organised in clusters at the plasma membrane, and probably kept in the active conformation by unknown interaction partners. Munc18 has been proposed to function in the formation and/or stabilisation of a Syntaxin-1/-SNAP-25 acceptor platform for the vesicular Synaptobrevin (Zilly et al., 2006). However, the work of Shen et al. (2007) indicates that Munc18 may stimulate fusion via binding to the assembled SNARE complex. Irrespective of the exact molecular mechanism, whose elucidation will require more time, genetic deletion of Munc18 in mice causes complete silencing of central synapses, indicating that Munc18 is an essential component of the synaptic vesicle release machinery (Verhage et al., 2000).

As is the case for Munc18, synapses lacking all Munc13 isoforms are completely silent (Augustin et al., 1999; Varoqueaux et al., 2002). Munc13 has been termed a “priming protein” after the initial analysis of Munc13-deficient synapses, which were shown to be electrophysiologically silent but did not display any change in the number of morphologically docked vesicles (Augustin et al., 1999; Varoqueaux et al., 2002). This finding was taken as a strong evidence for the existence of a biochemical “priming” modification, following a docking step. However, recent advancement in morphological techniques allowed to reveal a strong reduction in the number of docked vesicles in *C. elegans* Unc-13 deletion mutants, which was not evident with conventional fixation methods (Gracheva et al., 2006; Weimer et al., 2006). This recent finding indicates that indeed docking and priming may represent different aspects of the same cell-biological process. Munc13/Unc-13 proteins have been shown to interact with free Syntaxin-1, and their binding has been shown to be necessary for their function (Betz et al., 1997; Madison et al., 2005; Stevens et al., 2005). Munc13 was therefore originally proposed to function in the “opening” of Syntaxin-1, since (1) *in vitro* it could only bind to its open form, and (2) the open form

of Syntaxin-1 could partially rescue the uncoordinated phenotype of *C. elegans* Unc-13 deletion mutants (Richmond et al., 2001). Although its exact mechanism of action has not yet been clarified unequivocally, members of the Munc13 protein family are candidates for enabling the formation of the SNARE complex (Wojcik and Brose, 2007). In addition to acting as essential regulatory components of the release machinery, Munc13 proteins are also key modulators of synaptic efficacy. Munc13 proteins are the main diacylglycerol (DAG)/phorbol ester receptors in hippocampal neurons, and are responsible for the DAG/phorbol ester mediated augmentation of neurotransmitter release (Rhee et al., 2002).

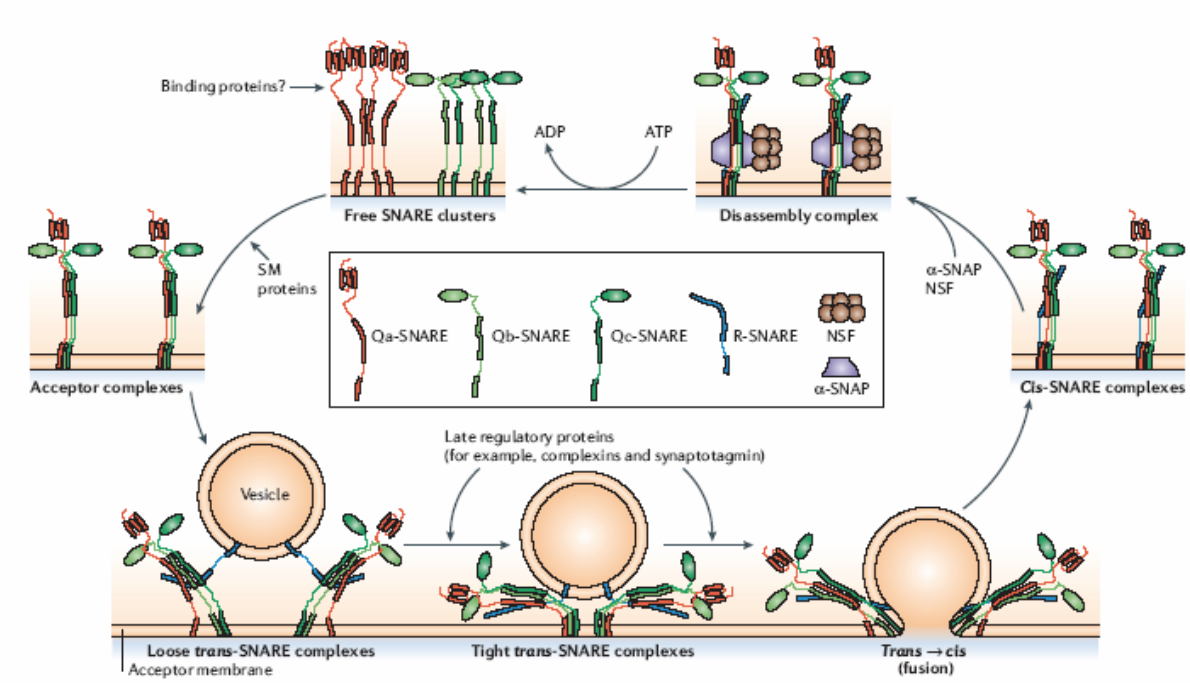

Figure 3 **The SNARE Cycle.** Free SNAREs exist in native membranes in active clusters, and are probably maintained in this reactive state by binding of unknown proteins. SM proteins assist in the formation of SNAP25/Syntaxin-1 acceptor complexes. *Trans*-SNARE complex formation with vesicular Synaptobrevin starts from a "loose" state, and proceeds to a "tight" state via binding of late regulatory proteins. After fusion, *cis*-SNARE complexes are formed, which are disassembled by the SNARE complex disassembly machinery NSF/SNAPs. This reaction guarantees that free “active” SNAREs are constantly regenerated. Image from Jahn and Scheller (2006).

Taken together, the results of the functional studies on Munc18 and Munc13 deletion mutant mice indirectly suggest that the formation of the *trans*-SNARE complex is the central molecular event of the priming step. All manipulations that

block or prevent its formation are likely to result in a total arrest of neurotransmitter release. However, direct evidence for a central role of the *trans*-SNARE complex in the priming reaction has been difficult to obtain (Jahn and Scheller, 2006; Xu et al., 1999).

As postulated by the "zippering" hypothesis, preformed Syntaxin-1/SNAP-25 acceptor complexes assemble in a *trans*-configuration with the synaptic vesicle SNARE Synaptobrevin. Unlike *in vitro*, where evidence of different states of the SNARE complex is scarce, the "zippering" reaction seems to proceed through intermediate states in a highly and specifically regulated fashion *in vivo*. Trans-SNARE complex assembly may proceed from a "loose" state, in which only the N-terminal portion of the SNARE motifs are zippered up, to a "tight" state, in which the zippering process is mostly completed. Functional studies in chromaffin cells indicate that both states exist in a dynamic equilibrium, they are fusion competent but exocytose with different kinetics in response to a rise in the Ca^{2+} concentration (Xu et al., 1999). The pool of vesicles in the "tight" configuration would contribute to the fast component of the release burst, while vesicles in the "loose" state would contribute to its slow phase. This interpretation provides molecular correlates of the different components of synaptic vesicle exocytosis kinetics. Several late regulatory proteins have been suggested to control these transition states of SNARE complexes in synaptic vesicle exocytosis (Jahn and Scheller, 2006). In particular, Complexins were shown to bind and stabilise the fully assembled *trans*-SNARE complex, which supports fast synaptic vesicle exocytosis (Pabst et al., 2002; Chen et al., 2002; Tang et al., 2006). Genetic deletion of Complexins indeed reduced the synchronous component of release (Reim et al., 2001). CAPS proteins were recently identified as essential components of the synaptic vesicle priming machinery and are necessary to support fast phasic neurotransmitter release (Jockusch et al, 2007). The molecular mechanism of CAPS function is still unknown. However, the presence of normal tonic release at CAPS-deficient synapses indicates that CAPS proteins may specifically function in stabilising the rapidly releasable state of vesicles, which supports evoked phasic release (Jockusch et al, 2007). Synaptotagmin-1 was also identified as a late regulator of the synaptic vesicle cycle. It is considered to be the Ca^{2+} sensor for synchronous synaptic vesicle exocytosis at CNS synapses (Geppert et al., 1991; Sudhof, 2002). Its C_2A and C_2B Ca^{2+} binding domains chelate Ca^{2+} ions and interact with membrane phoshoplipids in a Ca^{2+} dependent manner (Bai and Chapman, 2004;

Brose et al., 1992; Perin et al., 1990). Synaptotagmin-1 was also shown to bind to the assembled SNARE complex in a partially Ca^{2+} dependent manner (Davis et al., 1999; Tang et al., 2006). Although some groups proposed that Synaptotagmin-1 may function in the assembly of the SNARE complex (Bhalla et al., 2006), it most likely functions after the *trans*-SNARE complex has been assembled, by interacting with it upon Ca^{2+} binding. Synaptotagmin-1 may therefore act as a mechanical transducer of the Ca^{2+} signal, which induces the metastable *trans*-SNARE complex to execute fusion (Sudhof, 2002).

Taken together, studies on late regulatory proteins indicate that the stability of the metastable *trans*-SNARE complex is highly regulated *in vivo*, and represents a key physiological regulation point for the fast component of synaptic vesicle exocytosis. In the light of the current knowledge of the basal molecular machinery of neurotransmitter release, we would define as "primed" a vesicle which is docked at the active zone, with tight *trans*-SNARE complexes formed (by the concerted action of Munc18 and Munc13) and stabilised (by Complexin and CAPS). The Ca^{2+} signal would be transduced by Synaptotagmin-1, which upon binding to the *trans*-SNARE complexes triggers fast fusion with the plasma membrane.

1.6 Synchronous and Asynchronous Forms of Neurotransmitter Release

Neurons exhibit two modes of Ca^{2+} triggered neurotransmitter release, which have been traditionally designated "synchronous" and "asynchronous". "Synchronous" release is the fast component which follows action potential stimulation with a delay of only tens to hundreds microseconds (Katz and Miledi, 1965; Barrett and Stevens, 1972, Borst and Sackmann, 1996; Sabatini and Regher, 1996). On the other hand, the definition of "asynchronous" release includes all forms of release that are not synchronously coupled to the stimulation.

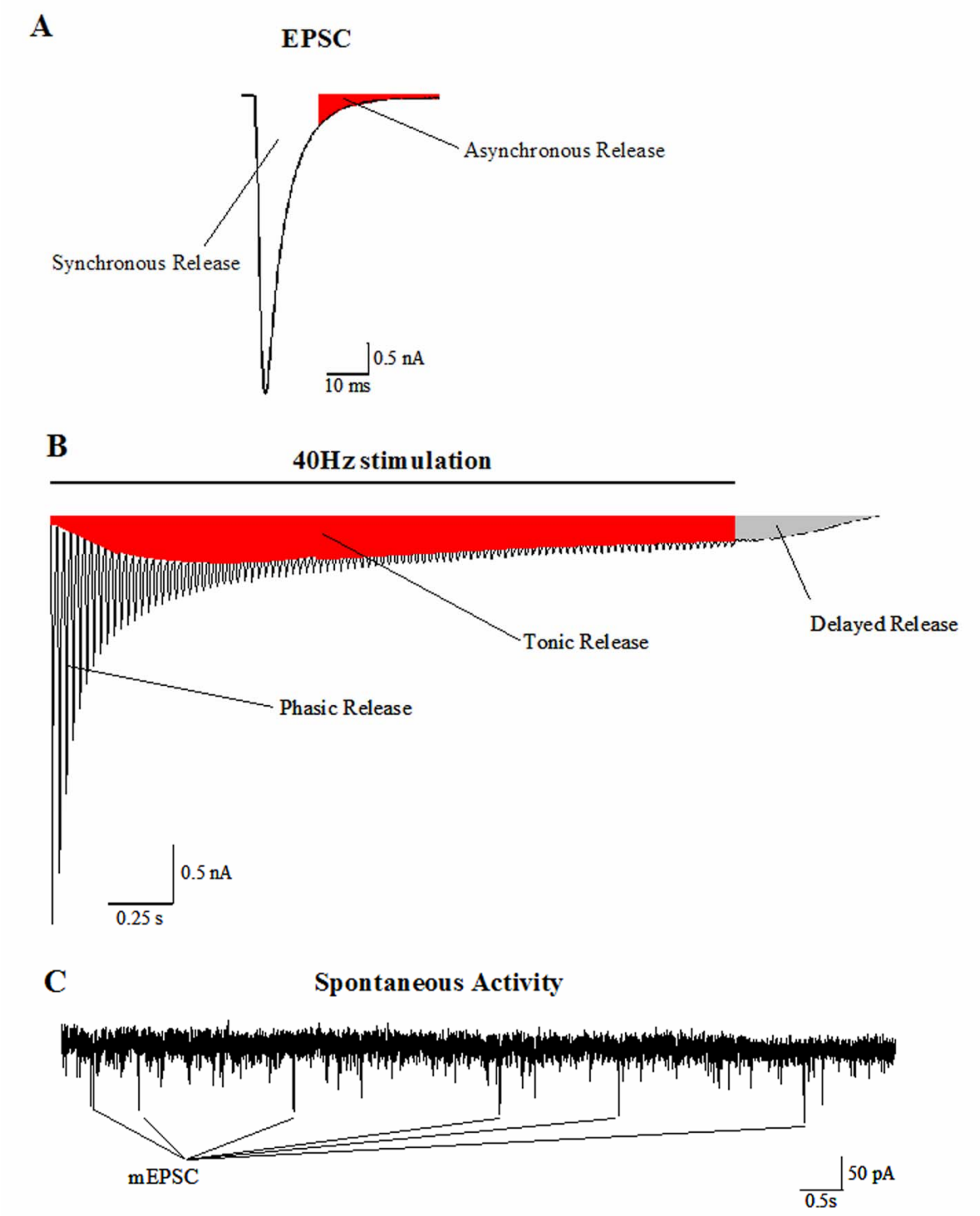

Figure 4 **"Asynchronous" Forms of Neurotransmitter Release.** Neurons exhibit two modes of Ca^{2+} triggered neurotransmitter release, which have been traditionally designated "synchronous" and "asynchronous". Four distinct forms of neurotransmitter release have been classified as "asynchronous": "asynchronous" release evoked by a single AP (A), Tonic release, evoked during AP trains (B), delayed release, after an AP train (B), and spontaneous neurotransmitter release (C). (A) Representative evoked EPSC, where the contribution of asynchronous

release is indicated in red. (B) Representative cumulative 40 Hz stimulation trace, where phasic, tonic (red) and delayed (grey) release are indicated. (C) Representative recording of spontaneous release events (mEPSCs). Some mEPSCs are indicated.

Synchronous release is believed to be responsible for maintaining timing precision throughout the brain, and for the synchronisation of the activity of neuronal ensembles that contribute to the generation of oscillatory network activities (Hefft and Jonas, 2005). On the other hand, the physiological relevance of asynchronous modes of release have been poorly investigated, even though under specific circumstances (e.g. during high-frequency stimulation trains) they can account for the majority of neurotransmitter being released from presynaptic terminals (Otsu et al., 2004; Lu and Trussell, 2000). To date, four distinct forms of neurotransmitter release have been classified as “asynchronous”:

1. “asynchronous” release evoked by a single AP
2. “asynchronous” release evoked during AP trains (tonic release)
3. “asynchronous” release after an AP train (delayed release)
4. spontaneous neurotransmitter release (miniature events)

After stimulation, initial synchronous release is followed by a slow “asynchronous” form of neurotransmitter release (Fig. 4A). This slow component of release was first identified at the frog neuromuscular junction (Barrett and Stevens, 1972) and later described also at central hippocampal synapses (Goda and Stevens, 1994). During high-frequency stimulation, neurons exhibit two different forms of release. When APs fire at high frequency, neurotransmitter release switches from a fast “phasic” to a slow form of “tonic” release during the train (Fig. 4B; Cummings et al., 1996; Lu and Trussel, 2000; Hagler and Goda, 2001; Altwood and Karunanithi, 2002). “Delayed” release refers to the asynchronous form of release, which operates after high-frequency stimulation trains, and accounts for the observed increase in mEPSC or the so-called “asynchronous tail” after the stimulus train (Barrett and Stevens, 1972; Goda and Stevens, 1994; Alturi and Regher, 1998; Fig. 4B). In addition to evoked “asynchronous” transmission, neurons exhibit spontaneous neurotransmitter release that is independent of action potentials (Otsu and Murphy, 2003; Zucker, 2005). This results in the appearance of so-called miniature postsynaptic currents, which represent single vesicles fusing with the presynaptic membrane (Fig. 4C).

The forms of release mentioned above (which for clarity will be termed asynchronous, tonic, delayed, and spontaneous, respectively) are indeed

“asynchronous” in nature, in the sense that by definition they are not synchronously coupled to the stimulation, or happen even in the absence of stimulation, as it is the case for spontaneous release. To date it is common use to refer to these distinct forms of release simply as “asynchronous”, even though this may be an inappropriate simplification. By superficial examination, it seems that they exhibit similar properties, which prompted the assumption that they are simply different manifestations of the same heterogeneous nature of the RRP.

The various forms of asynchronous release show a similar dependence on Ca^{2+} concentrations. An increase or decrease of intracellular Ca^{2+} concentrations increases or decrease all forms of asynchronous release (Cummings et al., 1996; Alturi and Regher, 1998; Otsu et al., 2004). Furthermore, substitution of extracellular Ca^{2+} with Sr^{2+} “desynchronises” neurotransmitter release, that is, drastically increases asynchronous at the expense of synchronous release. Sr^{2+} can substitute for Ca^{2+} in triggering neurotransmitter release. However, due to its slower clearance (Xu-Friedmann and Regehr, 1999 and 2000) it leads to a greater increase in residual divalent ion concentration in the presynaptic terminal.

To account for these experimental findings, the “residual Ca^{2+} hypothesis” was formulated. This hypothesis postulates that the residual Ca^{2+} concentration in the presynaptic terminal can modulate the relative amount of asynchronous and synchronous release observed either after single AP stimulation or during and after AP trains. Accumulation of Ca^{2+} in presynaptic terminals as a result of activity would result in an increase in asynchronous release, while a decrease in residual Ca^{2+} would would have the opposite effect. However, it remained to be explained how the Ca^{2+} concentration itself would be responsible for the dual kinetic nature of the neurotransmitter release process at central synapses.

Three alternative hypothesis have been formulated to account for this biphasic nature of Ca^{2+}-evoked neurotransmitter release: (1) “synchronous” and “asynchronous” release share the same Ca^{2+} sensor but differ in the coupling to Ca^{2+} channels (Sakaba et al., 2005); (2) different Ca^{2+} sensors with distinct properties mediate “synchronous” and “asynchronous” release (Sun et al., 2007); (3) “synchronous” and “asynchronous” release are mediated by the same Ca^{2+} sensor but use different vesicle sub-pools (Wolfel et al., 2007; Schneggenburger and Neher, 2000). The first hypothesis implies a heterogeneous distribution of synaptic vesicles with respect to their distance to Ca^{2+}-channels. Closely coupled vesicles respond

rapidly to Ca^{2+} influx, while the same Ca^{2+} sensor on more distant vesicles senses a smaller apparent Ca^{2+} concentration, therefore mediating their release less efficiently and more slowly. In this paradigm, “asynchronous” release originates from a population of vesicles that are not (yet) coupled to Ca^{2+} cannels (Sakaba et al., 2005). The second hypothesis postulates the existence of two separate Ca^{2+} sensors with different affinities, a low-affinity fast sensor for “synchronous” and a high-affinity slow sensor for “asynchronous” release (Sun et al., 2007). Competition of the two sensors for the same pool of synaptic vesicles at different intracellular Ca^{2+} concentrations would then account for the biphasic nature of neurotransmitter release. The “synchronous” Ca^{2+} sensor would win during pulses of high Ca^{2+} concentration, while the “asynchronous” Ca^{2+} sensor dominates during sustained phases of lower Ca^{2+} concentrations. The third hypothesis postulates that a different “state” of the vesicle is responsible for the two forms of release. A different maturation state and/or protein composition of the release machinery would then essentially define two subsets of vesicles fusing with distinct kinetics.

In conclusion, several forms of neurotransmitter release at central synapses have been classified as “asynchronous”. According to the “residual Ca^{2+}” hypothesis, “asynchronous” release is due to accumulation of Ca^{2+} in the presynaptic terminal as a result of activity. A heterogeneity of the synaptic vesicle pools has been postulated to explain how “residual” Ca^{2+} can elicit neurotransmitter release with different kinetics.

1.7 NSF and SNAPs: The SNARE Complex Disassembly Machinery

Genes that are essential for various steps in the secretory pathway were identified for the first time in a classical genetic screen in Saccharomyces cerevisiae (Novick et al., 1980). In this screen, several mutations causing disruption of specific secretory transport steps were isolated. Among the 23 complementation classes, which were originally identified, the Sec17 and Sec18 mutations led to impairment of multiple intracellular transport steps, indicative of a generalised membrane fusion defect. Mammalian homologues of Sec17 and Sec18, termed SNAPs and NSF, were subsequently identified as soluble factors that are required to support vesicular transport in a mammalian cell-free system (Wilson et al., 1989; Clary et al., 1990). In particular, the three SNAP isoforms (α-, β- and γ-SNAP) were isolated from bovine

brain (Clary et al., 1990), and it was later shown that β-SNAP is a brain specific isoform (Whiteheart et al., 1993). A classical biochemical study, which shed light onto the molecular mechanisms of NSF and SNAP function, was performed by Söllner et al. (1993a). Their elegant work showed that ATP hydrolysis by NSF was associated with the disassembly of a pre-existing SNARE complex, providing the first evidence for the existence of a SNARE assembly-disassembly cycle that underlies membrane fusion. Following this finding, efforts concentrated on the elucidation of the site of action of the SNARE complex disassembly reaction in the synaptic vesicle cycle.

Initially, a model was proposed according to which fusion itself was mediated by the action of NSF on a pre-assembled SNARE docking complex (Soellner et al., 1993b). However, after the discovery that NSF is not involved in fusion itself (Mayer et al., 1996) and that the SNAREs Syntaxin and Synaptobrevin are aligned in parallel, with their transmembrane domain next to each other (Hanson et al., 1997; Lin et al., 1997), it became apparent that SNARE assembly, rather than disassembly, might provide the energy required for fusion. Subsequently, a number of observations supported this second model, which has gained widespread acceptance in recent years (Chen et al., 2001; Jahn and Scheller, 2006). The SNAP/NSF disassembly machinery is currently believed to act after fusion, by mediating the recycling of free “active” SNAREs after disassembling spent “inactive” *cis*-SNARE complexes.

1.8 The SNAP Protein Family

Protein sequence alignments show that α- and β-SNAP are highly homologous (83% sequence identity) while γ-SNAP is a more distantly related isoform (25% and 23% identical to α- and β-SNAP, respectively) that may belong to a different SNAP subfamily (Clary et al., 1990). γ-SNAP may bind to a different membrane receptor protein or to a different SNARE complex site as compared to α- and β-SNAP (Whiteheart et al., 1992). α- and β-SNAP are essential for intercysternal Golgi transport, whereas γ-SNAP is not necessary for transport but increases the binding of α- and β-SNAP to membranes (Wilson et al., 1992). Furthermore, α- and β-SNAP, but not γ-SNAP, were are absolutely required for ER-Golgi transport (Peter et al., 1998). Taken together, these data indicate that γ-SNAP may have a different

functional role than α- and β-SNAP (Whiteheart et al., 1993; Puschel et al., 1994; Nishiki et al., 2001).

To date, only three studies hae examined the distribution of the three SNAP isoforms (Whiteheart et al., 1993; Puschel et al., 1994; Nishiki et al., 2001). The first study employed Southern blotting analysis to study the expression pattern of the three SNAP isoforms in mouse tissues. While α- and γ-SNAP mRNAs were found to be expressed in all tissues examined (heart, brain, spleen, lung, liver, muscle, kidney, testis), β-SNAP mRNA was restricted to the brain. The second study by Puschel et al. (1994) analysed temporal and spatial expression patterns of α- and β-SNAP mRNAs in mouse brain. By *in situ* hybridisation the authors detected α-SNAP mRNA as early as embryonic day 10 (E10), whereas the β-SNAP mRNA was first detected at P0 by Southern blotting approach. High α- and β-SNAP mRNA levels for were detected in the hippocampus. Only one study addressed the distribution of the three isoforms at the protein level (Nishiki et al., 2001). The authors generated isoform-specific antibodies and studied the expression and subcellular localisation of the three SNAP isoforms in the rat nervous system. The authors confirmed previously published results and showed that α- and γ-SNAP are ubiquitously expressed in several rat tissues whereas β-SNAP is specifically expressed only in the brain. To analyse protein distribution at the cellular level in the nervous system, the authors performed immunohistochemical localisation studies. The comparative analysis was performed only for the α- and β-SNAP isoforms because due to strong unspecific nuclear staining of the anti-γ-SNAP antibody it was not possible to define the localisation of γ-SNAP. The detailed analysis revealed three major differences in distribution between the α- and β-SNAP isoforms. (1) In the hippocampus, β-SNAP immunoreactivity was detected only in the CA3 region, while α-SNAP was expressed in all cellular layers. (2) In the retina, β-SNAP seemed to be absent from neuronal cell bodies, while α-SNAP reactivity was detected. (3) In the cerebellum, strong β-SNAP immunoreactivity was found in synapse-rich regions of the molecular layer and glomeruli in the granular layer, while α-SNAP immunoreactivity was lower. Both isoforms, however, were detected throughout the brain in synaptic and non-synaptic regions. The subcellular distribution of the three isoforms was analysed by biochemical (subcellular fractionation) and ultrastructural (silver-enhanced immunogold EM) methods. The distribution of the three isoforms in subcellular brain

fractions was found to be almost identical. The three isoforms were detected in membrane and soluble fractions, and were not significantly enriched in the crude synaptic vesicle fraction. On the other hand, the ultrastructural localisation and quantification of α- and β-SNAP immunoreactivities showed a modest enrichment of β-SNAP at postsynaptic densities (18.2%) as compared to α-SNAP (4.1%). Unfortunately, the sample numbers in this immunolocalisation study were quite low as only 20 synapses were analyzed (Nishiki et al., 2001).

In summary, studies on the localisation of the SNAP isoforms consistently indicated major differences in their temporal and spatial expression profiles. α- and γ-SNAP are probably ubiquitous isoforms, while β-SNAP is a postnatally expressed brain specific isoform. To date, however, only one study addressed the distribution and ultrastructural localisation of α- and β-SNAP in the brain. The subtle differences reported in this single study require validation and further investigations.

1.9 The Role of the SNARE Disassembly Machinery in Regulated Exocytosis

Major efforts have been directed at the elucidation of the functional role of SNARE recycling in regulated exocytosis. Genetic, pharmacological, and biochemical manipulations of the SNARE disassembly machinery have been performed, either targeting NSF or SNAPs.

1.9.1 Functional Studies on NSF

The most detailed information on the functional role of NSF in synaptic transmission originates from the analysis of the temperature-sensitive paralitic Comatose mutation in Drosophila (Pallanck et al., 1995; Kawasaki et al., 1998). The great advantage of the Comatose mutant is that at the restrictive temperature an acute and fast inactivation of NSF is achieved, which provides a useful system to study its acute function in synaptic transmission. Synaptic transmission was analysed at the neuromuscular junction (Kawasaki et al., 1998) and at a central synapse within the giant fiber patway (Kawasaki et al., 1999). It was shown that at the restrictive temperature, single AP evoked transmission at synapses was normal. On the other hand, upon repetitive stimulation neurotransmitter release depressed much more

strongly and faster in mutants as compared to controls. Furthermore, accumulation of SNARE complexes and of physically-docked vesicles at presynaptic sites was observed in mutants at the restrictive temperature. These results were taken as evidence for a role of NSF in the activity-dependent maintenance of the RRP, i.e. in the priming process of synaptic vesicles.

Several other studies have examined the role of NSF in regulated secretion and seem to corroborate the hypothesis of NSF activity being required for priming the release process. One study examined the role of NSF using injection for NSF peptides into the presynaptic terminal of the squid giant axon (Schweitzer et al., 1998). Two peptides were found to inhibit release, probably by inhibiting SNAP-mediated stimulation of the ATPase activity of NSF. In this microinjection study, NSF was shown to reduce the degree and to slow down the kinetics of neurotransmitter release. However, in a subsequent study the same inhibitory peptides were tested for their effect in neurotransmitter release at the crayfish neuromuscular junction (Parnas et al., 2006). In this case, the peptides inhibited release but had no effect on its time course. A related study on PC12 cells (Banerjee et al., 1996) indicated that NSF functions in a priming step but is not directly involved in fusion.

Taken together, above studies suggest a role for NSF in the maintenance of the RRP. Inhibition of its activity resulted in a reduction in Ca^{2+} regulated exocytosis, which was shown to be activity-dependent. These experiments were taken as evidence for a priming defect after NSF perturbation that arises from a limited supply of free SNAREs for subsequent rounds of fusion.

1.9.2 Functional Studies on SNAP isoforms

Functional studies to assess the role of SNAPs in Ca^{2+} regulated exocytosis were performed on different model systems. In chromaffin cells, catecholamine release in the presence of exogenous α-SNAP (either included in the patch pipette or applied to permeabilised cells) was shown to be increased (Kibble et al., 1996; Xu et al., 1999; Morgan and Burgoyne, 1995). High-resolution capacitance measurements showed that α-SNAP increases the amplitude of the exocytotic burst and the slow release component without changing their kinetics.

Effects of α-SNAP on neurotransmitter exocytosis were so far analysed in three different synapses, (1) the squid giant synapse (DeBello et al., 1995), (2) the crayfish

neuromuscular junction (He et al., 1999), and (3) the Drosophila neuromuscular junction (Babcock et al., 2004). In the first two studies, recombinant α-SNAP protein was microinjected into presynaptic terminals. In both synapses, exogenous α-SNAP increased neurotransmitter release without significantly affecting the kinetics of the release process. At the Drosophila neuromuscular junction, α-SNAP levels were increased via a transgenic approach. Intriguingly, this study showed that increased α-SNAP levels resulted in reduced neurotransmitter release. To date, however, this is not the only indication for a negative function of α-SNAP in Ca^{2+} regulated exocytosis. Several other studies also showed that excess α-SNAP might indeed result in inhibition of exocytosis. Addition of α-SNAP was shown to inhibit cell-free fusion reactions, including sperm acrosome exocytosis (Tomes et al., 2005), yeast vacuole fusion (Wang et al., 2000), secretory granule fusion in PC12 cells, and liposome fusion (Barszczewski et al., 2007). In the latter study, it was proposed that α-SNAP inhibits exocytosis by binding directly to free Syntaxin-1, thereby preventing its interaction with the other SNARE partners.

α-SNAP has been the isoform of choice in all of the studies mentioned above. The β-SNAP isoform, on the other hand, has not been investigated systematically. To date, in fact, only two functional studies compared the role of α- and β-SNAP isoforms in Ca^{2+} regulated exocytosis in chromaffin cells (Suldow et al., 1996; Xu et al., 2002). While in the first study both isoforms were found to stimulate exocytosis to the same extent, in the second study, β-SNAP was far less efficient than α-SNAP in stimulating exocytosis.

On aggregate, multiple functional studies indicated that an oversupply of α-SNAP might enhance exocytosis in various cellular systems, including bovine chromaffin cells, the squid giant synapse, the crayfish neuromuscular junction, and pancreatic β-cells. However, a significant number of studies indicated that excess of α-SNAP can inhibit fusion. As regards the β-SNAP isoform, its functional role has been investigated only superficially. Although several biochemical findings indicate that α- and β-SNAP may be functionally equivalent, two comparative functional studies yielded contradictory results (Suldow et al., 1996; Xu et al., 2002).

1.9.3 A New Function of α-SNAP in Regulating Apical Membrane Trafficking - HYH Mutant Mice

Recently, an unexpected role for α-SNAP in apical membrane trafficking has been proposed, based on the analysis of the "Hydrocephaly with Hop-gait" (HYH) mutant mouse. HYH is a recessive mutation that arose spontaneously in the C75L/10J mouse strain, and two independent studies identified it as a missense mutation (M105I) in the α-SNAP protein (Chae et al., 2004; Hong et al., 2004). Both studies showed that this mutation results in a drastic reduction of α-SNAP levels (approximately 50 % of wild-type levels) as a consequence of either mRNA (Chae et al., 2004) or protein (Hong et al.,, 2004) instability. Chae et al. (2004) showed that the single aminoacid change did not alter protein folding, and *in vitro* disassembly of the SNARE core complex was comparable in the presence of HYH mutant or wild-type α-SNAP (2004). Based on these data, it was concluded that HYH is a hypomorphic mutation that results in low levels of protein but does not affect protein function *per se*.

HYH mice suffer from progressive hydrocephalous. They show a remarkably small cerebral cortex at birth and die postnatally from progressive enlargement of the ventricular system. Chae et al. (2004) suggested that the small HYH cortex may result from altered cell fate. Neural progenitor cells displayed altered cell fate, accompanied by altered localisation of many apical proteins implicated in regulation of neural cell fate (e.g. E-cadherin, β-catenin). Therefore, it was concluded that α-SNAP may be essential for apical protein localisation and cell fate determination in neuroepithelial cells (Chae et al., 2004).

1.10 Aim of the Present Study

The first aim of my study was to elucidate the role of SNARE recycling in synaptic vesicle exocytosis at synapses. The experimental approach was based on the genetic impairment of SNAP-components of the disassembly machinery. I reasoned that genetic manipulations targeting SNAPs would be more specific than perturbing NSF function as NSF is involved in several cellular processes which are unrelated to its well-described SNARE complex disassembly activity (Zhao et al., 2007; Whiteheart and Matveeva, 2004; Hanley et al., 2002; Lee et al., 2002; Noel et al.,

1999). Essentially, attempts to study SNARE recycling after genetic manipulation of NSF activity would be expected to lead to pleiotropic effects, which could complicate and confound the interpretation of the results. In contrast, SNARE cycle regulation seems to be the only physiologically relevant function of α- and β-SNAP. Although several putative interaction partners for α- and β-SNAP have been identified by Yeast Two Hybrid screens, indicating additional roles for SNAPs, evidence for the physiological relevance of these interactions is lacking (Martin et al., 2006).

Based on above arguments, I aimed to genetically target SNAPs in order to study the functional role of the SNARE recycling machinery in central synapses. Unfortunately, previous genetic approaches to study SNAP function have not been successful. The NSF/SNAP machinery does not only operate at synapses, but its constitutive function is essential for the maintenance of the secretory pathway throughout development. Thus, complete removal of SNAPs resulted in total arrest of membrane trafficking and early cell death. A targeted null mutation of α-SNAP is embryonically lethal in mice (Chae et al., 2004), consistent with results of RNA interference studies in *C. elegans* that indcated lethality at the two-cell stage after SNAP knock-down (Piano et al., 2000). In view of these dfficulties, I took advantage of the following genetic mouse models:

1. β-SNAP deletion mutant mice (generated by Dr. G. Meyer).
2. HYH mutant mice, which bear a hypomorphic mutation in the α-SNAP gene.

I aimed to combine the β-SNAP deletion with the HYH mutation to generate a "genetic SNAP knock-down" mouse model, in which a strong reduction in total SNAP levels and a consequent strong impairment of the SNARE disassembly machinery are expected. I therefore used double-mutant mice as a model to investigate the physiological role of SNARE recycling in synaptic transmission.

The second aim of my study was to investigate a possible direct role of α- and β-SNAP in synaptic vesicle exocytosis. The existing literature contains conflicting models concerning α- and β-SNAP function (cfr. 1.10.2), and, to date, it has not been established whether α- and β-SNAP are functionally equivalent or serve different roles in regulated exocytosis. To address this questions, I aimed to analyse synaptic transmission in (1) β-SNAP deletion and HYH mutant mice, and (2) in wild-type neurons over-expressing either α- or β-SNAP. I anticipated that these functional physiological studies under conditions of altered α- and β-SNAP protein expression

levels would provide me with direct evidence for a role of the two isoforms in synaptic transmission at central mammalian synapses.

Materials and Methods

2.1 Materials

2.1.1 Chemicals and Reagents

Agarose	Sigma-Aldrich GmbH Life-Technologies Gibco-BRL GmbH
Alkaline Phosphatase	Roche Diagnostics GmbH
Ammonium Persulfate (APS)	Sigma-Aldrich GmbH
Aprotinin	Roche Diagnostics GmbH
ATP/GTP	Sigma-Aldrich GmbH
Bacto-Peptone	DIFCO Laboratories GmbH
Bacto-Yeast Extract	DIFCO Laboratories GmbH
BSA	Pierce Biotechnology
Calcymicin	Calbiochem
Comassie Brilliant Blue R250	BioMol Feinchemikalien GmbH
DMSO	Sigma-Aldrich GmbH
DNaseI	Roche Diagnostics GmbH
DNTPs	Pharmacia Biotech GmbH
Dry Milk	Nestle
ECL Reagent	Amersham-Buchler GmbH & Co
Ethidium Bromide	Sigma-Aldrich GmbH
Exonuclease I	USB
Glucose	Sigma-Aldrich GmbH
Glycine	Sigma-Aldrich GmbH BioRad Laboratories GmbH
Goat serum	Life Technologies Gibco BRL GmbH
Hepes	BioMol Feinchemikalien GmbH Sigma-Aldrich GmbH
Imidazole	Sigma-Aldrich GmbH
IPTG	BioMol Feinchemikalien GmbH
Kainic Acid	Sigma-Aldrich GmbH
Luria Broth (LB) Medium	Sigma-Aldrich GmbH

Leupeptin	Roche Diagnostics GmbH
Lysozyme	Sigma-Aldrich GmbH
MK-801	Sigma-Aldrich GmbH
Ni^{2+}NTA beads	Qiagen GmbH
PBDU	Sigma-Aldrich GmbH
PBS	PAA Chemical Company
Pfu polymerase	Stratagene GmbH
PMSF	Roche Diagnostics GmbH
Polyacrylamide (AMBA solution)	BioRad Laboratories GmbH
Ponceau S	Sigma-Aldrich GmbH
Protein Assay	BioRad Laboratories GmbH
Protein Molecular Weight Standards	BioRad Laboratories GmbH Fermentas GmbH
Proteinase K	Roche Diagnostics GmbH
Protein-G Sepharose (4 Fast Flow)	Pharmacia Biotech GmbH
Restriction Endonucleases	Roche Diagnostics GmbH New england Biolabs
RNAse A	Sigma-Aldrich GmbH
SAP (Shrimp Alkaline Phosphatase)	USB
Salmon Sperm DNA	Sigma-Aldrich GmbH
SDS	Roche Diagnostics GmbH
Secondary Antibodies	BioRad Laboratories GmbH
Sucrose	Sigma-Aldrich GmbH
T4 DNA Ligase	Roche Diagnostics GmbH
Taq-Polymerase	ABI, Weiterstadt or Qiagen GmbH
TEMED	BioRad Laboratories GmbH
Tris Base	Sigma-Aldrich GmbH
Triton X-100	Roche Diagnostics GmbH

TTX	Tokris Cookson Inc.
Tween 20	Sigma-Aldrich GmbH
X-Gal	BioMol Feinchemikalien GmbH

2.1.2 Kits

Plasmid Mini-, Midi and Maxi Kits	Qiagen GmbH
Nettex DNA Extraction Kit	Nettex Biotechnology
QIAquick Gel Extraction Kit	Qiagen GmbH
QIAquick PCR Purification	Qiagen GmbH
Quick Change	Stratagene GmbH
SP6 Cap-Scribe RNA Polymerase Kit	Roche Diagnostics GmbH

2.1.3 *Apparatus*

1.5 ml Eppendorf Shaker	Eppendorf GmbH
Centrifuges	Beckmann Instruments GmbH Eppendorf GmbH Heraeus GmbH
Developer	Agfa-Gevaert GmbH
DNA Sequencer	Applied Biosystems
DNA/RNA Spectrophotometer	Pharmacia
Electroporation Apparatus (Bacteria)	BioRad Laboratories GmbH
Electroporation Apparatus (BHK21 cells)	BioRad Laboratories GmbH
Electroporation System for Agarose Gels	Life-Technologies Gibco-BRL GmbH
Electroporation System for SDS-PAGE	BioRad Laboratories GmbH
Freezer	Libherr
Gel Drier	Biometra GmbH
Gel Photography Apparatus	Intas GmbH
Heating Block	Eppendorf GmbH
Incubators	Adolf Kuehne AH, Heraeus GmbH New Brunswig Scientific GmbH
Odyssey Imaging System	LI-COR IRDye 800 infrared dye, Rockland Immunochemicals

PCR Machine	Biometra GmbH
pH Meter	Knick, Schuett GmbH
Pipettes, Pipetteboy	Gilson and Brandt GmbH
Refrigerators	Libherr
Shaking Incubator	New Brunswig Scientific GmbH
Sonicator	B. Braun Biotech International GmbH
Sterile Bank	Heraeus GmbH
Water Bath	Biometra GmbH

2.1.4 *Materials*

Dyalysis Membranes	Spectrum Medicals
ECL Films	Amersham-Buchler & Co
Electroporation Cuvettes (Bacteria)	BioRad Laboratories GmbH
Electroporation Cuvettes (BHK21 cells)	BioRad Laboratories GmbH
Plastic Tubes	Greiner, Falcon und Brandt
Reaction Eppendorf Tubes	Eppendorf
Whatman 3MM Chr	Whattmann International Ltd
Whatmann-Cellulose Filter Nr.1	Biometra GmbH

2.1.5 *Materials and Media for Cell Culture*

Albumine, Bovine	Sigma-Aldrich GmbH
B-27 Supplement	Life Technologies Gibco BRL GmbH
Cell Culture Flasks	Firms Greiner, Costar, Falcon and Nunc
Collagen	BD Biosciences
Cysteine	Sigma-Aldrich GmbH
DMEM (Dulbecco's MEM)	Life Technologies Gibco BRL GmbH
Fetal Calf Serum	Life Technologies Gibco BRL GmbH
GlutaMAX TM I	Life Technologies Gibco BRL GmbH
HBSS (Hank's balanced salt solution)	Life Technologies Gibco BRL GmbH
L-Glutamine	Life Technologies Gibco BRL GmbH
MITO	BD Biosciences
Neurobasal Medium	Life Technologies Gibco BRL GmbH

OptiMEM	Life Technologies Gibco BRL GmbH
Papain	Worthington Biomedical Corporation / Cell Systems
PBS	PAA Biochemical Company
Penicillin/Streptomycin	Life Technologies Gibco BRL GmbH
Poly-L-Lysine	Sigma-Aldrich GmbH
Trypsin EDTA	Life Technologies Gibco BRL GmbH
Trypsin Inhibitor	Sigma-Aldrich GmbH

2.1.6 *Vectors*

pLEXN	Vojtek et al., 1993
PCDNA-3	Invitrogen
pET28a	Novagen, Merk Biosciences GmbH
pQE30	Qiagen GmbH
pQE9	Qiagen GmbH
pSFV1	Life-Technologies Gibco-BRL GmbH
PSFV-Helper	Life-Technologies Gibco-BRL GmbH
pVP16	Vojtek et al., 1993

2.1.7 *Primary Antibodies*

α/β-SNAP	Monoclonal, Synaptic Systems
Actin	Polyclonal and Monoclonal, Sigma Aldrich
α-SNAP	Polyclonal, provided by Prof. Takahashi Monoclonal, Exalpha
β-SNAP	Polyclonal, provided by Prof. Takahashi
CamKII a	Polyclonal, Sigma Aldrich
Complexin1/2	Polyclonal, Synaptic Systems
CSP	Polyclonal, Synaptic Systems
GABA-A α1	Polyclonal, Chemicon
GABA-A β	Monoclonal, Chemicon
GluR1	Polyclonal, Chemicon

GluR2	Monoclonal, Chemicon
GluR2/3	Polyclonal, Chemicon
GluR6/7	Polyclonal, Upstate
γ-SNAP	Polyclonal, Synaptic Systems
His x 6	Monoclonal, Qiagen GmbH
MAP2	Monoclonal, Chemicon
Munc-13-1 (40)	Polyclonal provided by Dr. Varoqueaux
Munc-18-1	Rabbit, Synaptic Systems
Myc (9E10)	Monoclonal, Sigma-Aldrich
Neuroligin1/3	Polyclonal provided by Dr. Varoqueaux
NMDAR	Monoclonal, Brose et al., 1994
NSF	Polyclonal, Synaptic Systems
Pick1	Polyclonal, Chemicon
PSD95	Monoclonal, AbCam
RIM1/2	Monoclonal, Transduction Laboratories
SNAP25	Polyclonal, Synaptic Systems
Synapsin	Monoclonal and Polyclonal, Synaptic Systems
Synaptobrevin 2	Monoclonal (69.1), Synaptic System
Synaptophysin	Monoclonal (7.2), Synaptic Systems
Synaptotagmin 1	Polyclonal, Synaptic Systems
Syntaxin 1	Monoclonal (78.2), Synaptic Systems
Syntaxin13	Polyclonal, Synaptic Systems
Tomosyn	Polyclonal, Synaptic Systems
vGAT	Polyclonal (Guinea Pig), Chemicon
vGlut1	Monoclonal, Chemicon

2.1.8 Secondary antibodies

Anti-mouse (from Goat)	Horse Radish peroxidase Conjugate, BioRad
Anti-mouse (from Goat)	Alexa Fluor 488-555 Molecular Probes
Anti-mouse (from Goat)	LI-COR IRDye 800 infrared dye, Rockland Immunochemicals

Anti-Guinea Pig (from Goat)	Horse Radish peroxidase Conjugate, BioRad
Anti-Rabbit (from Goat)	Alexa Fluor 488-555 Molecular Probes
Anti-Rabbit (from Goat)	Horse Radish peroxidase Conjugate, BioRad
Anti-Rabbit (from Goat)	LI-COR IRDye 800 infrared dye, Rockland Immunochemicals

2.1.9 Oligonucleotides

The following oligonucleotides are given in 5' to 3' direction, and were made by I. Thanhaeuser, D. Schwerdfeger and F. Benseler with the department-owned Oligo synthesizer (ABI 5000 DNA/RNA Synthesizer).

1	β-SNAP Genotyping (WT allele) 5'	TTT ACA GAA ACT GCG TCC CAC A
2	β-SNAP Genotyping (WT allele) 3'	TTC ATT TGC CAG AGT GAC TTG
3	β-SNAP Genotyping (KO allele) 5'	TTT ACA GAA ACT GCG TCC CAC A
4	β-SNAP Genotyping (KO allele) 3'	GAG CGC GCG CGG CGG AGT TGT TGA C
5	HYH Genotyping 5'	CAC TCT GAC CAG GTT GCC CGG
6	HYH Genotyping 3'	GTC TGT ATA GAT CTC AAT TGC TCT T
7	β-SNAP Mutagenesis 5'	GCC ATC GAG ATC TAT GAG CAG GTG GAA GCA AAC
8	β-SNAP Mutagenesis 5'	GTG TTT GCT GCC ACC TGC TCA TAG ATC TCG ATG GC
9	α-SNAP cloning into PCDNA3 5'	CGC GGA TTC GTC ATG GAC ACC TCC GGG AAG CAG G
10	α-SNAP cloning into PCDNA3 3'	CGC GAT ATC TCA GCG CAG GTC TTC CTC ATC A
11	β-SNAP cloning into PCDNA3 5'	CGC GGA TCC GAC ATG GAC AAC GCA GGG AAG GAG CG
12	β-SNAP cloning into PCDNA3 3'	CGC GAT ATC TCA CTT GAG GTC TCC ATC TCC T

13	α-SNAP *in-situ*	ACC TTG CGC TCC GCT TCA GCC AGC AGC GCC ATA GCC TCA GCC TGC
14	β-SNAP *in-situ*	ACT CGC TTC TCG GCC TCC GCC ATA AGC TGG ACC GCT TCT CGC TCC

2.1.10 cDNA Clones

α- and β-SNAP in pLEXN	Provided by Dr. Meyer G
pVP16 constructs	Provided by Dr. Meyer G
α-SNAP in pET28a	Provided by Dr. Fasshauer D
β-SNAP in pQE30	Provided by Prof. Betz H
NSF in pQE9	Provided by Dr. Fasshauer D
α- and β-SNAP in pSFV1	See 2.2.15 for cloning strategy

2.2 Methods

2.2.1 Production of Competent Bacteria

100 ml LB medium were transfected with a single colony of the desired bacterial strain and incubated while shaking over night at 37°C. Cells were diluted to 1:100 in one litre of LB-medium and shaken at 37°C until an OD_{600} of 0.5 to 0.7 was reached. Cells were recollected by centrifugation (15 min at 4000 x g_{max}) at 4°C and resuspended in one litre of ice-cold 10% Glycerine in sterile H_2O. Cells were washed with 0.5 and 0.25 litres of 10% Glycerine in water, and after the last washing step they were resuspended in 4 ml of 10% Glycerine, aliquoted, flash frozen in liquid Nitrogen, and stored at -80°C.

2.2.2 Electroporation of Plasmid DNA into Competent Bacteria

40 µl of competent bacteria were thawed on ice. An apropriate amount of DNA (1 µl Ligation or 1 µl of a 1/1000 dilution of a plasmid preparation) was then added, mixed and incubated for one minute on ice in an electroporation cuvette (0.1 cm, BioRad). Subsequently, an electric pulse (E. coli pulser, BioRad) of 1.80 kV was administered. The cells were then immediately removed from the cuvette with 0.9 ml LB-Medium and allowed to recover for 1 hour, at 37°C in a shaking incubator. After recovery, the

cells were carefully centrifuged and the pellet resuspended in 100 μl of LB-Medium and plated on selection plates.

2.2.3 DNA Plasmid "Mini" Preparation

This method from Holmes et al. (1981) is used for the quick analysis of clones after transformation to determine the success of transfer of the plasmid DNA into the bacterial cells, e.g. after ligation. Single colonies were chosen and incubated over night at 37°C in 2 ml selection tubes. 1.5 ml of these cultures were decanted into eppendorf tubes and centrifuged for 60 seconds at full speed. The supernatant was removed, and pellets were resuspended in 300 μl STET (0.8% sucrose, 0.5% Triton X-100, 50mM Tris/Cl pH 8, 50mM EDTA, 25ml lysozyme 10mg/ml). The mix was centrifuged at full speed for 10 minutes, pellets were removed and 100 ml 7.5 M NH_4Ac and 400 ml isopropanol were added to the supernatant. The mix was centrifuged for 30 minutes at full speed. Pellets were air dried at room temperature for 1 minute, and resuspended in 50 μl TE (10 mM Tris/Cl pH7.4, 1 mM EDTA pH 8.0).

2.2.4 Plasmid Preparation from Qiagen protocols

Plasmid DNA preparation from the "mini", "midi" and "maxi" QIAGEN purification kits allow for the isolation of supercoiled plasmid DNA, which can be used for sequencing or subcloning. The procedures were carried out as outlined in the QIAGEN plasmid purification handbook. DNA concentration was measured by spectophotometric analysis, according to the extinction coefficient at 260 nm for double stranded DNA: 1 OD_{260} = 50 mg/ml.

2.2.5 Restriction Digests

Restriction enzymes were purchased together with the appropriate 10 x concentrated buffer for optimal reaction conditions. Restriction digests of Plasmid DNA were performed by incubating restriction reaction mixtures for 1.5 to 2 hours at the enzyme specific temperature. Preparative restriction mixes were prepared as follows:

Preparative Restriction Mix	
Plasmid DNA	1-2 μg
Restriction Buffer 10x	10 μl
Restriction Enzyme	1.5 μl
(BSA 10x)	10 μl
To 100 μl final volume with water	

2.2.6 Dephosphorylation of the 5' End with Alkaline Phosphatase

Vectors digested with single restriction enzyme are treated with shrimp alkaline phospatase (SAP) before ligation with the desired insert to prevent autoligation of the vector. The dephosphorylation mix was prepared by following producer´s guidelines, and the reaction was allowed to proceed for 20 minutes at 37°C.

2.2.7 Ligation

T4 DNA ligase was used to ligate both sticky and blunt DNA ends. Ligation reactions were allowed to proceed for 16 hours at 16°C or on melting ice. Ligation mixes were prepared as follows:

Ligation Mix	
Vector (from gel extraction)	1-2 μl
Ligation Buffer 10x	2 μl
T4 Ligase	1.5 μl
To 20 μl final volume with Insert solution	

To increase the colony yield of the ligation, DNA was precipitated by using the "Quick" DNA Precipitation protocol (see below) and the total amount of precipitated DNA was resuspended in 2 μl and electroporated in competent bacteria.

2.2.8 "Quick" DNA Precipitation

DNA contained in Ligation Mixes (18 μl) was precipitated for at least one hour at –80°C in the presence of Ammoniumacetate (7.5 M, 2 μl) and Ethanol (100%, 60 μl). After 15 minutes centrifugation at full speed a tiny white pellet was visible, which was washed with 70% ethanol before being resuspended in 2 μl distilled water.

2.2.9 DNA Sequencing

All DNA synthesis and sequencing was carried out by D. Schwerdfelger, I. Thanhaeuser and F. Benseler at the MPI for Experimental Medicine, using the department-owned Oligo Synthesizer, ABI 5000 DNA/RNA Synthesizer, and the Applied Biosystems 373 DNA Sequencer (modified from Sanger et al., 1977).

2.2.10 Agarose Gel Electrophoresis

Agarose gel electrophoresis is used to separate, identify and purify negatively charged DNA fragments based on their size. DNA bands are made visible with ethidium bromide, and can be photographed in UV-Light (254 or 314 nm). Usually 0.7 to 2% gels are used. Agarose was dissolved by heating in 100 ml of the required 1x TBE buffer, and 0.5 mg/ml Ethidium Bromide was added. Samples were mixed with 6x Probe Buffer (0.25% Bromophenol Blue, 40% Sucrose in H_2O) to a final 1x concentration, and loaded into the wells. DNA fragments are separated at constant voltage (80-120 V) in TBE running buffer (50 mM Tris-Base, 50 mM Boric Acid, 2mM EDTA pH8.0).

2.2.11 Isolation of DNA fragments from Agarose Gels

Single electrophoretic DNA bands can be excised from the gel and the containing DNA can be eluted and used for further applications. For this purpose, I used the QIAquick PCR purification Kit. The protocol, outlined in the QIAquick Spin Handbook for purifying PCR fragments, was provided by the producers.

2.2.12 Genomic DNA Isolation from Mouse Tail Samples

Quick isolation of genomic DNA from mouse tails was performed using the Nexttec 3.0 Kit according to the manufacturer's guidelines. This quick protocol allowed fast genotyping during the preparation of cultures (see below). 1 µl purified DNA was used for the genotyping PCRs.

2.2.13 Polymerase Chain Reaction

In vitro enzymatic DNA amplification is achieved via PCR (Mullis et al., 1992). The PCR reaction mix included double-strand template DNA, single-strand primers, deoxyribonucleosides (dNTPs), high-fidelity Pfu-polymerase, buffer and salt. Taq-

polymerase is used for DNA synthesis for genotyping reactions. Reaction mixes were as follows:

PCR with Pfu-Polymerase	PCR for Genotyping
1 μl (50-500ng) Template DNA	1 μl Tail DNA
1 μl 5' Primer (5 pmol)	1 μl 5' Primer (5 pmol)
1 μl 3' Primer (5 pmol)	1 μl 3' Primer (5 pmol)
1 μl dNTP-Mix (2.5 mM each)	1 μl dNTP-Mix (2.5 mM each)
2 μl 10x Polymerase Buffer	2 μl 10x Polymerase Buffer
1 μl 1 ml Pfu Polymerase	1 μl Red Taq Polymerase
Final volume to 50 μl with H_2O	Final volume to 20 μl with H_2O

Basic PCR cycling parameters were as follows:
Step 1: 95°C for 5 minutes
Step 2: 95°C for 30 seconds
Step 3: Annealing temperature for 30 seconds
Step 4: 72 °C for extension time (30-40 cycles from step 2)
Step 5: 72°C for 10 minutes

2.2.14 Genotyping PCRs

β-SNAP genotyping was performed on mouse genomic DNA by separate amplification of wild-type and knock-out alleles. The wild-type allele was amplified with primers number 1 and 2, and the knock-out allele with primers 3 and 4. Amplification conditions used were identical for both amplifications: Annealing temperature 60°C, 1 minute extension time.

HYH genotyping was performed by direct sequencing of the point mutation G (in wild/type) to A (in HYH mutant). A fragment of approximately 200 base pairs containing the point mutation was directly amplified from genomic DNA by using primers number 5 and 6. Amplification conditions were as follows: Annealing temperature 58°C, 1 minute extension time.

Before the sequencing reaction, the following reaction mix was incubated at 37°C for 40 minutes, and then at 80°C for 20 minutes, in order to clean the PCR reaction

mix from excess primers and dNTP which would interfere with the sequencing reaction:

Amplification Mix	5 μl
Shrimp Alkaline Phosphatase	0.5 μl
Exonuclease I	0.5 μl
H_2O	4 μl

2.2.15 Cloning of α- and β-SNAP into pSFV1 for Semliki Forest Virus Generation

The mouse β-SNAP sequence was generated by mutagenesis PCR using bovine β-SNAP in pQE30 and the Quick Exchange Kit with the overlapping mutagenic primers number 7 and 8. Amplification conditions were chosen according to guidelines of manufacturers.

Subsequent cloning of mouse β-SNAP was performed using the positive product of this mutagenic reaction, which was confirmed by sequencing. α-SNAP, on the other hand, was amplified from a pLEXN construct. Both fragments were amplified with primers containing EcoRV/BamHI restriction sites (primers 9-10 for α-SNAP, and 11-12 for β-SNAP), and subcloned into pcDNA3-IRES-EGFP. A fragment containing α- or β-SNAP and the IRES sequence was then excised with BamHI/ClaI and subcloned into pSFV1. The final construct (α- or β-SNAP in pSFV1) allows the simultaneous expression of α- or β-SNAP and EGFP.

2.2.16 Primary Mouse and Rat Neuronal Cultures

2.2.16.1 Media and Solutions

Solution 1

2 mg Cystein, 10 ml DMEM, 1 mM $CaCl_2$ (stock 100 mM), 0.5 mM EDTA (stock 50 mM).

Papain Solution

20-25 units of Papain per 1 ml of solution 1 were mixed and bubbled with carbogen (95% oxygen, 5% carbon dioxide) for 10-20 minutes (until the solution was clear). The papain solution was sterolized by filtration through a 0.2 mm filter.

Stop Solution

25 mg albumine, 25 mg trypsin inhibitor, 9 ml Dulbecco's MEM (DMEM), 1 ml FCS. The solution was kept in a water bath at 37°C until use.

DMEM Complete

50 ml DMEM, 10% FCS, 2 ml GlutaMAX TM I, Pen/Strep 1:100.

Neurobasal Complete

100 ml Neurobasal, 2 mM GlutaMAX TM I, 2 ml 1x B-27 supplement, Pen/Strep 1:100

2.2.16.2 Astrocyte Culture for Mouse Neuronal Autaptic Cultures

Autaptic neurons were cultured on astrocyte feeder cells. These feeder cells were prepared on small microdots of permissive substrate, where astrocytes can adhere. Small microdots (a few μm^2 in size) of permissive substrate (collagen) were prepared on glass coverslips. Than astrocytes were plated onto these microdots top. To make a microdot plate, 0.15% agarose gel was liquefied, pipetted onto glass coverslips, and quickly sucked off again. Agarose forms a non-permissive substrate where cells are reluctant to attach. Coverslips were then sterilised for 20-30 minutes under UV-light and left to dry for a few hours. Next, the sticky collagen/ Poly-D-Lysine (PDL) substrate was applied on top of the agarose to form "islands" on which cells readily attach. The PDL/acetic acid/collagen coating solution (3:1:1 acetic acid, PDL, collagen) was stamped onto the agarose in small dots using a custom-made stamp, and coverslips were then re-sterilised for 20-30 minutes under UV light.

Mouse cortices from newborn animals were digested for 20 minutes in Trypsin/EDTA at 37°C with gentle agitation (1 ml/cortex). The supernatant was carefully discarded, and stop solution (approx 1ml per cortex) was added and incubated for 15 min at 37°C. After discarding the supernatant, 0.2 ml of prewarmed FBS Medium (10% FBS, MITO, Pen/Strep, in DMEM) was added, and brains were

gently triturated with a yellow tip, left to settle down, and the supernatant was transferred to prewarmed FBS Medium. Cells were counted, and 800.000 cells were plated into a T-75 culture flask. The medium was exchanged the day after plating, and cells were left to grow in a monolayer until confluence was reached. Cells were then treated with Trypsin (5ml Trypsin/EDTA), counted and plated at a density of 12.000 cells per well of 6-well plates containing microdot-coated coverslips.

2.2.16.3 Treatment of Coverslips for Culturing Primary Neurons (Continental Cultures)

To attain direct adhesion of cultured neurons, the surface of coverslips was coated with PDL in sterile atmosphere. The coverslips were incubated with PDL for at least one hour (usually overnight) at 37°C. The coverslips were then washed twice with sterile water, once with HBSS and then incubated with Complete Neurobasal Medium at 37°C until cell plating.

2.2.16.4 Mouse Neuronal Cultures

The individual brains were quickly removed from newborn pups (HYH mutant, β-SNAP deletion mutant, or wild-type mice) and collected in HBSS at room temperature. Hippocampi were dissected out and transferred immediately to 0.5 ml Papain solution, pre-warmed at 37°C, and incubated for approximately 1 hour at 37°C with gentle agitation. Papain was removed by moving hippocampi to the wall of the tube, 0.5 ml pre-warmed Stop Solution was added, and the hippocampi were incubated for 15-20 minutes at 37°C with gentle agitation. All the supernatant was removed and 200 µl pre-warmed Complete Neurobasal Medium was added. The hippocampi were gently triturated 10-20 times with a yellow tip, and after leaving the tubes to stand for 1-2 minutes the supernatant was transferred to 1 ml of pre-warmed Complete Neurobasal Medium. A second trituration step was used to increase the yield of the preparation, if necessary. Cells were counted using the Naubauer Counting Chamber (4x4 grid x 1000 cells/ml) and approximately 90.000-240.000 were plated out per well in 6 well plate for continental cultures, while 4.000 cells were plated per well in 6 well astrocyte-plate for autaptic cultures. The medium was not changed.

In the case of SNAP double mutant neurons, genotyping was performed in parallel with the preparation of neuronal cultures. At the moment of dissection, HYH

mutant brains were clearly identified based on their characteristic anatomical abnormalities (see 3.4.1). Genotypes were confirmed by sequencing. After dissection, hippocampi were kept in Complete Neurobasal Medium at 37°C under gentle shaking for approximately 2 hours before being transferred to papain solution, while quick β-SNAP genotyping was performed in parallel from tail samples.

2.2.16.5 Rat Neuronal Continental Cultures

The brains from rat embryos (E18.5) were dissected out and collected in a dish with HBSS, and the hippocampi were removed and pooled in a 1 ml Falcon tube. The hippocampi were washed 3 times with HBSS, then 200 µl Trypsin-EDTA was added to 1800 µl HBSS, and left for 20 min in the 37°C bath. After incubation, the hippocampi were washed 5 times with HBSS and transferred to a 2 ml Eppendorf-cup, where 1600 µl HBSS was added with 400 µl DNase I (0.01% final). The hippocampi were triturated slowly with a yellow tip. The triturated cells were then filtered through a cell strainer into a 50 ml Falcon tube, and complemented to a volume of 20 ml with complete DMEM. 10 µl of the neuron solution was counted, and cells were plated at a density of 360.000 cells per well in 6 well plates. The media was exchanged the following day to serum-containing Neurobasal.

2.2.16.6 Immunocytochemistry on Autaptic Hippocampal Neurons

Autaptic neuronal cultures at 9-15 DIV were quickly washed with PBS and fixed with 4% PFA in PB Sucrose Buffer (130 mM Na_2HPO_4, 50 mM NaH_2PO_4, 320 mM Sucrose, pH 7.4) for 10-15 minutes at room temperature. Also all the following steps were performed at room temperature. After three washing steps with PB (130 mM Na_2HPO_4, 50 mM NaH_2PO_4, pH 7.4), a blocking/permeabilisation step was performed by incubating the cells in Blocking buffer (1xPB, 5% Goat Serum, 0.05% Triton) for 30 minutes, after which a primary antibody containing solution (in blocking buffer) was applied and incubated for 1 hour at room temperature (or over night at 4°C). After three washed with PB, fluorochrome-labelled secondary antibody in Blocking buffer was applied, and incubated for 1 hour at room temperature. After 3 final washes with PB and one quick wash with distilled water, coverslips were mounted with the embedding medium Moviol and left to dry over night at room temperature.

2.2.16.7 *In-Vitro* Packaging of Semliki Forest Virus

The procedure involves electroporating host cells in the presence of both Helper construct (providing structural and replicational proteins *in trans* required to produce the virus) and pSFV1 construct (containing the gene of interest) mRNAs. Semliki Forest Virus is a retroviral-based virus, and RNA needs to be packaged into reconstituted viral particles. Only if both Helper and pSFV1 mRNAs are expressed together in the same cell, virus particles are assembled, which contain only the pSFV1 mRNA. Viral particles are therefore replication-incompetent and only carry the gene of interest.

In vitro transcription of capped mRNAs was performed with SP6 Cap-Scribe RNA polymerase from pSFV-Helper and pSV1 constructs, according to the manufacturer's instructions. mRNAs were then purified by standard phenol/chloroform extraction procedures, and precipitated in the presence of ethanol. The RNA concentration was estimated a by absorbance at 260 nm, aliquoted and stored at -20°C.

Semliki Forest Viruses were produced in BHK21 tk-ts13 host cells. These cells were cultured in the presence of complete growth medium (2.5% FCS in DEM, 100 U Pen/Strep) in T-75 cell culture flasks. Once 80% confluence was reached, cells were washed with Opti-MEM, incubated with Trypsin/EDTA (2.5%) for 2-3 minutes at 37°C until cells detached, and resuspended in complete growth medium. Cells were pelletted by mild centrifugation (800 x g_{max} for 2 minutes) and washed two times with Opti-MEM. Before the last washing step, cells were counted in a Neubauer chamber and were then resuspended at a density of $1x10^7$ cells per ml in ice-cold PBS. 800 μl of the cell suspension were mixed with 10 μg Helper mRNA and 10 μg pSFV1-construct mRNA, and electroporated at 300 V (1 pulse of 0.25 msec). The electroporated cell suspension was then transferred to a T-75 flask containing 9 ml complete Neurobasal Medium (100 ml Neurobasal, 1 ml GlutaMAX TM I, 2 ml 1x B-27 supplement, 1x Pen/Strep), and left grow at 37°c for 24-30 hours. Expression of GFP can be directly monitored by observation under a fluorescence microscope, and once optimal fluorescence intensity was reached, the supernatant was harvested and stored at -80°C in 450μl aliquots.

Activation of the virus was done by incubating at room temperature for 45 minutes 450 ml virus aliquot with 450 μl pre-warmed complete Neurobasal medium and 1 aliquot of Chymotrypsin (100 μl, 2 mg/ml stored at -20°C). The Chymotrypsin digest was stopped by adding 1 aliquot Apoprotinin (100 μl, 6 mg/ml stored at -20°C) and

incubation for 10 minutes at room temperature. Activated viruses were used for up to 2 weeks. Autaptic neuronal cultures were infected with 40-60 μl viruses expressing α-SNAP, β-SNAP or HYH mutant. After 6-10 hours, a bright GFP signal was visible under the fluorescence microscope.

2.2.17 Biochemical Experiments

2.2.18 Sodium-Dodecyl-Sulfate-Polyacrylamide-Gel Electrophresis (SDS-PAGE)

In SDS polyacrylamide gel electrophoresis, proteins are separated based on their molecular size as they migrate in an electrical field through pores in the gel matrix towards the anode. Pore sizes decrease with increasing acrylamide concentrations.

2.2.18.1 Buffers and Solutions

Stacking Gel Buffer
0.5M Tris/Cl pH 6.8, 0.4% SDS

Separating Gel Buffer
1.5 M Tris/Cl pH 8.8, 0.4% SDS

AMBA Solution
30% acrylamide/N,N'-Methylene-bis-Acrylamide Solution

10% APS
10% Ammonium Persulfate in dH_2O
Running Buffer (per Litre)
25 mM Tris Base, 190 mM Glycine, 1% SDS, pH 8.8

BioRad Prestained SDS-PAGE Wide Range Standards: 250-150-100-75-50-37-25-20-15-10 kDa.
Fermentas SDS-PAGE Wide Range Markers: 170-130-100-70-55-40-35-25-15-10 kDa.

2.2.18.2 SDS-PAGE Gel Composition

	Separation Gel (for 2 gels)	Stacking Gel (for 2 gels)
AMBA (30%)	X ml (for desired concentration)	0.4 ml
Buffer	2.5 ml	0.75 ml
H_2O	10 - X ml	1.85 ml
10% APS	60 μl	60 μl
TEMED	6 μl	6 μl

2.2.18.3 Preparation of and Running SDS-PAGE Gels

After pouring the separation gel, the surface was covered with water-saturated butanol to obtain a smooth surface of the gel. After polymerisation of the gel, the butanol was removed and the remaining volume above the gel was filled with stacking gel solution and the comb was inserted. After the gel was polymerised, the protein samples were mixed with SDS sample buffer and boiled at 100°C for 5 minutes before loading on the gel. The gel chamber was filled with SDS running buffer and the electrophoresis was performed at constant voltage of 90-120V.

2.2.19 Standard and Colloidal Comassie Blue Stainings

After electrophoresis the stacking gel was discarded and the separation gel was stained. Gels were incubated for 15-30 min in 25% (v/v) isopropanol, 10% (v/v) acetic acid and 0.15% (w/v) Comassie Brilliant Blue R-250 while shaking. Then the gel was destained in 30% (v/v) methanol and 10% (v/v) acetic acid for 15 min. After scanning the gel on the computer-scanner it was dried in the gel drier for long-term storage. The high-sensitivity Colloidal Coomassie Staining was performed as follows. A fixation step (40% ethanol, 10% acetic acid) of at least 10 minutes was followed by two washes with water, a staining step with Dye Stock Solution (80% dye stock solution, 20% methanol), and extensive washes in 1% acetic acid, until a clear band pattern in the gel was obtained. The Dye Stock Solution contained 0.1% Comassie Brilliant Blue G250, 2% orto-phosphoric acid and 10% ammonium sulphate.

2.2.20 Transfer of Proteins from Acrylamide Gels to Membranes: Western Blotting

Western Blotting (or immunoblotting) is used to identify specific antigens on proteins separated by SDS-PAGE and transfered to nitrocellulose membranes. The identification relies on the specificity of antibody-antigen reactions. Proteins were first separated by SDS-PAGE, and the antigens were electrophoretically transferred at 250 mA for 2 hours, or overnight at 40 mA, to a nitrocellulose membrane. The process was subsequently monitored by reversible Ponceau-S staining. The transferred proteins bound to the surface of the membrane, providing access to reactions with immunodetection reagents.

2.2.20.1 Buffers and solutions

Blot Buffer

25 mM Tris Base, 190 mM Glycine, 20% Methanol

Ponceau-S Solution

0.1% (w/v) Ponceau-S, 5% Acetic Acid

2.2.21 Immunostaining of Blots with HRP-Labelled Secondary Antibody and Visualisation with Enhanced Chemiluminescence (ECL)

For immunoblotting, a primary antibody was used which recognises a specific epitope on the protein of interest. Unspecific binding was inhibited additionally by the use of blocking solution containing either protein or detergent blocking agents. To detect the antigen-antibody reaction, a horseradish peroxidase (HRP)-labelled secondary antibody was used, which binds to the first unlabelled antibody (indirect staining method). The active components of the ECL system are luminol and H_2O_2. The peroxidase reduces the hydrogen peroxide, and the resulting oxygen oxidises the luminol, which releases light. The chemiluminescence is then enhanced through appropriate enhancers and visualised on Amersham Hyperfilm films.

2.2.21.1 Buffers and solutions

1x TBS

10 mM Tris/HCl, 150 mM NaCl, pH 8.0

Blocking buffer

5% milk powder, 5% goat serum, 1x TBS, 0.1% Tween 20

Washing Buffer

1x TBS, 0.1% Tween 20

2.2.21.2 Procedure

Number of washes	Buffer	Time (min)
1	Blocking Buffer	30 (or overnight at 4°C)
1	Blocking Buffer and 1° Ab	60 (or overnight at 4°C)
4	Blocking Buffer	5
1	Blocking Buffer and 2° Ab	60
3	Blocking Buffer	5
3	Washing Buffer	5
2	TBS 1x	5

The above incubations were done at room temperature under moderate shaking. Occasionally, blocking or incubation with primary antibody were performed overnight at 4°C. After the last washing step of the above protocol, the membrane was placed on a glass plate and ECL signal development was performed according to the manufacturer's instructions. A clean transparency was placed on top of the membrane and the membrane was exposed to Amersham Hyperfilm film for appropriate times.

2.2.22 Immunostaining of Blots with Infra-Red Labelled Secondary Antibody and Visualisation with the Odyssey System

The Odyssey TM Imaging System allows to accurately quantify proteins in Western Blot analysis using advanced infrared imaging. Odyssey is uniquely equipped with two infrared channels for direct fluorescence detection on membranes using infrared labelled antibodies, Alexa Fluor 680-labelled secondary antibodies and LI-COR IRDye 800 infrared dye-labelled secondary antibodies. With two detection channels, two separate target samples can be simultaneously probed on the same blot. Infrared detection produces a wider linear range than other fluorescent imaging systems because low background fluorescence results in higher sensitivity. The

procedures with ECL or Odyssey detection are essentially the same, the only significant difference being that all incubations from the addition of the secondary antibody onwards are done in the dark, and that Tween-20 is excluded from the Blocking solution only in the Blocking step.

2.2.23 Determination of Protein Concentrations

The determination of protein concentrations was carried out using the BCA protocol, and following the instructions provided by Protein Assay from the Bio-Rad company. This assay is based on Cu^{+2} reduction and the selective colorimetric detection of the cuprous cation (Cu^{1+}) by Bicinchoninic acid.

2.2.24 Mouse Brain homogenate and Triton X-100 Solubilised Brain Membrane (P2) Fractions

2.2.24.1 Buffers and Solutions

Homogenisation Buffer

50 mM Hepes/NaOH pH 7.4, 5 mM EDTA

Solubilisation/IP Buffer

50 mM Hepes/NaOH pH 7.4, 150 mM NaCl, 1% Triton X-100, 5 mM EDTA

Protease inhibitors (1 mM PMSF, 1 μg/μl Leupeptin and Aprotinin) were included in all buffers.

2.2.24.2 Procedure

All steps after the removal of the mouse brain were done on ice and all the centrifugation steps were done at 4°C. One mouse brain was placed in 0.5-3 ml ice-cold Homogenisation Buffer and homogenised at 900 rpm (ten strokes) with a Glass-Teflon homogeniser. After centrifugation of the homogenate for 10 minutes at 900 x g_{max}, the nuclear pellet was discarded. The supernatant is the final “whole-brain homogenate” sample, which was usually employed for Western Blotting experiments. Homogenate aliquots were mixed with 3x Laemmli Loading Buffer to 1x final concentration, and used immediately or stored at –20 C for later use.

"Whole-brain homogenate" was processed to obtain "Triton X-100 Solubilised Brain-Membrane Fractions". For this purpose, brain homogenates were centrifuged at 20.000 x g_{max} for one hour. Supernatants were discarded, and pellets resuspended in Homogenisation Buffer. After determination of the protein concentration, samples were adjusted to 3-4 mg protein per ml with homogenisation buffer, and then mixed 1:1 with Solubilisation Buffer 2x, and incubated for 10-15 minutes at 4°C on a rotating wheel. Samples were then centrifuged at 100.000 x g_{max} for 1 hour, and supernatants were collected into fresh tubes and immediately used for further applications. The supernatant represents the "Triton X-100 Solubilised Brain-Membrane" fraction, which was used for Syntaxin I co-immunoprecipitation experiments and NSF/SNAPs binding assays (see below).

2.2.25 Lysates of Cultured Neurons

Continental cultures of mouse and rat neurons were quickly washed with ice-cold PBS, and lysed with Lysis Buffer (see above, whole brain homogenisation) for 30 minutes with moderate shaking at 4°C. A cell scraper was used to remove more efficiently the cells from the coverslip. The lysate was centrifuged at 100 x g_{max} for 10 minutes, and the supernatant directly used for Western blotting analysis, or stored at -20°C after addition of Laemmli Buffer.

2.2.26 Expression and Purification of His-tagged α-SNAP, β-SNAP and NSF

BL21-D3 bacteria were transformed with pET28a-α-SNAP, and a glycerol stock of a positive clone was made. pQE30-β-SNAP and pQE9-NSF were transformed into XL1Blue bacteria, and glycerol stocks were also made from positive clones. All three recombinant proteins were purified by taking advantage of the His tag, with the Ni^{2+}NTA system. Starter cultures were inoculated with α- , β-SNAP (100 ml) or NSF (300 ml) overexpressing bacteria and grown overnight at 37°C. The cultures were diluted 1:10 in the morning, and grown until an OD_{600} of approximately 0.6 was reached. Protein expression was induced with IPTG (0.5 mM final concentration). After 3-4 hours at 37°C (room temperature for NSF), bacteria were pelletted at 4000 x g_{max} for 15 minutes, and resuspended in 10 ml Lysis Buffer (50 mM Hepes/NaOH pH 7.4, 300 mM NaCl, 10 mM Imidazole). Cells were lysed by sonication (1 continuous 1-minute pulse at 50% power), Triton X100 at 0.1% final concentration

was added, and the lysate was incubated on ice for 30 minutes. After ultracentrifugation (100.000 x g_{max} for 1 hour) the supernatant was applied to 1 ml (bed volume) of pre-washed and equilibrated Ni^{2+}NTA beads (washed 4 times with Lysis Buffer), and incubated on a rotating wheel at 4°C for 1 hour to allow binding of recombinant proteins. Beads were then washed three times with Wash Buffer (50 mM Hepes/NaOH pH 7.4, 300 mM NaCl, 20 mM Imidazole), and proteins were eluted with 1 ml Elution Buffer (50 mM Hepes/NaOH pH 7.4, 300 mM NaCl, 0.5M Imidazole) two consecutive times. Eluted fractions containing recombinant SNAPs were dyalised against dialysis buffer (50 mM Hepes/NaOH pH 7.4, 150 mM NaCl) overnight at 4°C, aliquoted, flash-frozen in liquid nitrogen and stored at -80°C. NSF was always prepared fresh before the experiment, due to its instability. Protease inhibitors were included in all steps. For NSF purification, ATP (0.5 mM) was included in all buffers, and EDTA (5 mM) was included in the eluted fraction.

2.2.27 SNAP/NSF *in vitro* Binding Assay

Freshly prepared Triton X-100 solubilised brain membranes from wild-type mice, and purified recombinant NSF, were incubated in the presence of recombinant α- or β-SNAP (from -80°C frozen aliquots). 1.2 ml solubilised membranes were used (1 mg/ml protein concentration), and NSF and SNAPs were included at $3\ \mu M$ final concentration in the reaction mix. The binding reaction was allowed to proceed for 1-2 hours at 4°C, then anti-Myc antibody 9E10 was added (8-10μg per reaction), and the reaction was allowed to proceed for an additional 2 hours at 4°C. 50 μl (bed volume) of pre-washed Protein-G coupled Beads were added to each tube, and incubated for 2 hours. Beads were then collected by centrifugation, washed with Solubilisation/IP buffer (cfr. 2.2.24.1) 3 times and then eluted with ATP/Mg^{2+} Elution Buffer (50 mM Hepes/NaOH pH 7.4, 150 mM NaCl, 10 mM $MgCl_2$, 5 mM ATP). Eluted fractions were loaded on SDS-PAGE gels and subjected to Western blotting or to mass spectrometric analysis. The latter was performed by Dr. Olaf Jahn of the Proteomics Group at the Max Planck Institute for Experimental Medicine. In all steps of the assay, except in the elution step, a constant concentration of EDTA (5 mM) and ATP (0.5 mM) was maintained to stabilise NSF and the reconstituted 20S complex.

2.2.28 Syntaxin-1 Co-Immunoprecipitation from Solubilised Brain Membrane Fraction

400 μl Triton X-100 Solubilised Brain Membrane Fraction (1-1.5 mg protein per ml) was incubated in with 6 μg Syntaxin I antibody for 2 hours at 4°C. Pre-washed Protein G coupled Sepharose beads were added, and samples were further incubated for 2 hours at 4°C on a rotating wheel. Beads were then collected by centrifugation, washed 3 times with Solubilisation/IP buffer (cfr. 2.2.24.1), dried with a syringe needle (Microbalance 3, 0.55mm x 25mm), and immediately resuspended in 40 ml of 2x Laemmli Buffer. Samples were boiled for 5 minutes at 100°C just prior to Western blotting analysis, and kept at -20°C for long-term storage.

2.2.29 Subcellular Fractionation

Subcellular fractions were kindly provided by S. Kalla, who performed subcellular fractionation experiments from Munc-13-1 EYFP knock-in mouse brains according to the protocol reported in Kalla et al. (2006).

2.2.30 *In-situ* Hybridisation

In-situ hybridisation experiments were performed by Randi Randi and Dr. Frederique Varoqueaux according to published standard procedures (Varoqueaux et al., 2006). Oligonucleotide number 13 was used for the specific hybridisation with α-SNAP mRNA, while oligo number 14 was used for β-SNAP.

2.2.31 Nissl Staining

Nissl staining experiments were performed by Randi Rawson and Dr. Frederique Varoqueaux. 8-Days old mice were perfused with 4% PFA, brains were removed and embedded for cryostat sectioning. Nissl staining was performed on sagittal brain slices according to published standard procedures (Varoqueaux et al., 2005).

2.2.32 Yeast Two-Hybrid System

2.2.32.1 Buffers, Media and Solutions

Salmon Sperm Carrier DNA

DNA from Salmon Testes was dissolved in TE at 10 μg/ml and incubated overnight at 4°C to give a homogeneous viscous solution. This solution was then sonicated twice for 30 seconds with a large probe at ¾ power. The DNA solution was then extracted and precipitated according to a Phenol/Chloroform DNA extraction protocol involving one extraction with TE saturated phenol, one with phenol:chloroform (1:1) and one with chloroform. The DNA was then precipitated by adding 1/10 volume of 3 M sodium acetate (pH 6.0) and 2.5 volumes of ice-cold ethanol (99%). The precipitate was collected by centrifugation at 12.000 x g_{max}, washed with 70% ethanol, partially dried under a vacuum and redissolved in TE at 10 mg/ml. This solution was then stored in aliquots at -20 C.

Z-buffer (per Litre)

60 mM Na_2HPO_4, 40 mM NaH_2PO_4, 10 mM KCl, 1 mM $MgSO_4$, pH 7.0, 2.7 ml β-mercaptoethanol

X-Gal Stock Solution

50 mg/ml 5-bromo-4-chloro-3-indolyl-b-D-Galactoside in dimethylformamide

YPAD (per Litre)

10 g bacto yeast extract, 20 g peptone, 0.1 g adenine, 100 ml 20% glucose, 1 ml ampicillin, 900 ml water.

YEPD-Agar (per Litre)

10 g bacto yeast extract, 20 g peptone, 900 ml water.

Selection Media (per Litre)

1.2 g yeast nitrogen base without amino acids, 5 g ammonium sulphate, 10 g succinic acid, leucine, lysine, threonine, tryptophane, uracile. 0.05 g of each of the following amino acids: aspartic acid, histidine, isoleucine, methionine, phenylalanine, proline, serine, tyrosine, and valine.The medium was autoclaved for 15 min, and after

cooling 100 ml 20% glucose was added, as well as X g threonine and aspartic acid (which cannot be autoclaved).

-UTL Media

As above with the following amino acids omitted: uracile, tryptophane and leucine.

-L+UT Media

As above with the following amino acid omitted: Leucine

Selection plates

As above for the selection media with 20 g agar added before autoclaving.

2.2.32.2 Transformation of DNA into Yeast

In this experiment, the yeast was transformed using a heat shock procedure with DMSO and salmon sperm carrier DNA. 10ml of YPAD was inoculated with a single colony of L40 and grown overnight at 30°C. This solution was then diluted to an OD_{600} of 0.4 in 50 ml YPAD and allowed to grow for an additional two hours. The cells were pelletted by centrifugation for 5 minutes at 1.278 x g_{max} and resuspended in 40 ml TE. The cells were centrifuged again, resuspended in 2 ml 100 mM LiAc/0.5x TE and incubated at room temperature for 10 minutes. The following was dispensed to tubes: 1 μg of each plasmid DNA, 100 μg denatured sheared salmon sperm DNA, 100 μl of the yeast suspension and 700 μl 100 mM LiAc / 40% PEG / 1x TE. This mixture was then incubated at 30°C for 30 minutes. 88 μl DMSO was added, and the solution was mixed and heat-shocked at 42°C for 7 minutes. The cells were pelletted and washed with 1ml TE, resuspended in 50-100 μl TE and plated onto the appropriate selection plate.

2.2.32.3 β-Galactosidase Test

β-galactosidase activity in the yeast clones positively correlates with the intensity of interaction of the proteins expressed by the test plasmids. The qualitative filter test was used for quick analysis of the clones. A nitrocellulose filter was placed carefully onto the yeast colonies, lifted and then placed (colonies side-up) on a pre-cooled aluminium boat floating in liquid nitrogen. After 30 seconds, the boat and filter were immersed for 5 seconds. The filter was then kept, colony side-up, at room

temperature until thawed. 5 ml of Z-Buffer and 50 μl 50 mg/ml X-Gal were placed in the cover of a Petri dish and one Whatman filter circle was placed in the mixture, followed by the nitrocellulose filter with colonies facing up. The plate was incubated at 30°C. Strong interactions yielded detectable colour in less that 30 minutes.

2.2.33 Electrophysiology

2.2.33.1 Whole-Cell Patch Clamp

In this technique, the membrane potential is held constant ("clamped") while the current flowing through the membrane is measured. Technically, a patch pipette with a tip diameter of approximately 1 μm is placed in contact with the plasma membrane. When little negative pressure is applied from the interior of the pipette, a very high resistance seal (Giga-seal – resistance typically 1-3GΩ) develops between the membrane patch and the glass of the pipette ("on-cell" configuration). Rupture of the membrane patch underlying the electrode surface (whole-cell configuration) allows direct communication between the interior of the electrode (filled with so called "internal solution") and the intracellular space. Voltage-clamp of the cell, which consists in maintaining membrane voltage at a constant fixed value, is then achieved using a negative feedback loop through a high-gain differential amplifier (Hodgkin and Huxley, 1952).

2.2.33.2 Experimental Set-up for Whole-Cell Voltage-Clamp and Data Analysis

The recording chamber was mounted in an inverted microscope (Olympus). Movements of the microelectrode were controlled with custom made piezoelectric manipulators mounted on mechanical manipulators. This equipment was mounted on a vibration-insulation table surrounded by a Faraday cage. Electrodes were made from borosilicate glass capillaries (1.50 mm outer diameter, 0.86 mm inner diameter). Capillaries were pulled using a Sutter 2000 filament-based horizontal puller. Electrodes were filled with standard internal solution (see below). A reference electrode consisting of a chlorided silver wire immersed in the perfusing solution was connected to the patch clamp amplifier ground. Electrode resistances were typically 2-4MΩ After the on-cell configuration was established, membrane voltage was clamped at -70mV. EPSCs were evoked by depolarising the cell from -70mV to 0 mV

for 2 ms. Currents were recorded using an Axon 700B amplifier (Axon Instruments), and acquired with a Windows PC computer via interface Digidata 1440A. Recordings were analysed using the Axograph 4.9 software. For curve fittings, the Igor Pro software was used. Statistics were analysed using the Instat 2.03 software with Student's t-test. Unless stated otherwise, error bars indicate the standard error of the mean (SEM).

2.2.33.3 Media and solutions

Base-Plus Extracellular Solution

140 mM NaCl, 2.4 mM KCl, 10 mM Hepes, 10 mM Glucose, 4 mM $CaCl_2$, 4 mM $MgCl_2$

Base Minus Extracellular solution

(as Base Plus solution, without $CaCl_2$ and $MgCl_2$)

Standard Internal Solution

KCl 136 mM, Hepes 17.8 mM, EGTA 1 mM, ATP/GTP regeneration system 1X

ATP/GTP regeneration system (10x)

6 mM $MgCl_2$, 40 mM ATP-Mg^{2+}, 3 mM GTP-Na_2, 150 mM Creatinephosphat, 50 U/ml Creatinephosphokinase

Hypertonic Sucrose Solution

0.5 M Sucrose in Base Plus Solution

Drugs were used at the following concentrations:

Drug	Final concentration
TTX	300 nM
Kainate	10 μM
PBDU	1 μM
Calcymicin	10 μM
MK-801	3 μM
Glycin	10 μM

3. Results

3.1 Brain Distribution and *In Vitro* Biochemical Properties of α- and β-SNAP

3.1.1 Similar Distribution of α- and β-SNAP in the Mouse Brain

SNAPs were originally identified as soluble cytosolic factors that support intercisternal Golgi transport *in vitro* (Clary et al., 1990). In brain, both α- and β-SNAP are expressed. To characterise the two isoforms in more detail, I first analysed their subcellular distribution in the mouse brain (Fig. 5B). Subcellular fractions were probed by Western blotting for α- and β-SNAP. As a control, I probed the fractions for Synaptophysin-1 and NMDAR-1 to evaluate the quality of the fractionation and to monitor the distribution of presynaptic and postsynaptic proteins. In Fig. 5B a typical distribution pattern for NMDAR-1 and Synaptophysin-1 are observed, the first being highly enriched in the synaptic plasma membrane fraction (SPM) and virtually absent from the crude synaptic vesicle fraction (LP2), and the latter being enriched in SPMs but also in the LP2 fraction. α- and β-SNAP, on the other hand, were identified in substantial amounts in all subcellular membrane and soluble fractions. They showed a very similar distribution pattern and were only moderately enriched in synaptic fractions. The only fractions in which α- and β-SNAP showed modest differential distributions were S3 (cytosolic) and LS1 (supernatant after lysed synaptosomal membrane sedimentation), with α-SNAP being more enriched in S3 and β-SNAP in LS1. This difference could reflect either a slightly higher solubility of the α-SNAP isoform, or a higher binding affinity of β-SNAP to membranes as compared to α-SNAP.

The subcellular distribution analysis shows that, with the exception of subtle differences probably arising from differential solubility and/or membrane affinities of the two isoforms, α- and β-SNAP are similarly distributed in mouse brain fractions, and are both slightly enriched at synapses.

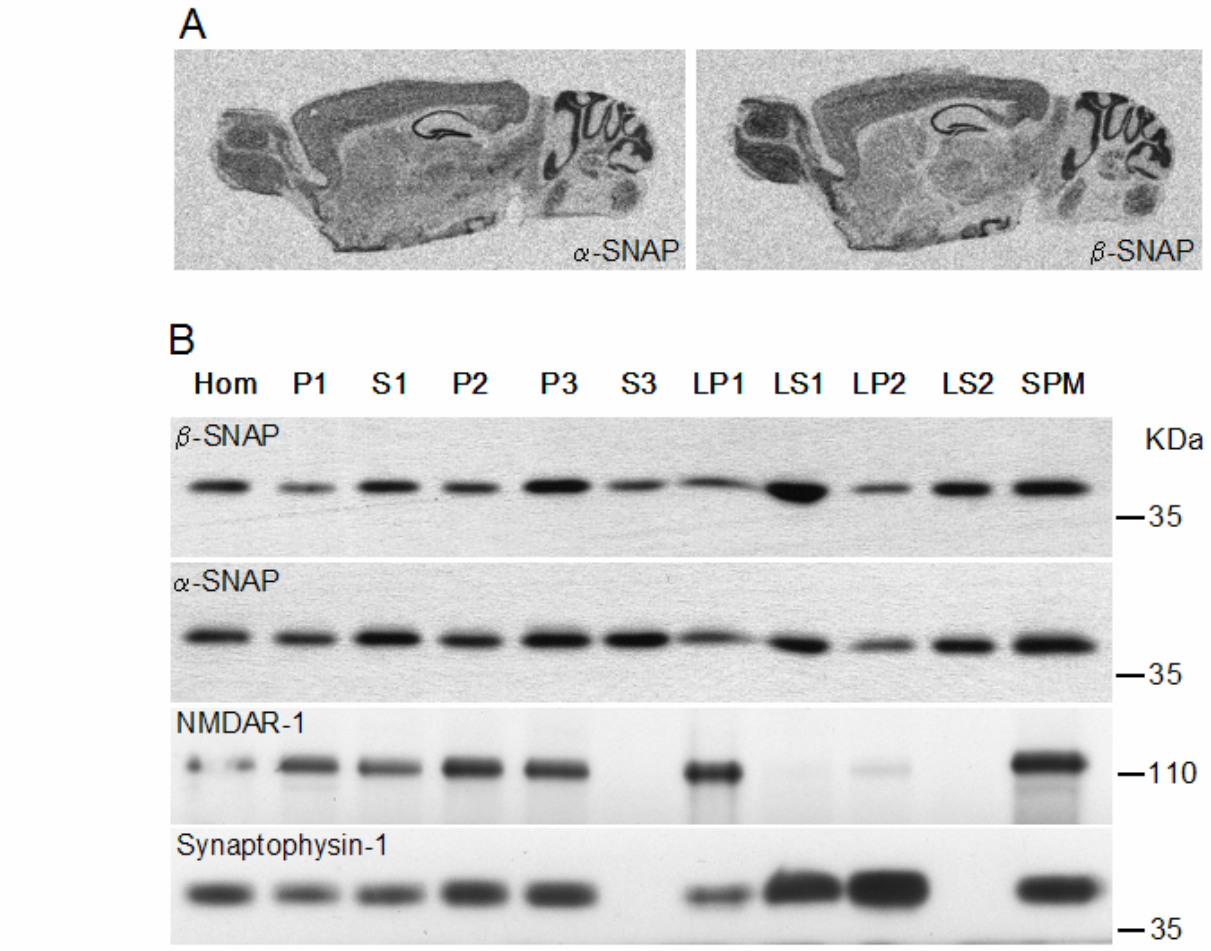

Figure 5 **Similar Distribution of α- and β-SNAP in the Mouse Brain.** (A) α- and β-SNAP mRNA distribution in adult mouse brain as determined by *in situ* hybridisation. Both mRNAs are widely expressed throughout the brain and are localized in the same brain areas. Highest signals for both mRNAs were found in olfactory bulb, hippocampus, cortex and cerebellar granule cell layer. (B) Immunoblots of subcellular fractions of brain homogenate from wild-type mice were analysed with antibodies against α- and β-SNAP. The distribution of a postsynaptic (NMDA-R1) and a presynaptic marker (Synaptophysin) was monitored to assess the quality of the subcellular fractionation. Typical distribution patterns for NMDAR-1 and Synaptophysin-1 are observed, the first being highly enriched in the synaptic plasma membrane fraction (SPM) and virtually absent from the crude synaptic vesicle fraction (LP2), and the latter being enriched in SPM but also in the LP2 fraction. α- and β-SNAP are present in both soluble and membrane fractions, and show a very similar subcellular distribution pattern in the mouse brain. Hom, Homogenate; P1, nuclear pellet; P2, crude synaptosomal pellet; P3, light membrane pellet; LP1, lysed synaptosomal membranes; LP2, crude synaptic vesicle fraction; SPM, synaptic plasma membranes; S1, supernatant after synaptosome sedimentation; S3, cytosolic fraction; LS1, supernatant after LP1 sedimentation; LS2, cytosolic synaptosomal fraction.

To study the expression pattern of α- and β-SNAP in the adult mouse brain, their mRNA distribution was analysed by *in situ* hybridisation (Fig. 5 A). Both α-SNAP and β-SNAP mRNAs were found to be widely expressed throughout the brain and were localized in the same brain areas. Highest signals for both mRNAs were found in olfactory bulb, hippocampus, cortex and cerebellar granule cell layer. In particular, the hippocampus showed an intense and clear labeling of the cell body layers (CA1, CA2, CA3 and dentate gyrus).

In conclusion, the mRNA distribution study revealed that α- and β-SNAP are widely expressed in the adult mouse brain and enriched in the same brain areas.

3.1.2 Differential Developmental Expression profiles of α- and β-SNAP in Mouse Brain and Hippocampal Cultures

While α-SNAP is a ubiquitous isoform, β-SNAP has been previously described as a postnatally expressed brain specific isoform (Whiteheart et al., 1993). To date however no detailed analysis of the developmental expression profiles of α- and β-SNAP in brain has been performed. I homogenised whole brains from mice between E12 and 3 months of age, and analysed them by Western blotting for the presence of α- and β-SNAP (Fig. 6A). Surprisingly, while α-SNAP levels were rather constant throughout the developmental stages tested and showed only a moderate increases in later stages, β-SNAP expression first appeared around birth and drastically increased during the first 2-3 weeks of postnatal life. The first weeks of postnatal life in mice are a critical time window for the establishment, formation and maturation of synaptic contacts throughout the whole brain (Xingjian and Bixby, 1993). Many synaptic proteins have been shown to have a similar expression pattern as β-SNAP, and this has been generally taken as an indication for a synaptic function of the respective proteins (Daly and Ziff, 1997; Bergmann et al., 1991; Catsicas et al., 1991).

I also analysed the developmental expression pattern of α- and β-SNAP in rat neuronal cultures (Fig. 6B). Postnatal *in vivo* neuronal development, the expression of several markers, and morphological and physiological properties of neurons can be recapitulated *in vitro* in the primary culture system (Wainer et al., 1991; Fuzshpan et al., 1989). As was the case for intact brain, I found that also in primary cultured neurons, β-SNAP expression is strongly upregulated during the first 2-3 weeks of *in*

vitro development, while α-SNAP expression shows only a moderate increase towards later stages (Fig. 6).

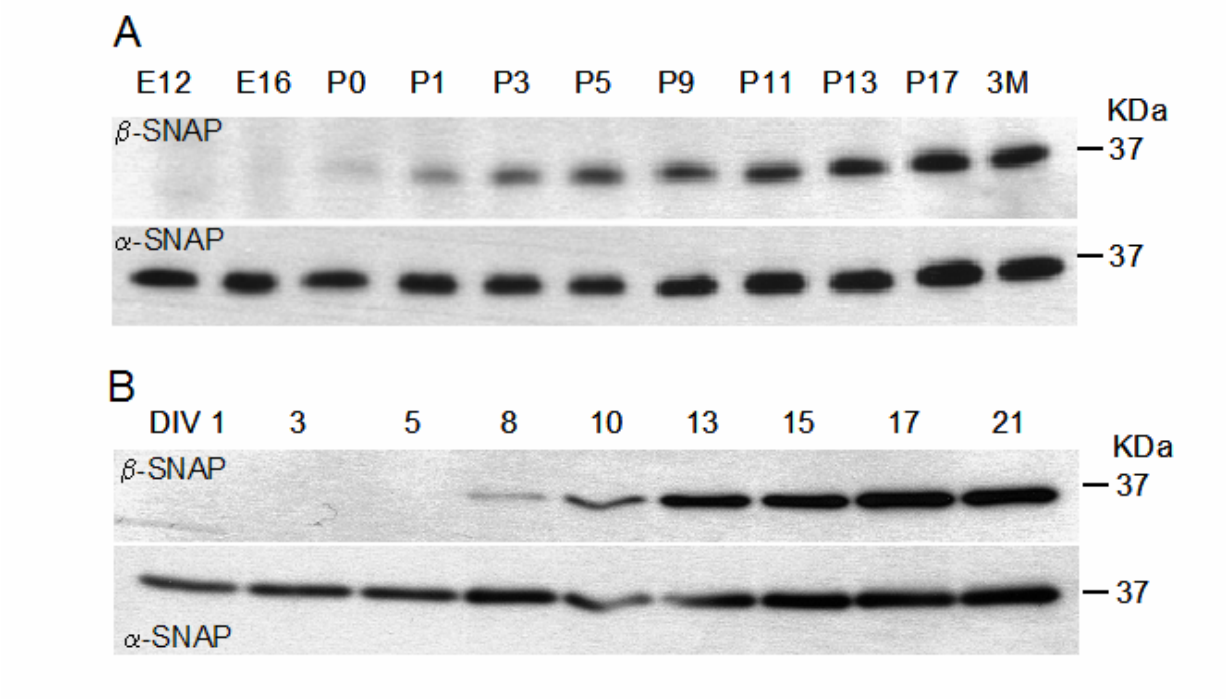

Figure 6 **Differential Developmental Expression Profiles of α- and β-SNAP in Mouse Brain and Hippocampal Cultures.** (A) Western blot analysis of α- and β-SNAP expression profiles in whole-brain homogenates from mice between E12 and 3 months of age (3M). α-SNAP levels are rather constant throughout the developmental stages tested (lower blot) while β-SNAP expression first appeared around birth and drastically increased during the first 2-3 weeks of postnatal life (upper blot). (B) Western blot analysis of α- and β-SNAP expression profiles in rat neuronal cultures. Like in intact brain, β-SNAP expression is strongly up regulated during the first 2-3 weeks of *in vitro* development, while α-SNAP expression shows only a moderate increase towards later stages.

In summary, the *in vitro* and *in vivo* developmental expression profiles of α- and β-SNAP indicate that α-SNAP expression is rather constant, while β-SNAP expression is strongly upregulated in neurons during the period of synapse formation.

3.1.3 Affinity Purification of α- and β-SNAP Interaction Partners from Solubilised Brain Membranes

SNAP receptors (SNAREs) were first purified and identified by Söllner et al. (1993). In an elegant biochemical assay they were able to reconstitute *in vitro* the 20S particle with recombinant NSF and α-SNAP, and to affinity purify the neuronal SNAREs from brain lysates. The assay consisted of the following components: (1) Myc-tagged recombinant NSF attached to a solid matrix via an anti-Myc antibody; (2) recombinant α-SNAP, and (3) detergent extract of a crude fraction from the grey matter of bovine brain. Recombinant NSF, α-SNAP, and brain lysates were incubated together in the presence of Mg^{2+}-ATP-γS (a non hydrolysable analogue of ATP), which allows the formation of stable 20S complexes consisting of the SNARE complex, NSF, and SNAPs. Stable assembled 20S complexes were then immunopurified via the Myc-tag of NSF and specifically eluted with Mg^{2+}-ATP. The bound 20S particles disassembled in the presence of Mg^{2+}-ATP and released stoichiometric amounts of α-SNAP and SNAREs. This final ATP-elution step introduced a greater level of specificity in the assay since only proteins released as the immediate consequence of ATP hydrolysis on the matrix are recovered in the eluate. With this biochemical assay, whose high specificity relies on the protein-protein interactions of the 20S components and on the ATP-hydrolysis elution, it was possible to isolate and successfully identify via microsequencing of protein fragments from the ATP eluted fraction the neuronal SNARE proteins Syntaxin-1, SNAP-25 and Synaptobrevin (Söllner et al., 1993). As mentioned above, this assay was carried out in the presence of α-SNAP.

To date, no biochemical data are available about the ability of the β-SNAP isoform to be incorporated into and to mediate ATP-disassembly of the 20S complex. Therefore, I adopted the original biochemical assay established by Söllner et al. (1993) to test the characteristics of the β-SNAP isoform and to compare it to α-SNAP. In two parallel assays, either α- or β-SNAP were included in the reaction mix, and all steps were performed in parallel as shown in Fig. 7A. Since recombinant α- and β-SNAP were added in excess for the binding reactions, the remaining endogenous SNAPs were likely out-competed, and the reconstituted 20S complexes were containing almost exclusively added recombinant α- or β-SNAP. The final ATP-

eluted fractions were separated by SDS-PAGE (Fig. 7B). Coomassie stained bands which were absent from “Beads” and “anti-Myc” control lanes were excised from the gel and subjected to mass spectrometric analysis.

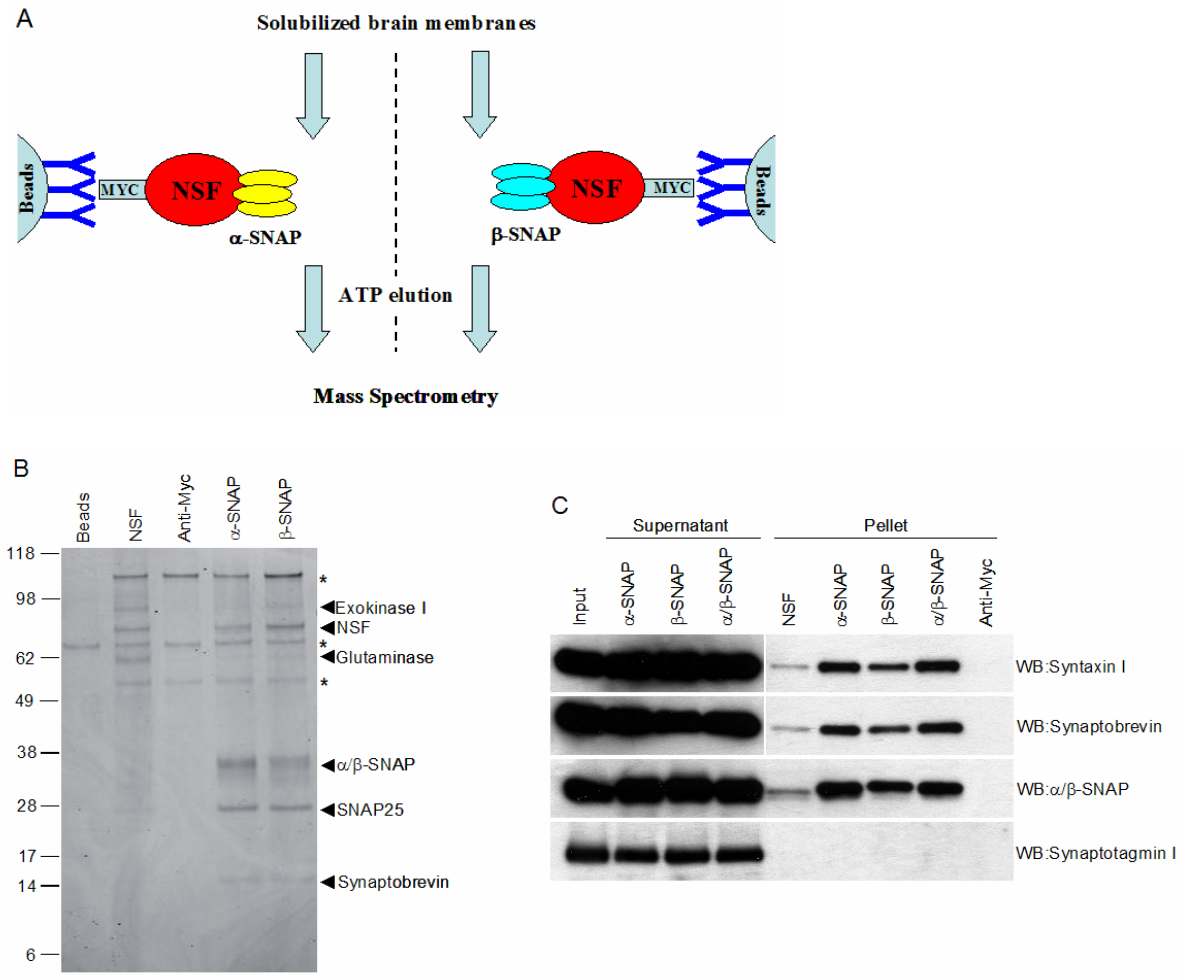

Figure 7 **Affinity Purification of α- and β-SNAP Interaction Partners from Triton-X100 Solubilised Brain Membranes.** (A) Schematic representation of the affinity purification procedure employed to isolate α- and β-SNAP interaction partners. Recombinant NSF and SNAREs from crude detergent brain extracts are assembled into 20S particles in the presence of either α- and β-SNAP. The SNAREs are incorporated stoichiometrically into the particles, which are then bound to anti-Myc coated-beads via the Myc-tag of recombinant NSF. Specific elution was performed in the presence of hydrolysable ATP (ATP/Mg^{+2}). (B) Representative SDS-PAGE gel stained with colloidal Coomassie blue, where (from left to right) elutates from control binding reactions (containing only agarose beads, beads plus NSF, beads plus anti-Myc antibody) and from specific reactions (containing complete reaction mixes with either α- or β-SNAP) were loaded. Visualised protein bands were excised from the gel and analysed by mass spectrometry. The neuronal SNAREs SNAP-25 and Synaptobrevin-2 were co-purified from

solubilised brain lysates with both α- and β-SNAP. Asteriscs (*) indicate unspecific bands, which were not included in the analysis. (C) Western blot of input, supernatants and eluted fractions (Pellets) for Syntaxin-1, Synaptobrevin-2, α/β-SNAP and Synaptotagmin-1. In addition to binding reactions containing either α- or β-SNAP, a parallel assay was included with both isoforms in a 1:1 ratio (α/β-SNAP lanes). Syntaxin-1 and Synaptobrevin-2 immunoreactive bands were slightly reduced in the β-SNAP pellet lane, compared to α- and α/β-SNAP lanes, indicating that β-SNAP may be incorporated into neuronal 20S complexes with slightly reduced affinity as compared to α-SNAP alone or to the situation where both α- and β-SNAP are present.

In the presence of only NSF (no α- and β-SNAP included in the assay) I identified Exokinase I and Glutaminase in the eluate (NSF lane, Fig. 7B). I did not further investigate the nature and specificity of these putative direct interactions.

When α- or β-SNAP were included in the assay, I was able to identify the neuronal SNARE proteins Synaptobrevin-2 and SNAP-25 in both eluted fractions at the expected molecular weights (15 and 25 kDa, respectively). Even though I expected Syntaxin-1 to be present in the eluate in stoichiometric amounts as compared to its cognate SNAREs, I was not able to identify it in the gel range representing 30-38 kDa. In this region, in fact, a diffuse band was visible in both α- and β-SNAP lanes (Fig. 7B), in which I could identify recombinant α- and β-SNAP, respectively. Since the molecular weights for SNAPs and Syntaxin-1 are very similar, it is likely that the excess of SNAPs used in the assay masked the co-migrating Syntaxin-1 and prevented its detection via mass spectrometry. Therefore, I performed a Western blot analysis for Syntaxin-1, which, as expected, was readily identified in both α- and β-SNAP eluted fractions (Fig. 7C). Interestingly, the Syntaxin-1 immunoreactive band in the β-SNAP lane was less intense than in the α-SNAP lane. In line with this finding, it has been reported that *in vitro* β-SNAP binds to assembled SNARE complexes with less affinity than α-SNAP (Schiavo et al., 1995). A faint Syntaxin-1 immunoreactive band was also detected in the NSF control lane, where no recombinant SNAPs were added. This probably reflected its binding via endogenous SNAPs to the recombinant immobilized NSF. In fact, Western blotting for α/β-SNAP showed a weak double band in the NSF control lane, indicating that endogenous SNAPs were indeed interacting with recombinant NSF and probably mediating binding to SNAREs (Fig. 7C). As expected, a similar pattern was observed for Synaptobrevin-2, which was strongly enriched in the α- and β-SNAP lanes as

compared to the NSF lane, where a weak immunoreactivity was detected. In contrast, Western blotting for Synaptotagmin 1 revealed the complete absence of the protein in all eluted fractions, even after long exposure of the blot (Fig. 7C and data not shown). This is consistent with previous reports, which indicated that Synaptogmin 1 and SNAPs compete for the same binding site on the SNARE complex (McMahon et al., 1995; Kee and Scheller, 1996).

In brain, both α- and β-SNAP isoforms are expressed. Therefore, to more closely mimic the *in vivo* situation *in vitro*, I performed a parallel assay were both isoforms were included in a 1:1 ratio. As shown in Fig. 7C (lane "α/β-SNAP"), both isoforms together were also very efficient in pulling-down SNARE proteins from the brain extract, as indicated by the Synaptobrevin-2 and Syntaxin-1 Western blotting.

On aggregate, the *in vitro* binding assays described above allowed me to describe several aspects of SNAP biochemistry which were previously unknown: (1) Although with slightly less efficiency than α-SNAP, the β-SNAP isoform can be incorporated into the 20S complex and can mediate its disassembly via ATP-hydrolysis; (2) "mixed" 20S complexes containing both SNAPs and "single" complexes containing either α- or β-SNAP are formed with similar efficiency; (3) α- or β-SNAP do not have different interaction partners.

3.2 β-SNAP Deletion Mutant Mice

In order to study the contribution of the brain-specific isoform β-SNAP to synaptic transmission, β-SNAP deletion mutant mice were generated by deletion of the first coding exon of the NAPB gene (Meyer et al., unpublished data). At birth, deletion mutant mice breathed, moved and suckled, and were indistinguishable from their littermates. However, starting from postnatal day 8, homozygous β-SNAP deletion mutant mice appeared slightly smaller than littermates. From postnatal day 11 onwards, they developed an epileptic syndrome characterized by severe recurrent epileptic seizures. Epileptic seizures started abruptly in mutant mice as an evident aberrant behaviour characterised by trembling, flickering movements of the tongue and increased motor activity. This pre-ictal period usually lasted between 10 to 30 seconds, and always evolved to a generalised "tonic-clonic" seizure. This seizure type is characterised by a first "tonic" phase, where all body muscles are contracted, followed by a second "clonic" phase, characterised by jerking movements of body

extremities resulting from rapidly alternating contraction and relaxation of the muscles. The ictal period usually lasted up to one minute and was generally followed by a very long period of quite ataxic behaviour, which is a common phenomenon after ictal events in mice (Frankel et al., 1994). Sometimes however double mutant mice did not recover after the tonic phase, and died during the seizure.

The characteristic progression of the seizure, evolving from defined behaviours that always preceded the generalised ictal event, may be indicative of a "secondarily generalized" seizure type. This type of seizure, which has been extensively studied and represents the most common seizure type in humans, arises from an initial primary electrical event in the brain, a “partial” seizure, which later becomes “generalized” and spreads to both brain hemispheres. A “partial” seizure is defined as a localised burst of electrical activity in a limited brain region, the so-called “focus” region. In support of the above behavioural observations, electroencephalographic (EEG) monitoring of the seizure events could be used to clearly define the epileptic phenotype of β-SNAP deletion mutant mice.

Most homozygous mutant mice died within the third postnatal week, but individual mice did survive up to the fifth postnatal week. As observed for several other epileptic mutant mice (Seyfried et al., 1980; Collins et al., 1968; Neumann et al., 1991; Sagane et al., 2005), the severity and recurrence of generalized tonic-clonic seizures are likely to be responsible for the lethality.

In summary, above data indicate that β-SNAP is not required for brain functions that support embryonic and perinatal life, but it plays a crucial role during postnatal life. This is consistent with its developmental expression profile, which starts around birth and reaches its maximum level within the second to third week of postnatal life (Fig. 6).

3.2.1 Unaltered Morphology and Protein Composition of β-SNAP Deficient Brains

I next analysed and compared brain structures of β-SNAP deletion mutant mice and wild-type control littermates. Sagittal sections from paraffin-embedded brains were made, and stained by the Nissl method (Fig. 8A). This method uses basic aniline to stain extranuclear RNA, and is used for the detection of Nissl bodies (rough endoplasmic reticulum) in the cytoplasm of neurons. This staining is commonly used

to study cell layering and cytoarchitecture of neurons in the brain. Light microscopic analysis of Nissl stained brain sections did not reveal any alteration in brain morphology and cytoarchitecture in β-SNAP mutant mice (Fig. 8A).

In order to study the composition of β-SNAP deficient brains at the molecular level, I analysed the expression of 42 candidate proteins in brain homogenates of control and β-SNAP mutant mice by Western blotting amd Enhanced Chemiluminescence detection (ECL) and Odyssey Infrared Imaging (Fig. 8B). I did not detect any difference in the expression levels of tested proteins between β-SNAP deficient and wild-type control brains.

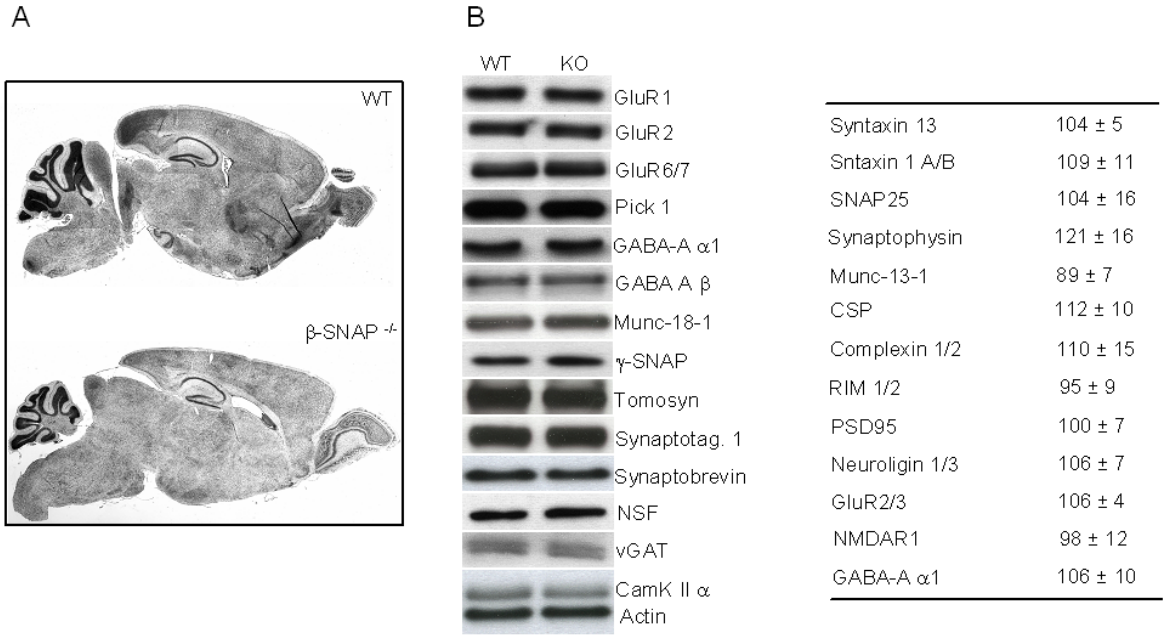

Figure 8 **Normal Morphology and Protein Composition of β-SNAP Deficient Brains.** (A) Sagittal sections from paraffin-embedded wild-type and β-SNAP deficient brains stained by the Nissl method. No alterations in brain morphology and cytoarchitecture in β-SNAP mutant mice were evident. (B) Expression levels of 42 candidate proteins in wild-type and β-SNAP deficient brain homogenates were analysed by Western blotting and Enhanced Chemiluminescence (left panel) or quantified by the Odyssey Infrared Imaging System (right panel) (N= 4). No changes in the protein levels between β-SNAP deficient and wild-type control brains were detectable. Data are expressed as % of control. Error bars indicate standard error of the mean.

Taken together, these results indicate that at the morphological and molecular level β-SNAP deficient brains are indistinguishable from control wild-type brains, and

that the β-SNAP deletion did not result in any parallel or compensatory change in the expression levels of a relatively large group of functionally related proteins.

3.2.2 Unaltered Synapse Number in β-SNAP Deficient Hippocampal Neurons

In order to characterize the synaptic phenotype of β-SNAP deficient neurons in more detail, I imaged and quantified glutamatergic synapses at the light microscopical level in single isolated neurons.

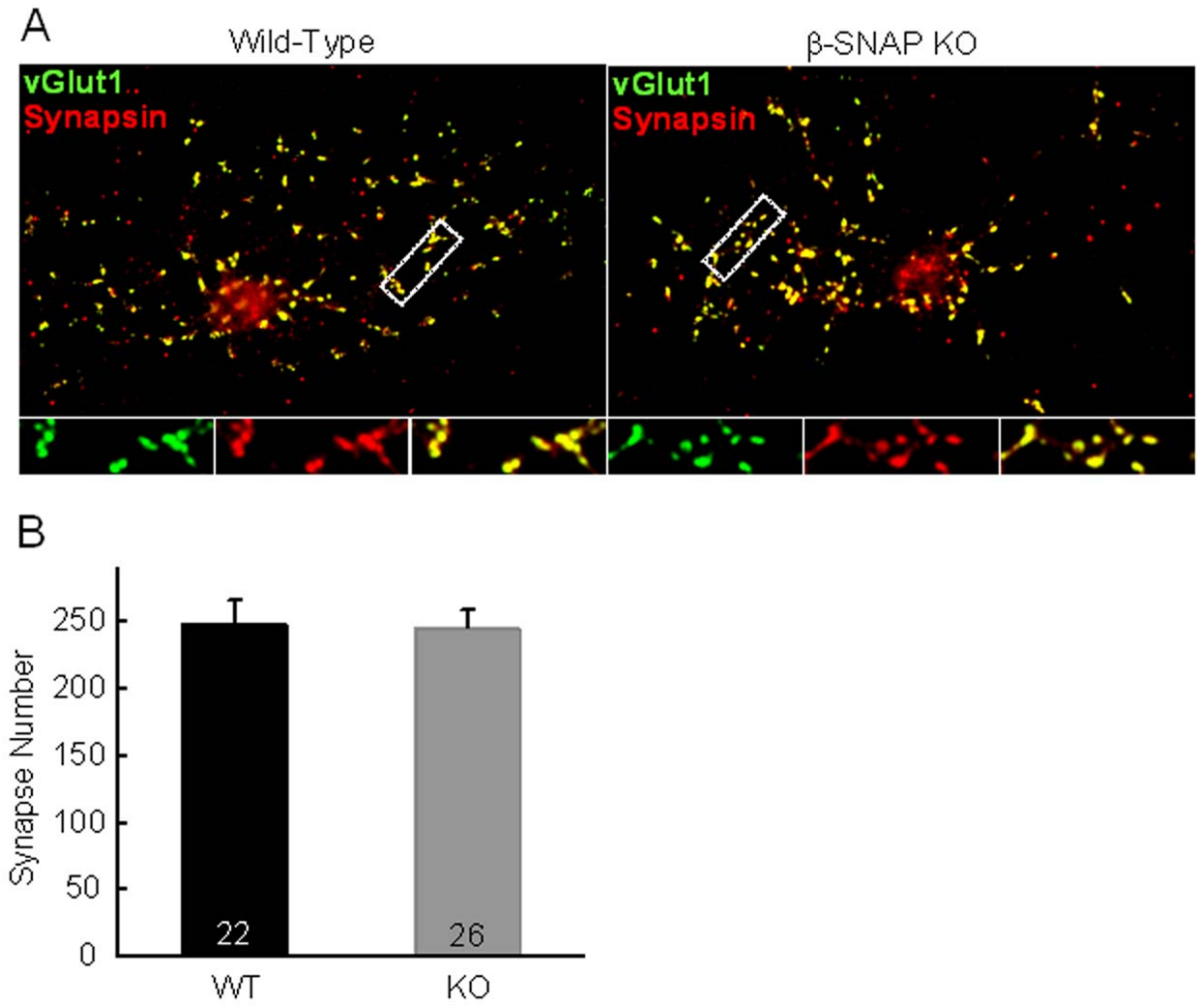

Figure 9 **Normal Synapse Density in β-SNAP Deficient Neurons.** (A) Example of immunofluorescence staining of autaptic neurons. Single glutamatergic boutons were identified by co-staining for the presynaptic markers vGluT-1 (green) and Synapsin (red). Insets show a magnification of the marked section (white box) in each neuron. (B) Total number of co-labeled puncta per neuron. No differences were observed between β-SNAP deficient and wild-type neurons. Numbers in bars indicate the number of cells analysed. Error bars indicate standard error of the mean.

For this purpose, I dissected P0 hippocampi from β-SNAP and wild-type control brains and cultured hippocampal neurons on astrocytes islands (1.4). Mutant cells grew very well in culture and were indistinguishable from control wild-type neurons as assessed by light microscopic observation. Neurons were fixed at DIV11-13. Single glutamatergic boutons were identified by co-staining for the presynaptic markers vGluT-1 and Synaptophysin (Fig. 9A). The total number of co-labeled puncta were counted for each isolated neuron. No differences were observed between β-SNAP deficient and wild-type neurons (Fig. 9B). These data indicate that both β-SNAP deficient and wild-type neurons form the same number of morphologically identified glutamatergic synapses in the autaptic culture system. β-SNAP is thus not required for synapse formation and maintenance.

3.2.3 Increase in High Molecular Weight (HMW) Neuronal SNARE Complexes in β-SNAP Deficient Brains

It is well established that the NSF/SNAP machinery is required *in vivo* for disassembling "spent" post-fusion *cis*-SNARE complexes, thus mediating the regeneration of "active" free SNAREs which are essential to support further membrane fusion reactions (Martin et al., 2006, Jahn and Scheller, 2006). The activity of the disassembly machinery is high in cells due to the high abundance of its components and to the high specific activity of NSF (Lang et al., 2002; Jahn and Scheller, 2006), and SNAREs are constantly maintained in a dissociated "active" state by NSF and SNAPs. Only experimental manipulations, which limit, impair or block the activity of the disassembly machinery, result in an accumulation of SNARE complexes (Lang et al., 2002). Given that β-SNAP deficiency might constitute such a manipulation, I measured the ratio of SNARE complexes to free neuronal SNAREs in β-SNAP deficient brains.

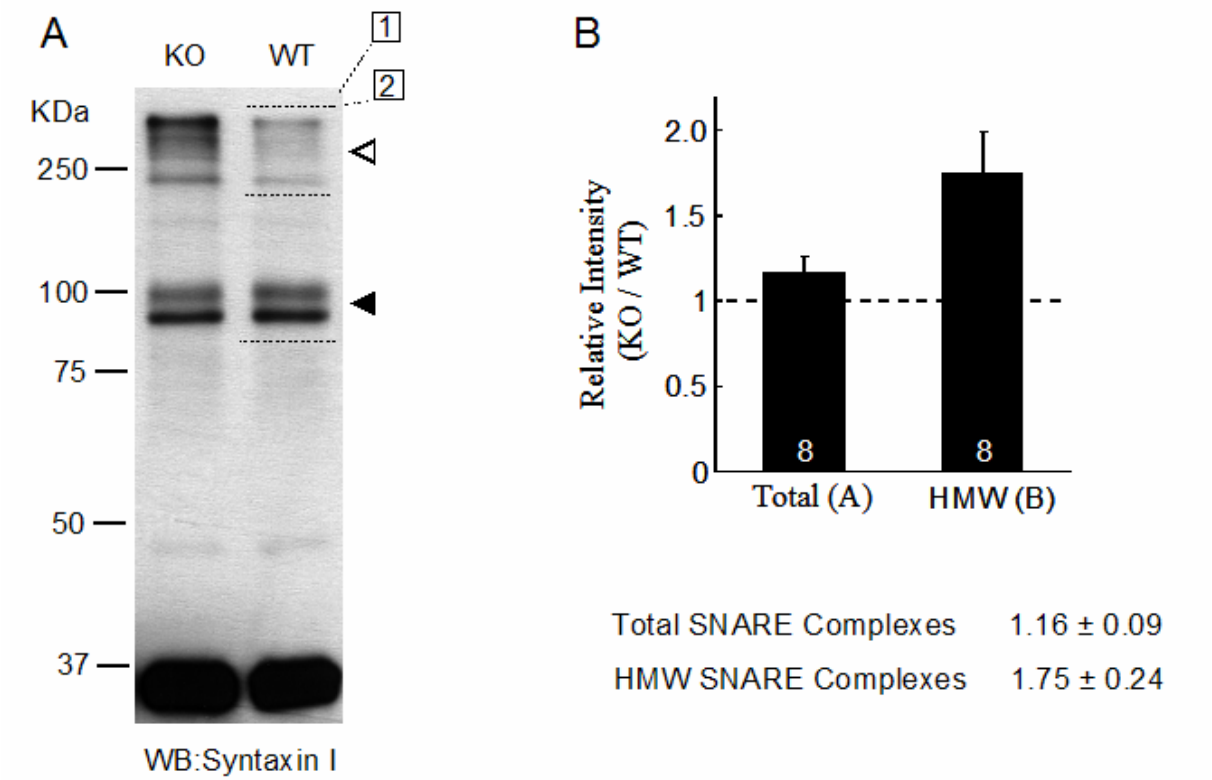

Figure 10 **Increase in High Molecular Weight Neuronal SNARE Complexes in β-SNAP Deficient Brains.** (A) Representative Western blot for the t-SNARE Syntaxin-1 in unboiled whole-brain homogenates from wild-type and β-SNAP knock-out mice. In addition to a band at the expected molecular weight of monomeric SNARE complexes (filled arrowhead), additional bands at higher molecular weights were identified (open arrowhead), which are generally attributed to oligomeric structures defined as high molecular weight (HMW) SNARE complexes. Dotted insets show blot areas used for quantification of total (1) and HMW (2) complexes. (B) Densitometric quantification of ECL signals for total and HMW SNARE complexes showed a selective increase in Syntaxin-1 containing HMW complexes in β-SNAP deficient brains as compared to wild-type controls, while total SNARE complexes were not significantly altered. Numbers in the bars indicate the number of independent experiments. Error bars indicate standard error of the mean.

To carry out this analysis I took advantage of the high stability of SNARE complexes, which are known to be resistant to disruption by the denaturing detergent SDS (Hayashi et al., 1994). To visualize these complexes in brain extracts, I performed a Western blot analysis for the t-SNARE Syntaxin-1 (Fig. 10A). This method has been used extensively for mouse brains and Drosophila head extracts (Otto et al., 1997; Xu et al., 2001; Sanyal et al., 2001; Tolar et al., 1998). SNARE complexes do not form in the presence of 1-2% SDS. Therefore, complexes present in SDS tissue extracts only reflect the amount present at the time of solubilization. By

using this Western blot approach I could detect a major band at the expected molecular weight (MW) of the free Syntaxin-1 monomer (37 kDa, Fig. 10A). In addition, several bands were visible at or above 80 kDa, i.e. one band around 80 kDa, probably corresponding to the neuronal SNARE complex whose calculated MW is 77 kDa (filled arrowhead), and additinal bands at even higher molecular weights (HMW, open arrowhead), which have been described in several other studies (Fasshauer et al., 1998; Poireer et al., 1998; Laage et al., 2000) and were proposed to reflect multimeric Syntaxin-1-containing SNARE complexes. Interestingly, a comparative analysis revealed a clear and highly reproducible increase in Syntaxin-1 containing HMW complexes in β-SNAP deficient brains as compared to wild-type controls, while both Syntaxin-1 levels and total SNARE complexes were not significantly altered (Fig.10B).

3.2.4 The Abundance of 20S Complexes is Decreased in β-SNAP Deficient Brains

The SNARE complex disassembly reaction mediated by the ubiquitous NSF/α-SNAP machinery has been studied extensively *in vitro* and *in vivo*, and the sequential biochemical equilibria which describe this reaction at the molecular level have been modeled (Fig. 3). The reaction is thought to proceed with the assembly of a multimeric protein complex (named 20S) which contains NSF, α-SNAP and the SNARE complex in a stochiometry of 1:3:1, respectively (Wimmer et al., 2001). However, the exact molecular composition of the 20S complex in brain, where in addition to α-SNAP also the β-SNAP isoform is present, is still unknown. This 20S complex can be stabilised by blocking the ATP-hydrolysing activity of NSF (e.g. with buffers containing ATPγS or ATP/EDTA) and isolated from biological samples. Therefore, I sought to analyse the composition of the 20S complex in wild-type brains, and to compare it to the 20S complex isolated from β-SNAP deficient brains. I expected this comparative analysis to be useful in order to reveal possible molecular alterations of the 20S complex in β-SNAP deficient brains.

As was shown by several pioneer studies in the field, the 20S complex can be isolated by gradient ultracentrifugation (Wilson et al., 1992; Wimmer et al., 2001). As the name indicates, the NSF-SNAP-SNARE complex has a sedimentation coefficient of about 20 S. Although this centrifugation method has been proven to be quite

reproducible and has been used successfully by several groups, it is rather laborious and requires a relative large protein sample. In recent years, an alternative method has been developed to study 20S complexes, which consists of an immunopurification of the complex from solubilized brain extracts with an anti-Syntaxin-1 antibody (McMahon et al., 1995; Chandra et al., 2005). I used this immunopurification method for my analysis. The results of these experiments are shown in Fig. 11.

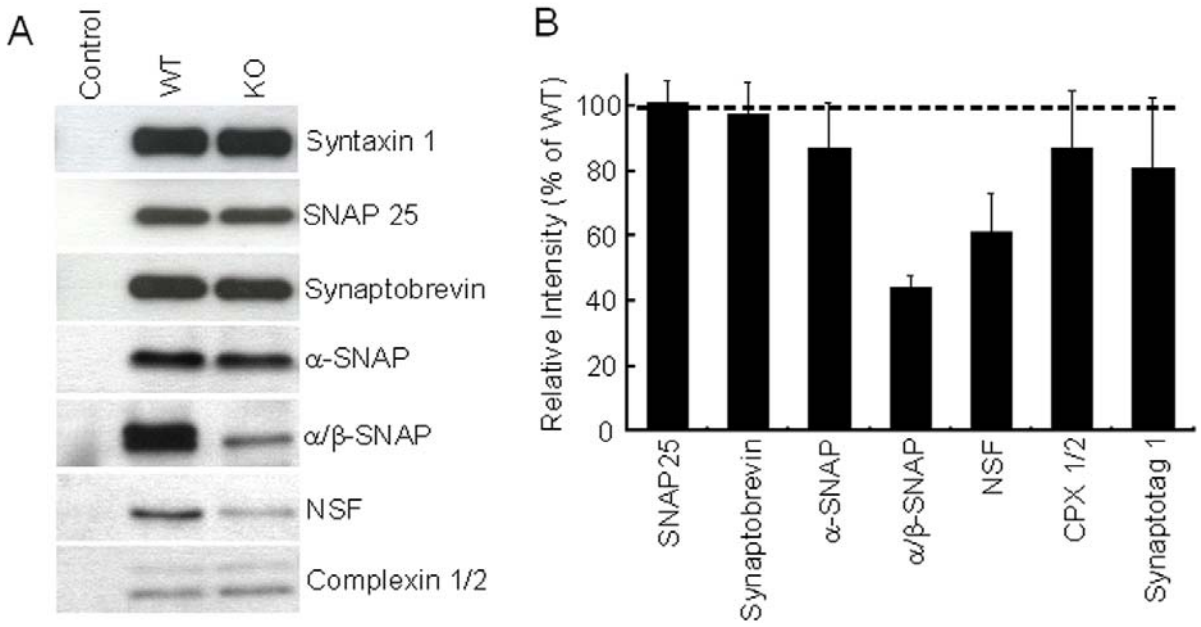

Figure 11 **Abundance of Neuronal 20S Complexes is Decreased in β-SNAP deficient brains.** (A) Representative Western blots of fractions immunoprecipitated with an anti-Syntaxin-1 antibody and analysed for the presence of components of the 20S complex: Syntaxin-1, SNAP-25, Synaptobrevin, α/β-SNAP and NSF. Complexins, which are SNARE complex associated proteins, were also analysed. (B) Relative densitometric quantification of ECL signals for components of the 20S complex and the SNARE complex associated proteins Complexin-1/2 and Synaptotagmin-1 in β-SNAP deficient samples. The comparative analyses showed that in β-SNAP deficient brains the 20S complex abundance was decreased by ~50% (N=4). Quantification of SNAP levels was done with the monoclonal antibody 77.2 (Synaptic Systems), which recognises both isoforms with the same affinity (data not shown). Quantification is expressed as % of wild-type controls. Error bars indicate standard error of the mean.

I tested the immunoprecipitated fractions by Western Blotting for the presence of the components of the 20S complex, and compared their amount in β-SNAP deficient

and wild-type control samples. Syntaxin-1 was immunoprecipitated very efficiently from both mutant and wild-type extracts (Fig. 11 and data not shown). From both wild-type and β-SNAP deficient brain extracts similar amounts of SNAP-25 and Synaptobrevin-2 were co-immuonprecipitated with Syntaxin-1 (Fig. 11A). In the wild-type sample both α- and β-SNAP were identified, while in the β-SNAP deficient sample only α-SNAP was present. The total amount of α/β-SNAP was reduced of ~50% in β-SNAP deficient samples (Fig. 11B). Importantly, the amount of co-immunoprecipitated α-SNAP did not change in the absence of β-SNAP. As expected, the reduction in total SNAP levels was paralleled by a similar ~50% reduction in coimmunoprecipitated NSF (Fig. 11B). The total amount of Complexins and Synaptotagmin-1, which were also co-immunoprecipitated with Syntaxin-1, were unchanged (Fig. 11B).

Above data represent the first indication that in wild-type brains 20S complexes contain both α- and β-SNAP. In my assay it was unfortunately not possible to discriminate whether both isoforms are part of the same 20S complex or whether each isoform is part of distinct α- and β-SNAP containing 20S complexes. The comparative analyses showed that in β-SNAP deficient brains the 20S complex abundance is decreased by ~50%. This finding can be explained by the absence of the β-SNAP isoform, which reduces the total SNAP pool by approximately 50%.

3.2.5 Glutamatergic Synaptic Transmission is Not Impaired in Autaptic β-SNAP Deficient Hippocampal Neurons

My data on the subcellular distribution of the β-SNAP isoform and other published data (Puschel et al., 1994; Nishiki et al., 2001) indicate that the β-SNAP isoform, like α-SNAP, is localized in the cytosol and moderately enriched at synaptic sites in neurons. Moreover, my data on mRNA expression showed that the β-SNAP protein is expressed throughout the hippocampus (Fig. 5), even though a previous immunohistochemical study did not detect any β-SNAP in cell bodies of the CA1 and CA2 fields in the rat hippocampus (Nishiki et al., 2001). The main experimental system I used to characterise synaptic phenotypes of SNAP deficient neurons electrophysiologically was the single cell autaptic culture system (Bekkers and Stevens 1991).

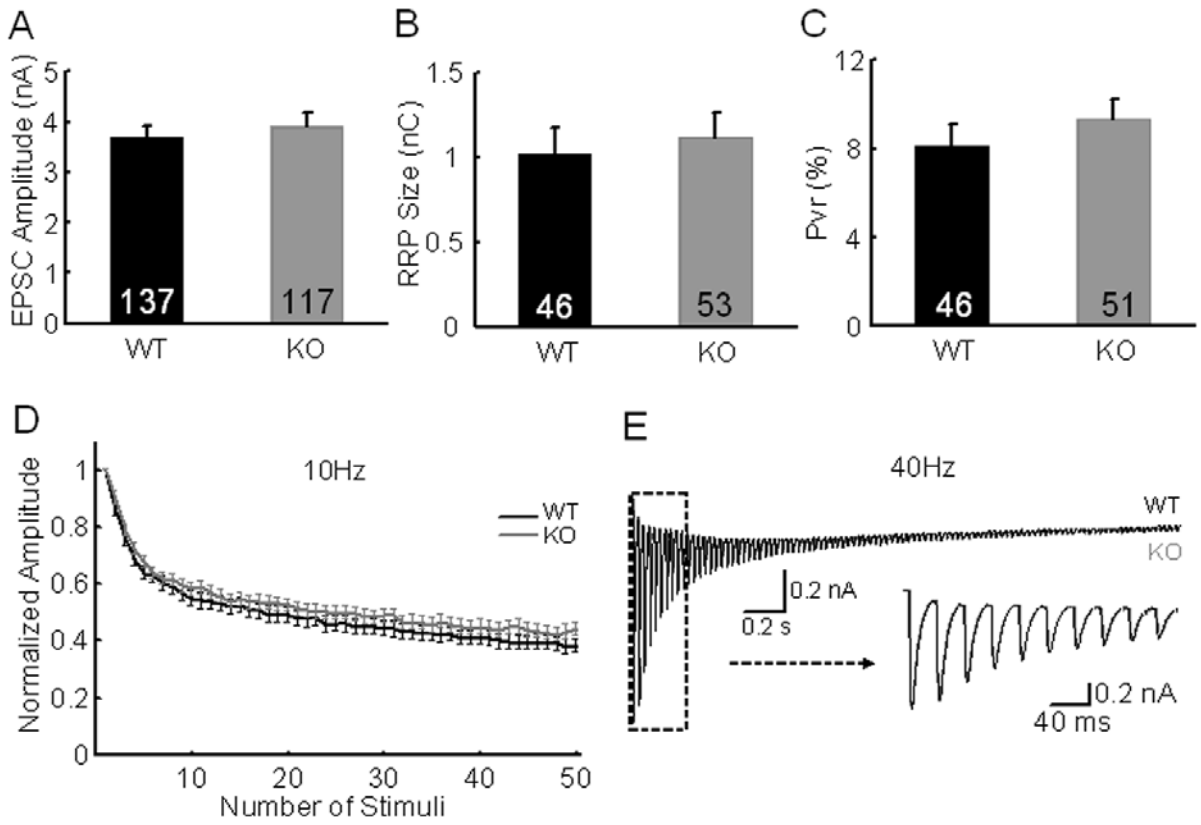

Figure 12 **Glutamatergic Synaptic Transmission is Not Impaired in β-SNAP Deficient Hippocampal Neurons.** To examine the functional consequences of the genetic deletion of the β-SNAP isoform, glutamatergic synaptic transmission was analysed in cultured hippocampal autaptic neurons. None of the tested parameters was found to be different between β-SNAP deficient and wild-type cells. The following parameters were analysed: (A) Mean EPSC amplitudes in wild-type (black) and β-SNAP deficient cells (grey); (B) mean RRP size estimated by the charge integral measured after release induced by application of 0.5 M sucrose solution; (C) mean vesicular release probability (P_{vr}), calculated by dividing the charge transfer during single EPSCs by the charge transfer measured during RRP release; (D) normalised EPSC depression during 10 Hz stimulation (WT, n=59; KO, n=60); (E) normalized average of continuous EPSC traces during 40 Hz stimulation. The inset in (E) shows a magnification of the marked section (box) of the overlapping cumulative traces (WT, n=100; KO, n=100). Numbers in the bars indicate the number of cells tested. Error bars indicate standard error of the mean.

This synaptic model system is uniquely suitable for determining key parameters underlying synaptic transmission. As all synapses originate from a single axon, different synaptic release modes can be quantified (evoked release by action potential or hypertonic solution, and spontaneous release). To examine the functional

consequences of the genetic deletion of the β-SNAP isoform, I studied glutamatergic synaptic transmission in cultured hippocampal autaptic neurons. This first part of the study was focused on glutamatergic neurons, which represent the most common neuron type in the mammalian brain. Glutamatergic transmission alone in fact accounts for ~80% of the total synaptic transmission in the brain. Moreover, glutamatergic neurons are by far the most extensively studied and characterized neuronal cell type in the brain, since they are the major contributors to information transfer and storage in the brain (Malenka and Bear, 2004). On the other hand, inhibitory GABAergic neurons, which are the second most frequent neuronal cell types in mammalian brain, are mainly responsible for local modulatory processes in neuronal networks (Jonas et al., 2004). They are less well characterized and highly heterogeneous. Indeed, a general classification of the subtypes of GABAergic neurons is still lacking (Yuste, 2005).

Autaptic responses were evoked by brief somatic depolarizations (2 ms). This stimulation generated an unclamped action potential, which was followed by an excitatory postsynaptic current (EPSC) with a delay of 2-4 ms. No differences in the amplitudes of evoked EPSCs were found between β-SNAP deficient and wild-type control neurons (Fig. 12A). A brief application of a hyperosmotic solution (0.5 M sucrose) has been widely used to deplete the primed vesicles of the readily releasable pool (RRP) (Stevens and Tsujimoto, 1995; Rosenmund and Stevens, 1996). The charge being transferred during the application can be taken as an estimate of the RRP. β-SNAP deficient neurons showed a similar response to hypertonic sucrose application as compared to wild-type control cells, indicating that the size of the RRP is unchanged in mutant cells (Fig. 12B). As a direct consequence of these data, the vesicular release probability (P_{vr}), which represents the fraction of the RRP being released by one single action potential stimulation, was also unchanged in β-SNAP deficient neurons (P_{vr} is calculated by the ratio of the EPSC charge over the sucrose charge) (Fig. 12C).

I next analysed short term synaptic plasticity in β-SNAP deficient neurons. I delivered one stimulation train consisting of 50 stimuli at 10 Hz. Under these stimulation conditions hippocampal synapses undergo short-term depression of evoked EPSCs, a phenomenon that is presynaptic in nature and has been correlated to RRP size, RRP refilling rates and P_{vr} (Liley and North, 1953; Dittmar and Regher, 1998; Junge et al., 2004). I analysed the extent and time course of depression of

evoked EPSCs. Both β-SNAP deficient and wild-type control neurons showed a similar pattern of depression (Fig. 12D), confirming that both RRP and P_{vr} were very similar in the two genotypes. Furthermore, RRP refilling during the stimulation train seemed not to be impaired since the extent of depression was not changed in β-SNAP deficient neurons.

There are two major types of neurotransmitter release, phasic release induced by single action potentials, and tonic release, which appears during high frequency trains. Stimulation at 10 Hz frequency is inefficient to trigger significant amounts of tonic release during the stimulation train. Therefore, to analyse this component of release, I delivered 100 stimuli at 40 Hz. This stimulation is also known to deplete the RRP, allowing to estimate the time course of pool depletion (Rosenmund et al., 1996; Rhee et al., 2002). As shown by the averaged cumulative 40 Hz traces in Fig. 12E, I found no difference between β-SNAP deficient and wild type neurons with regard to the time course of EPSC depression and the amount of tonic release elicited by the train.

Taken together, these data indicate that basic synaptic transmission and short-term synaptic plasticity are not altered in β-SNAP deficient glutamatergic hippocampal neurons.

3.3 HYH Mutant Mice

3.3.1 Glutamatergic Synaptic Transmission is Not Impaired in HYH Mutant Hippocampal Neurons

HYH mice suffer from progressive hydrocephalus, and already at birth (P0) they present drastic alterations of brain morphology. The hippocampus is smaller and malformed as compared to wild-type control littermates (Chae et al., 2004; Batiz et al., 2006). Since my aim was, like for β-SNAP deficient neurons, to analyse glutamatergic synaptic transmission of HYH mutant neurons, I cultured hippocampal neurons from P0 HYH mutant animals. By observation at the moment of dissection, hippocampi from HYH mice looked much smaller and malformed as compared to controls. Despite the obvious anatomical malformation of the hippocampi, dissociated HYH neurons grew very well in culture and, based on light microscopic observation, they were indistinguishable from control wild-type neurons. Using whole-cell

recordings of isolated cultured neurons I measured the whole-cell capacitance of mutant neurons (C_m). C_m can be used as an estimate for the size of the voltage clamped region of the neuron, which corresponds approximately to the neuronal cell body and proximal dendrites (Chitwood et al., 1999). HYH and control neurons showed very similar C_m values (Wild Type, 49.0 ± 2.3 pF, n = 22; HYH, 53.2 ± 3.3 pF, n = 19). To indirectly assess the size of the dendritic tree of cultured neurons, I applied kainate to single autaptic neurons and measured the amplitude of the recorded postsynaptic current. Kainate is known to activate the surface-expressed pool of AMPA and kainate receptors. The surface expression of these receptors is developmentally regulated, and the total surface fraction is a reflection of both the developmental stage and the size of the dendritic tree of the neuron. The current response to kainate application was not changed in HYH mutant cells as compared to wild-type neurons (wild-type, 206 ± 44 pA, n = 25; HYH, 198 ± 37 pA, n = 23). Taken together, these data indicate that despite malformations of the hippocampus, dissociated HYH hippocampal neurons are morphologically indistinguishable from wild-type control neurons in the autaptic system.

I next analysed glutamatergic synaptic transmission in cultured autaptic hippocampal HYH neurons. Like for the analysis of β-SNAP deficient neurons, I analysed both basic synaptic transmission and short-term synaptic plasticity during high frequency stimulations (HFS) (Fig. 13). None of the measured basic parameters (evoked EPSC amplitudes, hypertonic sucrose charge, P_{vr}) nor the time course of EPSC depression during high frequency stimulation were changed in HYH mutant neurons. Notably, also the amount of tonic release elicited during 40 Hz stimulation train was unaltered (Fig. 13E). Thus, glutamatergic synaptic transmission of cultured autaptic hippocampal neurons is not affected by the HYH mutation of α-SNAP.

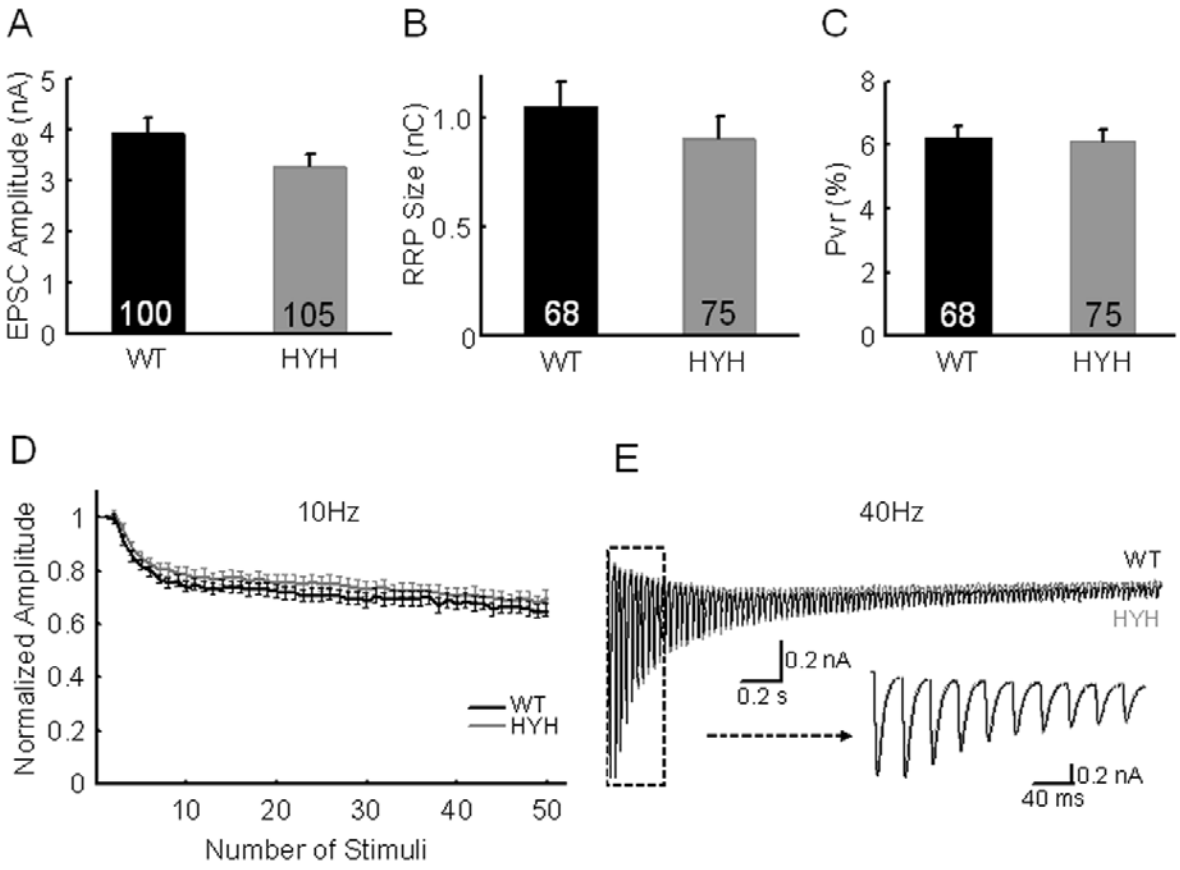

Figure 13 **Glutamatergic Synaptic Transmission is Not Impaired in HYH Mutant Hippocampal Neurons.** To examine the functional consequences of the spontaneous HYH mutation of α-SNAP, glutamatergic synaptic transmission was analysed in cultured hippocampal autaptic neurons. None of the tested parameters were found to be different between HYH mutant and wild-type cells. The following parameters were analysed: (A) Mean EPSC amplitudes in wild-type (black) and HYH mutant cells (grey), (B) mean RRP size estimated by the charge integral measured after release induced by application of 0.5 M sucrose solution, (C) mean vesicular release probability (P_{vr}), calculated by dividing the charge transfer during single EPSCs by the charge transfer measured during RRP release, (D) normalised EPSC depression during 10 Hz stimulation (WT, n = 71; HYH, n = 86), (E) normalized average of continuous EPSC traces during 40 Hz stimulation. The inset shows a magnification of the marked section (white box) of the overlapping cumulative traces (WT, n = 54; HYH, n = 51). Numbers in the bars indicate the number of cells measured. Error bars indicate standard error of the mean.

3.4 SNAP Double Mutant Mice

α- and β-SNAP show very high sequence identity (83% identical amino acids), and were postulated to be functionally equivalent *in vivo* (Suldow et al., 1996). In line with this hypothesis, my results showed that both isoforms were able to be incorporated into and to disassemble reconstituted 20S complexes *in vitro*. No evidence was found for differential interaction partners of α- and β-SNAP by Yeast Two-Hybrid screening (Martin et al., 2006) and by biochemical binding assays (Fig.7). My data thus support the hypothesis of a possible functional equivalence between α- and β-SNAP.

If α- and β-SNAP are indeed functionally equivalent, the lack of an obvious electrophysiological phenotype in β-SNAP deficient or HYH mutant glutamatergic neurons could be due to redundancy by α-SNAP. Removal of or reductions in the expression levels of compensatorily active isoforms is a valid and useful strategy to unmasking the functional role of a given protein (see for example Schlüter et al., 2004; Varoqueaux et al., 2006; Reim et al., 2004; Jockusch et al., 2007). To achieve this in the present study, I crossed β-SNAP deletion mutant mice with the HYH α-SNAP mutants. HYH mice were previously shown to display a 50% decrease in α-SNAP levels (Chae et al., 2004; Hong et al., 2004). As shown in the representative blot in Fig. 15C, crossing of the two mutations indeed resulted in a strong decrease in total SNAP levels (for quantification see Fig. 15B).

I crossed heterozygous β-SNAP/HYH mutant mice and analysed the phenotype of the offspring littermates. Both homozygous single mutants are alive at birth and indistinguishable from wild-type littermates at least during the first postnatal week. On the other hand, all homozygous β-SNAP/HYH double mutants observed so far were found dead at birth. Therefore, double mutant animals between 17 and 19 days of embryonic development (E17-E19) were analysed. At this developmental stage, double mutant mice were reacting to stimuli and showed no sign of obvious impairment. As controls, β-SNAP$^{+/+}$/α-SNAP$^{HYH/+}$ or β-SNAP$^{+/+}$/α-SNAP$^{+/+}$ animals were used.

3.4.1 Unaltered Morphology, Cytoarchitecture and Protein Composition of SNAP Double Mutant Cultured Hippocampal Neurons

I cultured hippocampal neurons from E17-E19 double mutant animals. Upon observation at the moment of dissection, double mutant brains showed all the neuropathological features of HYH brains. Cerebral hemispheres were smaller and displaced dorsally, and the dorsal midline structure was enlarged and evident between the displaced hemispheres (Chae et al., 2004). Like for HYH mice, hippocampi from double mutant mice were also much smaller and malformed compared to control littermates. Despite the neuroanatomical brain malformations, SNAP double mutant neurons grew very well in culture (both continental and autaptic) and, by light microscopic observation, were indistinguishable from control neurons.

As described for HYH cultured neurons, I measured whole-membrane capacitance (C_m) and current responses to the application of kainate in double mutant neurons in order to detect gross changes in cell size. None these parameters revealed a difference between SNAP double mutant and control neurons (Fig. 18D; C_m, Ctrl, 57.89 ± 1.94 Unit; DMut, 62.92 ± 2.17 Unit; n Ctrl = 110; n DMut = 92). In addition, I analysed dendritic morphology by determining the dendrite branching index, which is defined as the ratio between the number of dendritic tips and the number of primary dendrites emerging from the cell body (Danzer et al., 2002; Cheung et al., 2007). For this purpose, cultured autaptic neurons were stained for the dendritic marker MAP2 (Fig. 14B-C) and primary dendrites and dendrite tips were counted. I found no statistically significant differences in the branching index (Fig. 14C) or in the number of primary dendrites (Control = 6.00, n = 36; Double mutant = 6.02, n = 21) between double mutant and control neurons. Based on these experiments, it can be concluded that cell size and overall dendrite length and branching are not affected by the HYH and β-SNAP deletion mutations.

I next analysed the protein composition of cultured hippocampal double mutant neurons (DIV17-21). The levels of several candidate proteins were analysed by Western blotting (Fig. 15).

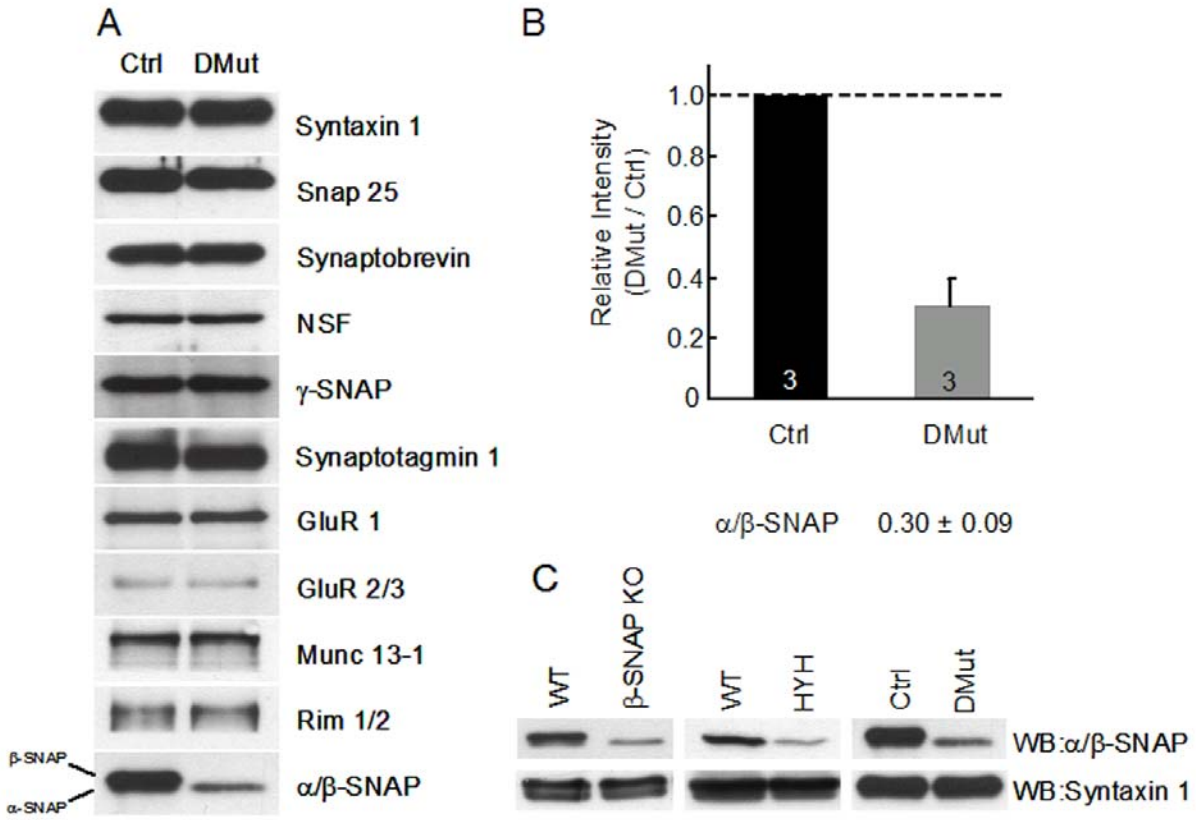

Figure 14 **Normal Protein Composition in SNAP Double Mutant Cultured Hippocampal Neurons**. (A) Expression levels of candidate proteins in double mutant (DMut) and control (ctrl) cultured hippocampal neurons were analysed by Enhanced Chemiluminescence. I found no obvious changes in total levels for any of the markers tested, except of SNAPs. (B) Densitometric quantification of ECL signals for total SNAP levels, detected with a monoclonal antibody, which recognises both isoforms with the same affinity. SNAP levels were reduced in double mutant neurons to ~30% of control levels. Numbers in the bars indicate the number of independent experiments. Error bars indicate standard error of the mean. (C) Representative Western blot showing SNAP levels in β-SNAP deficient, HYH and SNAP double mutants compared to controls (whole-brain homogenates for β-SNAP KO and HYH; cultured hippocampal neurons for SNAP double mutant). Western blotting for Syntaxin-1 is also shown as a loading control. Crossing β-SNAP deletion with HYH mice indeed resulted in a further decrease in SNAP levels as compared to single mutants.

I found no obvious change in the levels of any of the markers tested. On the other hand, total SNAP levels (as determined with a monoclonal antibody which recognises both isoforms with the same affinity, see Fig. 11A-B) were reduced in double mutant neurons to ~30% of control levels (Fig. 15A-B). This is consistent with previously

published work, which showed that α-SNAP levels are decreased to ~50% in HYH mice (Chae et al., 2004; Hong et al., 2004).

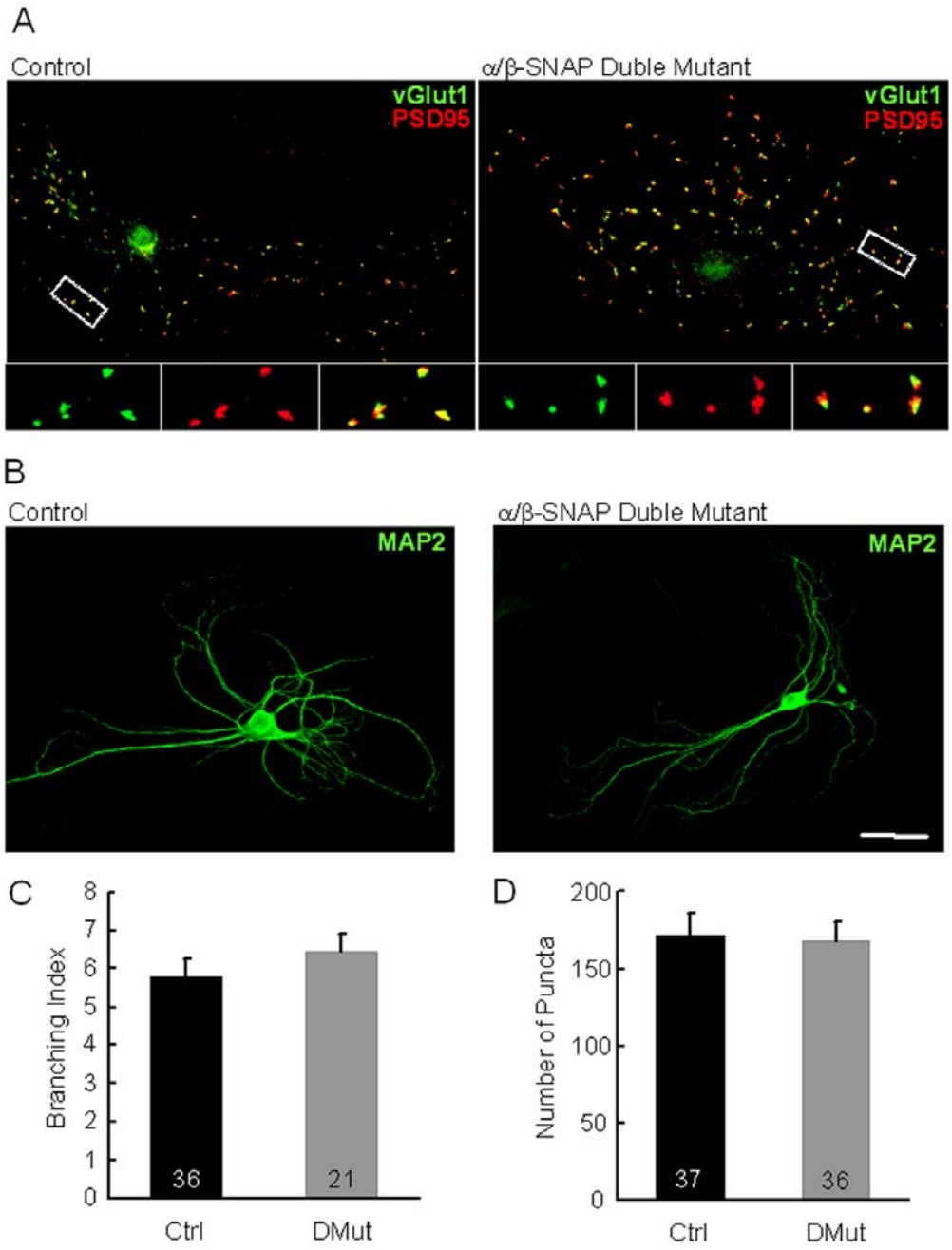

Figure 15 **Normal Morphology and Synapse Density in SNAP Double Mutant Cultured Hippocampal Neurons.** (A) Example of fluorescence staining of autaptic neurons. Single glutamatergic boutons were identified by co-staining for the presynaptic markers vGluT-1 (green) and PSD95 (red). Insets show a magnification of the marked section (white box) in each neuron. (B) Representative dendrite morphology in double mutant and control neurons, analysed with MAP2 staining (green). (C) The number of distal dendritic tips and proximal dendrites were counted, and the branching Index, defined as the ratio of number

of dendritic tips per number of primary dendrites, was calculated. No difference was found between double mutant and control neurons, indicating that dendrite branching was normal in double mutant neurons. (D) Total co-labeled vGluT-1/PSD95 puncta for each isolated neuron were counted. No differences were observed between double mutant and control neurons. Numbers in the bars indicate the number of cells. Error bars indicate standard error of the mean.

In order to characterize the synaptic phenotype of double mutant neurons in more detail, I imaged and quantified glutamatergic synapses at the light microscopical level in single isolated neurons (DIV 11-15) (Fig. 14A-D). Single glutamatergic synapses were identified by co-staining for the presynaptic marker vGluT-1 and the postsynaptic marker PSD95. Typical co-labelled synaptic puncta, where pre- and postsynaptic markers showed partial overlap (inset Fig. 14A), were counted. I did not find any difference in the total number of morphologically identified synapses between double mutant and control neurons (Fig. 14D).

Taken together, above results indicate that double mutant neurons develop normally in culture. Overall morphology, dendritic branching and extension, protein composition and total number of morphologically identified synapses are not affected by the HYH/β-SNAP double mutation.

3.4.2 Neuronal SNARE Complexes Accumulate in SNAP Double Mutant Embryonic Brain

As for the β-SNAP deletion mutant mouse, I also analysed the neuronal SNARE complex in double mutant mice. Because of the perinatal lethality of the double mutant mouse, I carried out this analysis on E17-E19 brains (Fig. 16). Many synaptic proteins are expressed at relatively low levels in late embryonic and newborn brains (Lou and Bixby, 1993, 1995; Daly and Ziff, 1997).

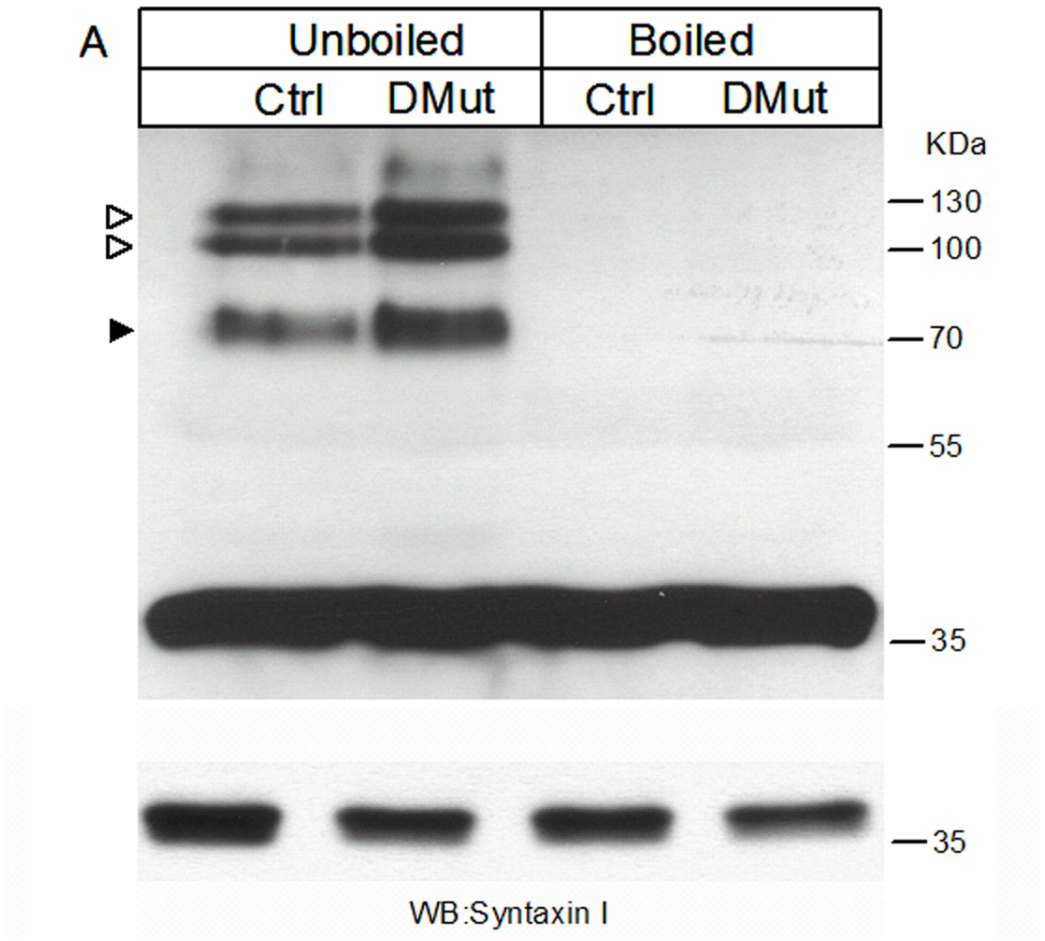

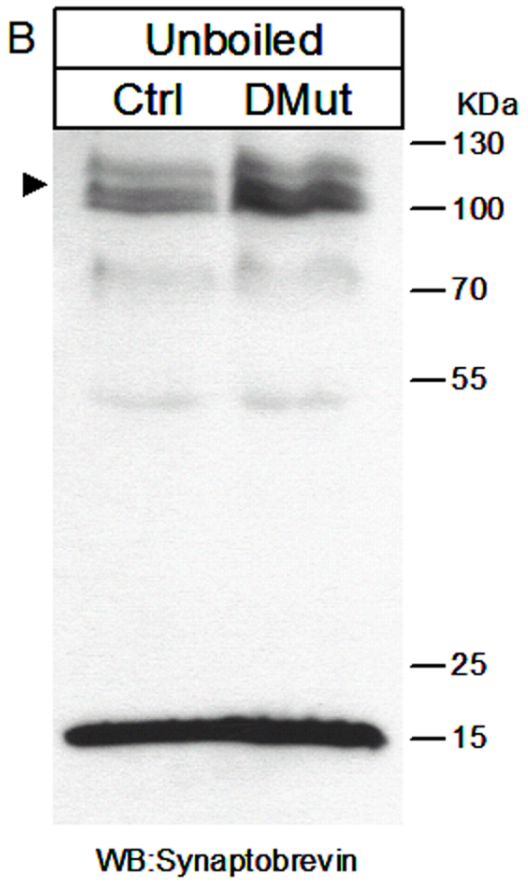

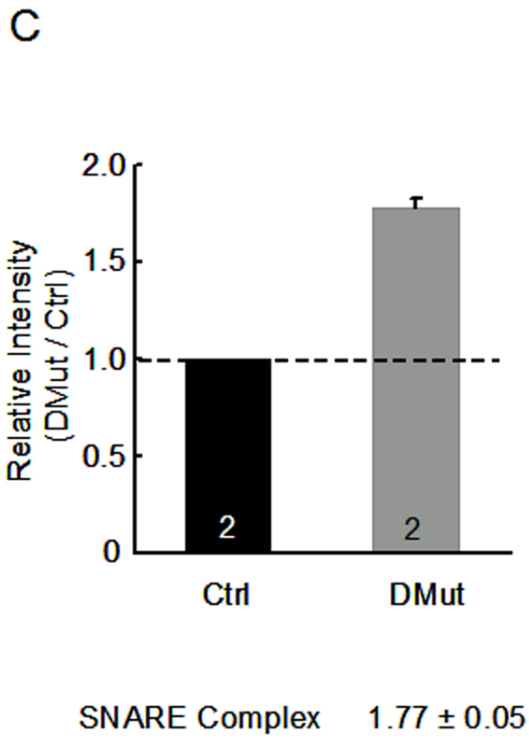

SNARE Complex 1.77 ± 0.05

Figure 16 **Neuronal SNARE Complexes Accumulate in SNAP Double Mutant Embryonic Brains.** (A) Representative Western blot analysis for the t-SNARE Syntaxin-1 of unboiled and boiled whole-brain homogenates from double mutant and control mice. In addition to a band at the expected molecular weight for monomeric SNARE complexes (filled arrowhead), additional bands at higher molecular weights were identified (empty arrows), probably representing High Molecular Weight (HMW) SNARE complexes. Compared to controls, double mutant brains showed a drastic increase in the amount of both SNARE core- and HMW-complexes. The lower panel shows a shorter exposure for monomeric Syntaxin-1. (B) Western blotting for Synaptobrevin was performed on unboiled brain homogenates from double mutant and control neurons to confirm that the signals observed with an anti-Syntaxin-1 antibody indeed arose from SNARE complexes. The representative blot shows the presence of reactive bands in the high molecular weight range, whose intensity was increased in the double mutant sample. This experiment indicates that the Syntaxin-1 immunoreactive bands in (A) indeed represent heteromeric SNARE complexes. (C) Densitometric quantification of ECL signals for total SNARE complexes showed a selective increase in double mutant compared to control brains. Numbers in the bars indicate the number of independent experiments. Error bars indicate standard error of the mean.

By 5-fold up-scaling of the total amount of sample employed in the Western blotting experiment, I was able to identify several Syntaxin-1 immunoreactive bands in the molecular weight range of 70-200 Kda, which selectively disappeared after boiling the samples (Fig. 16A). SNARE complexes are stable in the presence of 1-2%SDS, but readily and irreversibly disassembled if boiling occurs (Otto et al., 1997). Boiled samples showed only one immunoreactive band around 37 kDa, the expected molecular weight of the Syntaxin-1 monomer (Fig. 16A). In unboiled samples, like for β-SNAP deficient brains, one band around 70/80 kDa was identified, probably corresponding to the neuronal SNARE core complex (calculated molecular weight 77 kDa) (Fig. 16A, full arrow). HMW complexes were also detected above 100 kDa, with two prominent and one minor band (Fig. 16A, open arrowheads). Compared to control samples, double mutant brains showed a drastic increase in the amount of both SNARE core and HMW complexes (total SNARE complexes were increased to 1.77 ± 0.05 of control levels, see Fig.16C) while total Syntaxin-1 levels were not significantly changed (Fig. 16C). Importantly, the same immunoreactive band pattern was found by Western blotting for Synaptobrevin-2, a component of the neuronal SNARE complex, indicating that the Syntaxin-1 immunoreactive bands I quantified in

the previous experiment were indeed representing heteromeric SNARE complexes (Fig. 16B, full arrow).

In conclusion, double mutant embryonic brains showed a ~80% increase in total SNARE complex abundance as compared to control littermate samples.

3.4.3 Electrophysiological Analysis of Glutamatergic Synaptic Transmission in Cultured Autaptic Double Mutant Hippocampal Neurons

3.4.3.1 Evoked and Spontaneous Synaptic Transmission

To test for a functional redundancy of α- and β-SNAP, I analysed glutamatergic synaptic transmission of double mutant autaptic neurons, where in addition to the absence of the β-SNAP isoform also α-SNAP expression is strongly reduced, leading to a ~70% decrease in total SNAP levels (Fig. 15B).

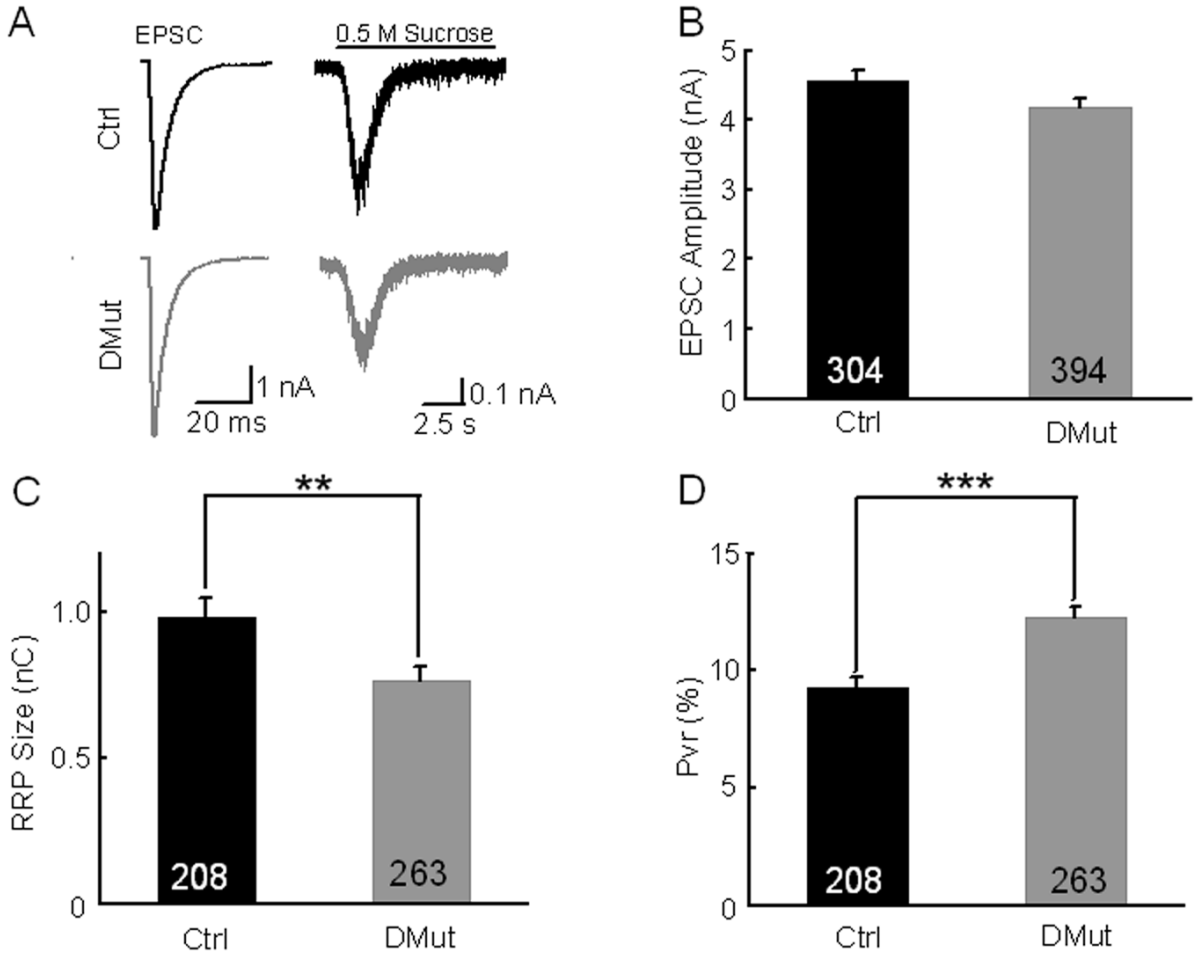

Figure 17 **Evoked Glutamatergic Synaptic Transmission in Autaptic Double-Mutant Neurons: Smaller RRP and Increased P_{vr}.** To determine the functional effects of a ~70% reduction in total SNAP levels, I analysed glutamatergic transmission in autaptic hippocampal neurons. The results indicate that, while evoked EPSCs in double mutant neurons were not significantly different from control neurons, the RRP size was significantly smaller (~25%) and P_{vr} was ~30% higher in double mutant neurons. (A) EPSC traces (left panel) and release induced by the application of 0.5 M sucrose solution for 9 s (right panel) in control (black) and double mutant (grey) neurons. (B) Mean EPSC amplitudes in control (black) and double mutant cells (grey). (C) Mean RRP size estimated by the charge integral measured after release induced by application of 0.5 M sucrose solution. (D) Mean P_{vr}, calculated by dividing the charge transfer during single EPSCs by the charge transfer measured during RRP release. Numbers in the bars indicate the number of cells. Error bars indicate standard error of the mean. Stars above two bars indicate a statistically significant difference.

Surprisingly, while evoked EPSCs in double mutant neurons were not significantly different from control values, the RRP size was ~25% smaller (Fig. 17A-B-C). Unaltered evoked EPSCs together with smaller RRP sizes indicate an increase in P_{vr}, which was indeed ~30% higher in double mutant neurons (Fig. 17D).

I also analysed spontaneous synaptic transmission by recording spontaneous miniature currents (mEPSC) (Fig. 18) in the presence of Tetrodotoxin (TTX), a Na^+ channel blocker, which prevents action potential generation. Under these conditions, evoked transmission is blocked and only spontaneously fusing quanta are recorded. Double mutant neurons showed no statistically significant differences from controls with regard to the amplitude or the frequency of mEPSCs (Fig. 18B-C).

The effects of the mutations on both RRP size and P_{vr} are predicted to have significant consequences for short-term synaptic plasticity (Zucker and Reger, 2002). I therefore monitored the stability of evoked EPSCs during trains of action potentials at 10 Hz frequency. As expected, double mutant neurons showed stronger and much faster depression during the simulation train (Fig. 19). Importantly and in accord with the increase in P_{vr}, depression in double mutant cells was already detectable with the second stimulus. A change in the ratio of the second to the first evoked EPSC in resonse to a stimulus pair (so called “Paired-Pulse Depression Ratio”) essentially reflects a change in P_{vr}, with an increased P_{vr} causing increased Paired-Pulse Depression and vice-versa (Zucker and Regher, 2002). Similarly, depression of evoked EPSCs during 40 Hz stimulation was faster in double mutant neurons (Fig. 19A-B).

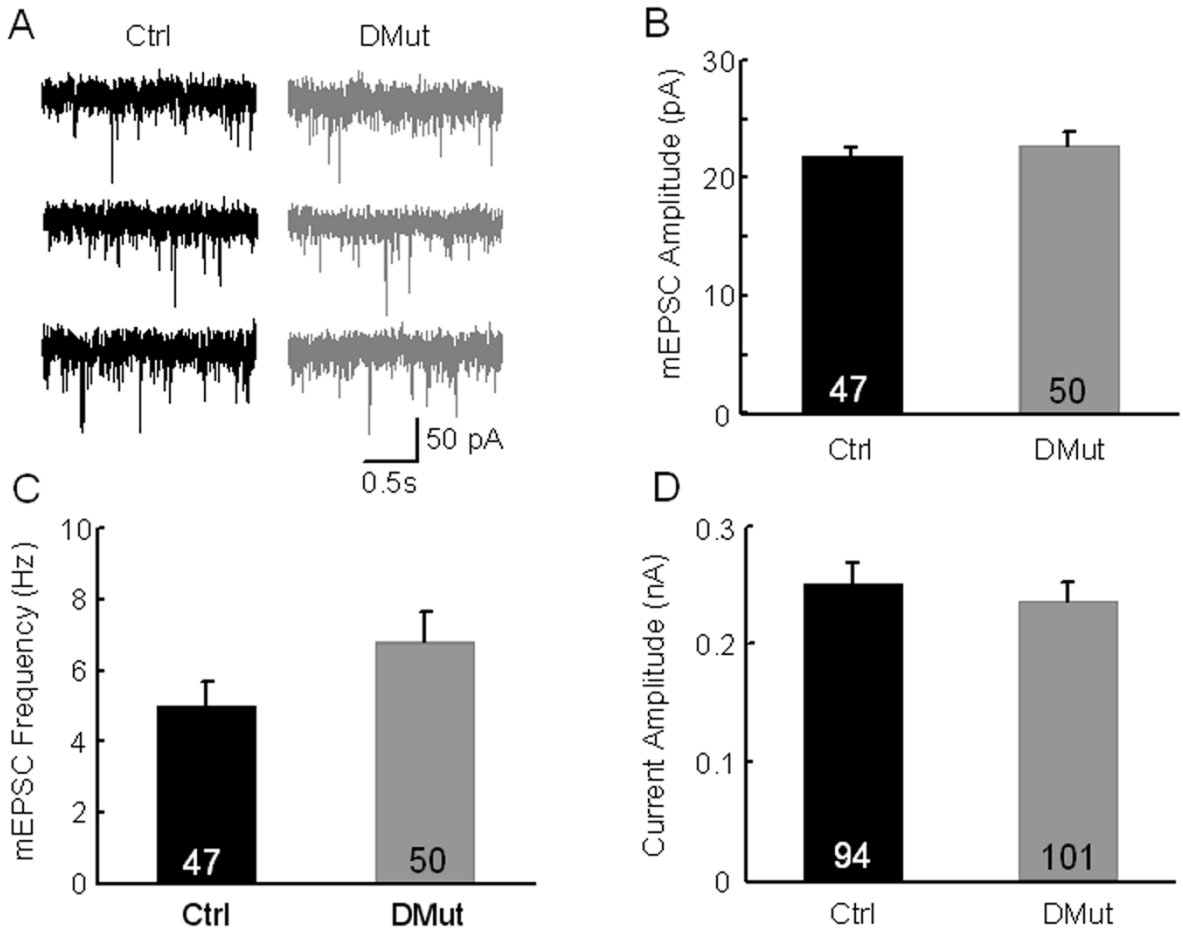

Figure 18 **Normal Spontaneous Glutamatergic Synaptic Transmission in Autaptic Double-Mutant Neurons.** Spontaneous synaptic transmission was analysed by recording spontaneous miniature currents (mEPSC) at a holding potential of –70mV in the presence of the Na^+ channel blocker Tetrodotoxin (TTX). Double mutant neurons showed no statistically significant difference in the amplitude or the frequency of mEPSCs. (A) Representative traces of mEPSC activity in control (black) and double mutant cells (grey). (B) Mean mEPSC amplitudes. (C) Mean mEPSC frequencies. (D) Similar current amplitude of responses to 10 μM Kainate application in double mutant and control neurons, indicating that the total pool of surface expressed glutamate (Kainate and AMPA-type) receptors is very similar between the two genotypes. Numbers in the bars indicate the number of cells tested. Error bars indicate standard error of the mean.

100 stimuli at 40 Hz are believed to deplete the RRP of hippocampal neurons (Moulder et al., 2005; Pyott and Rosenmund, 2002). Elmqvist and Quatsel (1965) developed a cumulative method to calculate the RRP size from the integral of the total synaptic charge being transferred during a stimulation train. In this method, the cumulative charge is plotted versus time and a linear fit to a steady-state phase is

extrapolated to a point on the y-axis, which reflects the RRP size. Like the RRP measure based on hypertonic sucrose application, this independent RRP measure yielded a similar relative estimate for the RRP change in double mutant neurons, with a ~28% reduction as compared to control data (Fig. 19D). Since the contribution of the tonic current is largely neglected by the linear fit, the RRP estimate obtained with this method mainly arises from the phasic component. Therefore, above data indicate that the RRP size and phasic release are decreased to the same extent in double mutant cells as compared to control neurons.

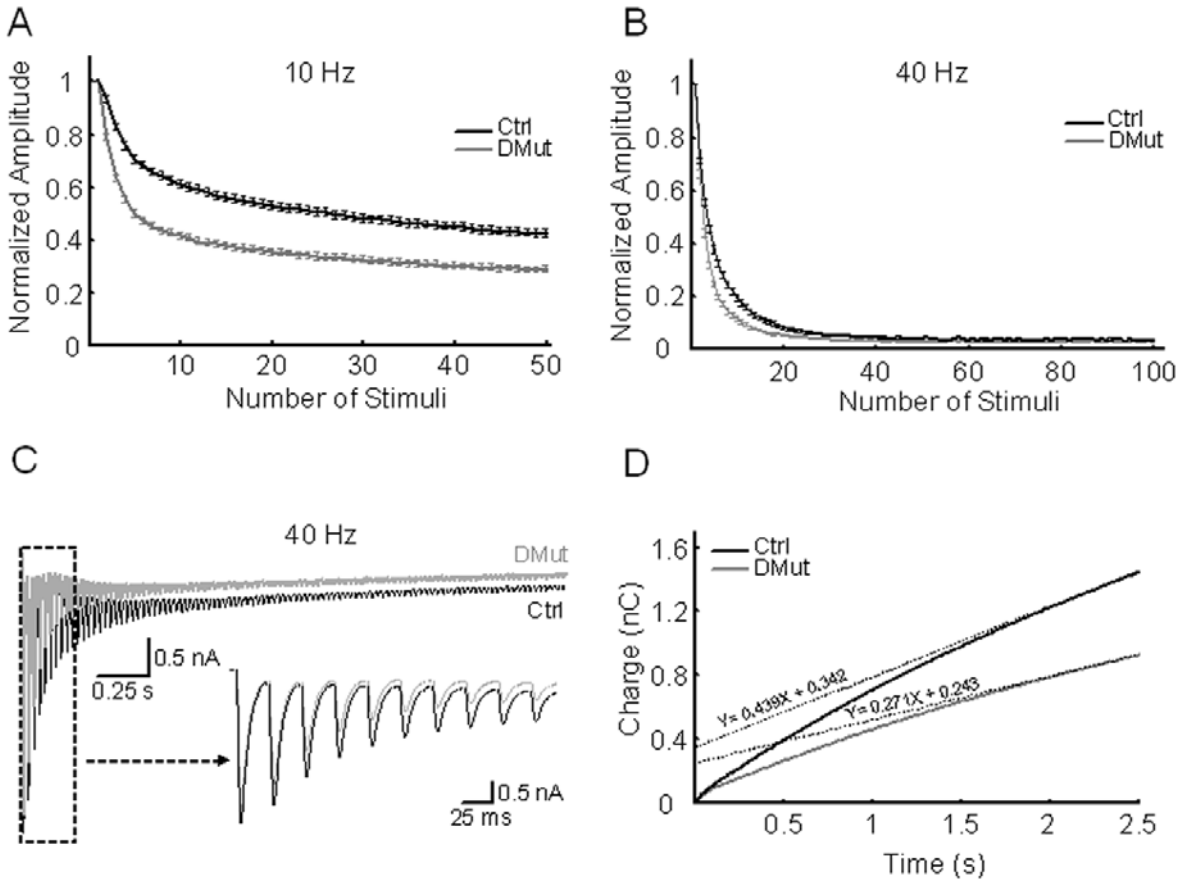

Figure 19 **Short-Term Synaptic Plasticity is Impaired in Double Mutant Neurons.** The effects of the mutations on both RRP size and P_{vr} are predicted to have significant consequences for short-term synaptic plasticity. As expected, double mutant neurons showed stronger and much faster EPSC depression during both 10 and 40 Hz stimulation trains. Interestingly, tonic release was reduced in double mutant neurons. (A) Normalised EPSC depression during 10 Hz (Ctrl, n = 234; DMut, n = 281). (B) Normalised EPSC depression during 40Hz (Ctrl, n = 151; DMut, n = 167). (C) Normalized average of continuous EPSC traces during 40 Hz stimulation. The inset shows a magnification of the

marked section (white box) for double mutant and control cumulative traces. (D) Integral of the total synaptic charge being transferred during the 40 Hz stimulation train. An extrapolation method yielded similar relative estimates for RRP size changes in double mutant neurons (intercept double mutant / intercept control = 0.243/0.342 ~ 28%). Numbers in the bars indicate the number of cells tested. Error bars indicate standard error of the mean. Stars above two bars indicate a statistically significant difference.

Surprisingly, the amount of tonic release elicited by the 40 Hz stimulation train was also drastically reduced in double mutant neurons, as shown in Fig. 19C by the shift in the steady-state current level after phasic release has decayed.

3.4.3.2 Unaltered Synaptic Release Probability and Munc-13-1 Dependent Enhancement of Synaptic Transmission

To investigate how the increase in P_{vr} in double mutant neurons affects the synaptic release probability (P_r), I estimated P_r by using the method developed by Rosenmund et al. (1993) (Fig. 20B). This method relies on the ability of the open-channel blocker MK-801 to progressively block activated NMDA channels in a use-dependent manner. In brief, once neurotransmitter release occurs at a given synapse, NMDA channels are opened and readily inactivated by MK-801. Therefore, during ongoing stimulation NMDA responses at activated synapses are progressively blocked. The use-dependent, progressive block of NMDA-EPSCs by MK-801 reflects therefore the release probability of neurotransmitter across all synapses of a given neuron. Double mutant and control neurons showed very similar decays of normalized NMDA responses in the presence of MK-801, indicating that the average probability of neurotransmitter being released at a given synapse was unchanged in double mutant cells (Fig. 20B).

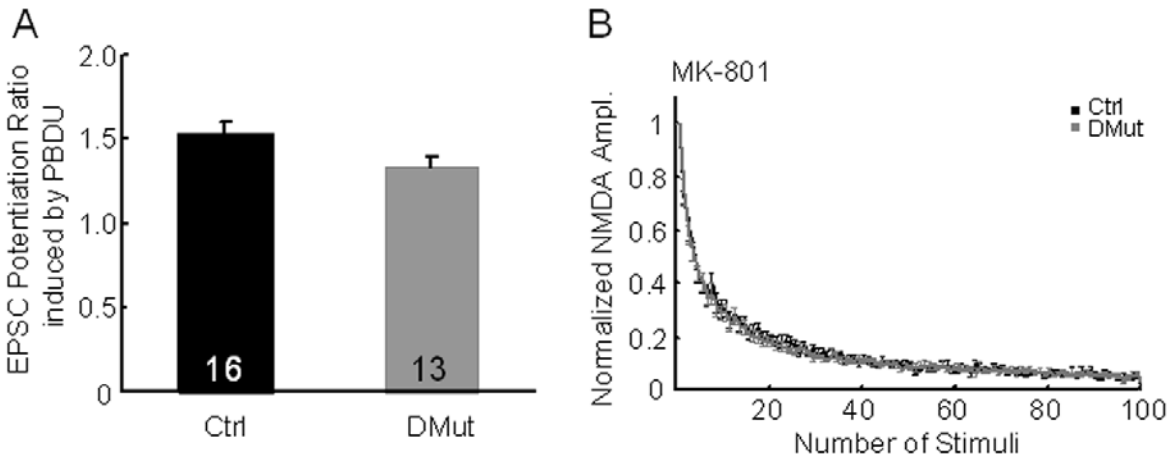

Figure 20 **Normal Synaptic Release Probability and Munc-13-1 Dependent Enhancement of Synaptic Transmission in Double Mutant Neurons.** To investigate how the increase in P_{vr} in double mutant neurons affects the synaptic release probability (P_r), I estimated P_r by analysing the progressive, use-dependent block of NMDA-EPSCs by the open-channel blocker MK-801. Double mutant (grey) and control (black) neurons showed very similar decay of normalized NMDA responses, indicating that the probability of synaptic neurotransmitter release is unchanged. (A) Averaged normalised NMDA-mediated amplitudes plotted against the stimulus number during application of MK-801 (Ctrl, n = 9; DMut, n = 12). Mean NMDA components relative to the AMPA component were not changed between double mutant and control neurons (Ctrl, 0.19 ± 0.015; DMut, 0.23 ± 0.027). (B) We tested for the functionality Munc-13-1 dependent priming processes in double mutant synapses by measuring PBDU potentiation of evoked EPSCs. EPSC potentiation induced by 1 μM PBDU. PBDU potentiation of evoked EPSCs was very similar between double mutant and control neurons, indicating that Munc-13-1 dependent priming reactions are not impaired in double mutant synapses. Numbers in the bars indicate the number of cells tested. Error bars indicate standard error of the mean. Note: Panels A and B need to be swapped.

A defect in RRP size may be indicative of a priming defect (Rhee et al., 2002). Therefore, we tested for the functionality of the priming factor Munc-13-1 in double mutant synapses by measuring the effects of PDBU on synaptic transmission (Fig. 20A). PBDU (β-Phorbol Ester analogue) is well known for inducing increases in presynaptic efficacy via its binding to the C1 domain of Munc-13-1 (Rhee et al., 2002). Double mutant and control neurons displayed a similar enhancement of evoked EPSC amplitudes in response to PDBU (Fig. 20A), indcating that Munc-13-1 is functioning normally at double mutant synapses.

3.4.3.3 Synaptic Vesicle Priming in SNAP Double Mutant Synapses

The best documented function for the SNARE complex disassembly machinery is to recycle “spent” *cis*-SNARE complexes after fusion. Experimental conditions which limit, impair or block the activity of the disassembly machinery have been shown to impair the priming process, that is, the rate at which new vesicles are recruited into the RRP after its depletion. Under these conditions, impaired SNARE disassembly limits the supply of free “active” neuronal SNAREs in the presynaptic terminal, leading to inefficient recruitment of vesicles into the RRP. In order to study the priming process in double mutant synapses in more detail, I analysed both Ca^{2+}-independent and Ca^{2+}-dependent RRP refilling rates.

3.4.3.3.1 Ca^{2+}-Independent RRP Refilling

To measure Ca^{2+}-independent RRP refilling, double pulses of hypertonic sucrose solution were applied at variable time intervals. The first pulse was applied to deplete the RRP, and the second to monitor its recovery (Fig. 21A). The charge integral of the second response was then plotted as a percentage of the first. RRP recovery was very similar between double mutant and control neurons (Fig. 21A), indicating that vesicle priming is not impaired at resting conditions in double mutant synapses. Both data sets were fitted with a double exponential function (τ_f = 2.4 s and τ_s = 10.1s).

Furthermore, in order to monitor basal synaptic vesicle cycling in the presynaptic terminal, I repetitively depleted the RRP by consecutive (every ~1 minute) hypertonic sucrose applications and monitored RRP recovery over time (Fig. 21B). Endocytosed synaptic vesicle have been shown to recycle back to the active zone within hundreds of milliseconds (Deak et al., 2004; Aravanis et al., 2003; Pyle et al., 2000; Stevens et al., 2000; Gandhi et al., 2003; Klingauf et al., 1998; Sara et al., 2002; Sun et al., 2002). Therefore, if recycling of synaptic vesicles is impaired in double mutant synapses, one would expect a stronger and faster decrease of responses to consecutive hypertonic sucrose applications over time, due to the progressive loss of the recycled synaptic vesicles of the RRP.

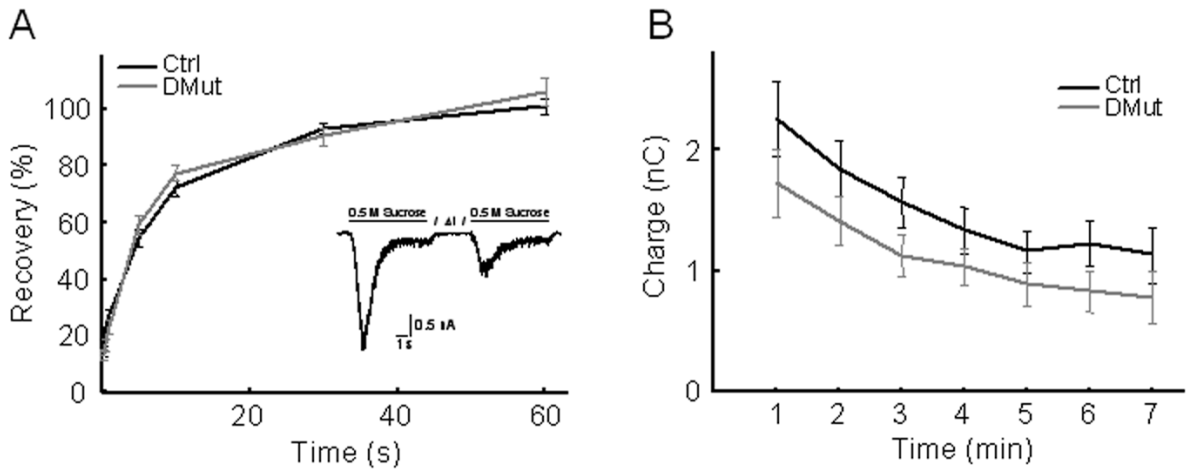

Figure 21 **Normal Ca^{2+}-Independent RRP Refilling and Basal Synaptic Vesicle Cycling at Double Mutant Synapses.** Ca^{2+}-independent RRP refilling was measured by applying two pulses of hypertonic sucrose solution at variable time intervals. The charge integral of the second response was then plotted as a percentage of the first (A). Double mutant and control neurons showed very similar kinetics of RRP recovery, indicating that vesicle priming is not impaired at resting Ca^{2+} concentrations. The recovery process was fitted with a double exponential function (recovery time constants, Tau1 = 2.4s; Tau2 = 10.1 s). To monitor synaptic vesicle cycling under resting Ca^{2+} conditions, responses to consecutive (every ~1 minute) hypertonic sucrose applications were monitored over time. Double mutant and control neurons showed similar responses to consecutive hypertonic sucrose applications (B), indicating that basal synaptic vesicle cycling occurs normally at double mutant synapses (Ctrl, n = 19; DMut, n = 14). Data shown are means ± standard error of the mean.

As expected, responses of both double mutant and control neurons were slightly decreasing over time, due to a well documented run-down phenomenon. However, the time course of this run-down was similar in mutant and control neurons, indicating that basal synaptic vesicle cycling occurs normally at double mutant synapses.

3.4.3.3.2 Ca^{2+}- and Activity-Dependent RRP Refilling

In a subsequent set of experiments, I analysed priming rates in mutant neurons in the presence of high intracellular Ca^{2+} concentration ($[Ca^{2+}]_i$.) High-frequency stimulation leads to an increase in $[Ca^{2+}]_i$, a condition under which refilling of the RRP is faster than at resting Ca^{2+} concentrations (Dittmann and Regher, 1998; Stevens and Wesseling, 1998; Wang and Kaczmarek, 1998). I employed two experimental

paradigms to study the effect of Ca^{2+} on the recovery of the RRP and synaptic transmission (Fig. 22): (1) I continuously stimulated the neuron at 10 Hz and intermittently depleted the RRP with a hypertonic sucrose pulse, and (2) I depleted the RRP with a hypertonic sucrose pulse and monitored recovery of the RRP under 10 Hz stimulation in normal osmolarity. The main difference between the two experimental paradigms is that in the first case high $[Ca^{2+}]_i$ is present before, during and after the hypertonic sucrose pulse, while in the latter case high $[Ca^{2+}]_i$ is present only after the sucrose pulse. Both experiments however gave similar results. As expected, due to their smaller RRP size, EPSC recovery in double mutant neurons reached a lower steady-state level as compared to control cells (Fig. 22A-C). The difference in the absolute EPSC steady-state levels between double mutant and control neurons is similar to that of RRP sizes measured by hypertonic sucrose applications (Fig. 17). To measure recovery rates of the RRP, I normalized the EPSC responses to the last value of the 10 Hz train (Schlüter et al., 2006). In both experiments, the time course of recovery of normalized EPSC responses was very similar between double mutant and control neurons (Fig. 22B-D), indicating that refilling rates after hypertonic sucrose depletion of the RRP were not changed in the presence of high $[Ca^{+2}]_i$.

Next, I analysed recovery rates after electrical discharge of the RRP. Instead of using hypertonic sucrose, a Ca^{2+}-independent method to trigger fusion, I used a high-frequency stimulation train (100 stimuli at 40 Hz) to deplete the RRP. EPSC recovery was then monitored by single action potential stimulations delivered at different times after RRP depletion. As shown in Fig. 23B, EPSC recovery after the 40 Hz stimulation train was markedly slower in double mutant neurons as compared to control cells. As previously reported, fitting of EPSC recovery rates with a double exponential function identified two kinetic components of RRP recovery (Silver et al., 1998; Sakaba and Neher, 2001; Schlüter et al., 2006). Both the fast and the slow component of EPSC recovery were significantly slower in double mutant neurons (Fig. 23A), indicating that refilling after high-frequency depletion of the RRP is strongly impaired in double mutant neurons.

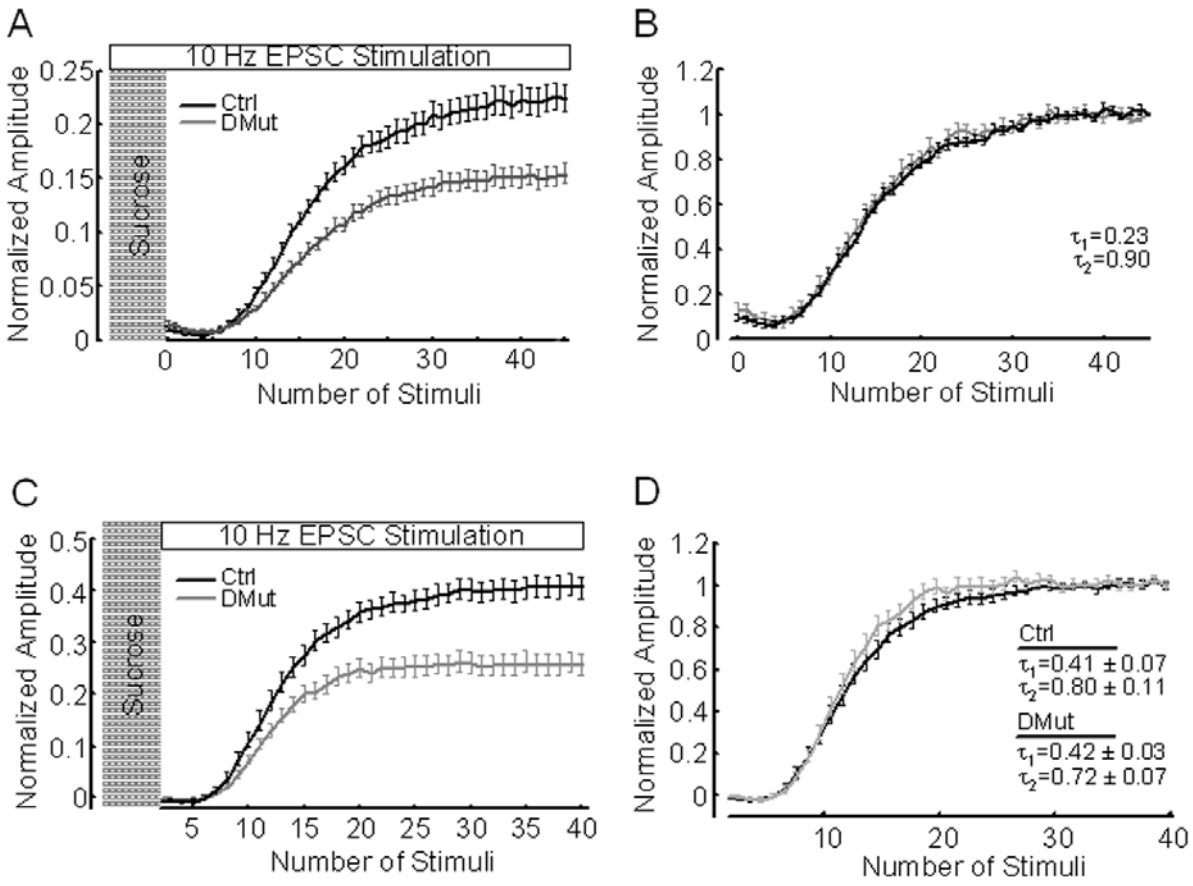

Figure 22 **Normal Ca^{+2}-Dependent RRP Refilling in Double Mutant Neurons after Hypertonic Sucrose Mediated RRP Depletion.** RRP refilling was analysed in the presence of high intracellular Ca^{2+} concentration. Two stimulation protocols were used: Intermittent RRP depletion via hypertonic sucrose in the presence of continuous 10 Hz stimulation (50 stimuli at 10 Hz - 50 stimuli at 10 Hz plus hypertonic sucrose – 50 stimuli at 10 Hz) (A), and hypertonic sucrose RRP depletion followed by 10 Hz stimulation to monitor recovery (hypertonic sucrose – 40 stimuli at 10 Hz) (C). Only EPSC recovery is shown in (A) and (C). In both experiments the time course of recovered EPSC responses normalised to the last value was very similar between double mutant and control neurons, as indicated in (B) and (D), respectively. (A) and (C) EPSC recovery monitored at 10 Hz stimulation frequency. EPSCs are normalised to the initial EPSC response (A: Ctrl, n = 127; DMut, n = 153. C: Ctrl, n = 33; DMut, n = 42). (B) and (D) Same as in (A) and (C), respectively, but EPSC responses are normalised to the last response of the 10 Hz train to allow direct comparison of recovery kinetics between double mutant and control neurons. Data shown are Mean ± standard deviation of the mean.

I next wanted to analyse EPSC recovery after complete depletion of neurotransmitter release. 100 stimuli at 40 Hz frequency can deplete the RRP, but are not sufficient to completely deplete total release. In fact, tonic release is still

prominent at the end of the train (Fig. 19). Therefore, I applied a stronger stimulation protocol (900 stimuli at 100 Hz) and monitored recovery of single action potential evoked EPSCs at different times after the stimulation train (Fig. 23B) (Sakaba, 2006). Also in this case, EPSC recovery was significantly slower in double mutant neurons as compared to controls (Fig. 23B). However, the relative difference of EPSC recovery time courses between mutant and control cells after 100 Hz stimulation was less than after 40 Hz stiumulation.

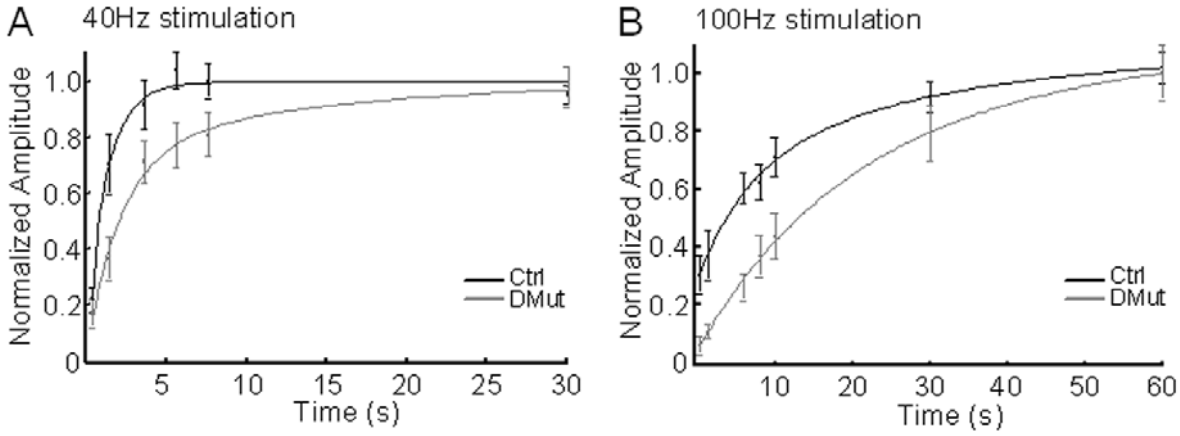

Figure 23 **Strong Impairment of RRP Recovery in Double Mutant Neurons after Electrical Discharge of the RRP.** The RRP was depleted by 100 stimuli at 40 Hz frequency, and then RRP refilling was followed by measuring the relative recovery of synaptic responses after 0.25, 1.3, 6, 8, 10 and 30 seconds (A). (B) RRP refilling monitored after 900 stimuli at 100 Hz. % recovery of EPSCs after 0.25, 1.3, 6, 8, 10, 30 and 60 seconds is shown (Ctrl, n = 15; DMut, n = 16). After electrical discharge of the RRP, EPSC recovery was markedly slower in double mutant neurons as compared to controls. Recovery time constants after 40 Hz (τ1- τ2): Ctrl = 0.51s – 1.29s; DMut = 1.78s – 12.19s. Recovery time constants after 100 Hz (τ1- τ2): Ctrl = 6.51s – 30.43s; DMut = 16.89s – 40.22s (Ctrl, n = 17; DMut, n = 18). Data shown are mean ± standard error of the mean.

Taken together, above results indicate that in double mutant neurons, Ca^{2+}-dependent and -independent refilling kinetics of the RRP are not impaired. On the other hand, RRP refilling is strongly impaired only when the RRP is completely depleted by a high frequency stimulation train (40-100 Hz).

3.4.3.4 Strong Reduction in Calcymicin-Induced Neurotransmitter Release in SNAP Double Mutant Neurons

A synaptic vesicle is functionally defined as “primed” when it can undergo fusion in response to a Ca^{2+} signal. Therefore, to determine the total pool of primed vesicles in the presynaptic terminal, I induced a massive increase in $[Ca^{2+}]_i$ and quantified the total charge response during the stimulus (representing the total amount of neurotransmitter being released). I used the Ca^{2+}-ionophore Calcymicin, which spontaneously inserts into the cell membrane and allows extracellular Ca^{2+} (4 mM) to flow into the cell to strongly increase the Ca^{2+} concentration in presynaptic terminals.

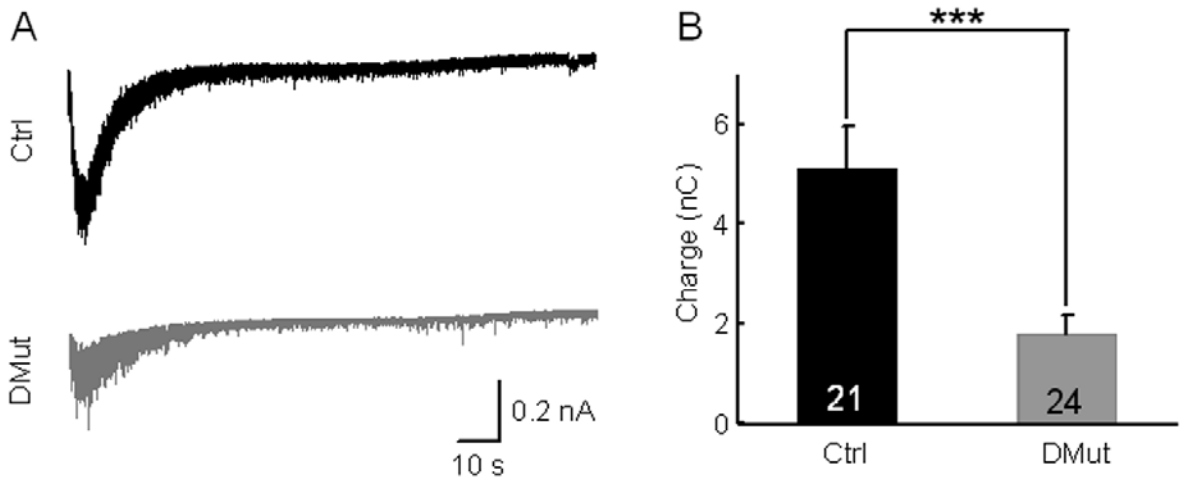

Figure 24 **Strong Reduction in Calcymicin-Induced Neurotransmitter Release in Double Mutant Neurons.** Spontaneous and evoked release monitored in the presence of the Ca^{2+} ionophore Calcymicin. EPSCs were monitored at 0.3 Hz during the two minutes application. (A) Representative traces from double mutant (grey) and control (black) neurons, where EPSCs were removed. (B) Total charge transfer induced by Calcymicin application. Double mutant neurons showed a drastic decrease (~60%) in the total charge response during the calcymicin application compared to control neurons. Numbers in the bars indicate the number of cells. Error bars indicate standard error of the mean. Stars above two bars indicate a statistically significant difference.

Double mutant neurons showed a drastic decrease (~60%) in the total charge response during the Calcymicin application as compared to control neurons (Fig. 24). On the other hand, the RRP size as estimated by hypertonic sucrose application was

only mildly reduced (~25%, Fig. 16C). These data indicate that the total number of primed vesicles which can undergo Ca^{2+}-mediated fusion is reduced by ~60% in double mutant neurons.

3.4.3.5 Strong Reduction in Neurotransmitter Release During 100 Hz Stimulation in SNAP Double Mutant Neurons

I next measured the total amount of neurotransmitter released during high-frequency stimulation in double mutant and control neurons. High-frequency stimulation can lead to increased $[Ca^{+2}]_i$, which is know to be critical for triggering tonic release. 100 stimuli at 40 Hz are not sufficient to completely deplete tonic release, which is still prominent at the end of the train (Fig. 19C), indicating that there is still neurotransmitter being released from presynaptic terminals. Therefore, I employed a much stronger stimulation (900 stimuli at 100 Hz), aiming to completely deplete tonic release.

In control neurons, this stimulation triggered a phasic release component which rapidly decayed within a few stimuli, and a prominent tonic component, which slowly decayed during the train (Fig. 25A). As expected, phasic EPSC responses from double mutant neurons decayed faster than controls. Surprisingly however, the tonic component was strongly reduced in double mutant neurons as shown in Fig. 25A. I quantified the size of the primed vesicles pool being released during the train by the cumulative method described above (3.4.3.1). Consistently with the Calcymicin data (Fig. 24), the total pool released during the 100 Hz stimulation was reduced by ~60% in double mutant neurons as compared to controls (Fig. 25D).

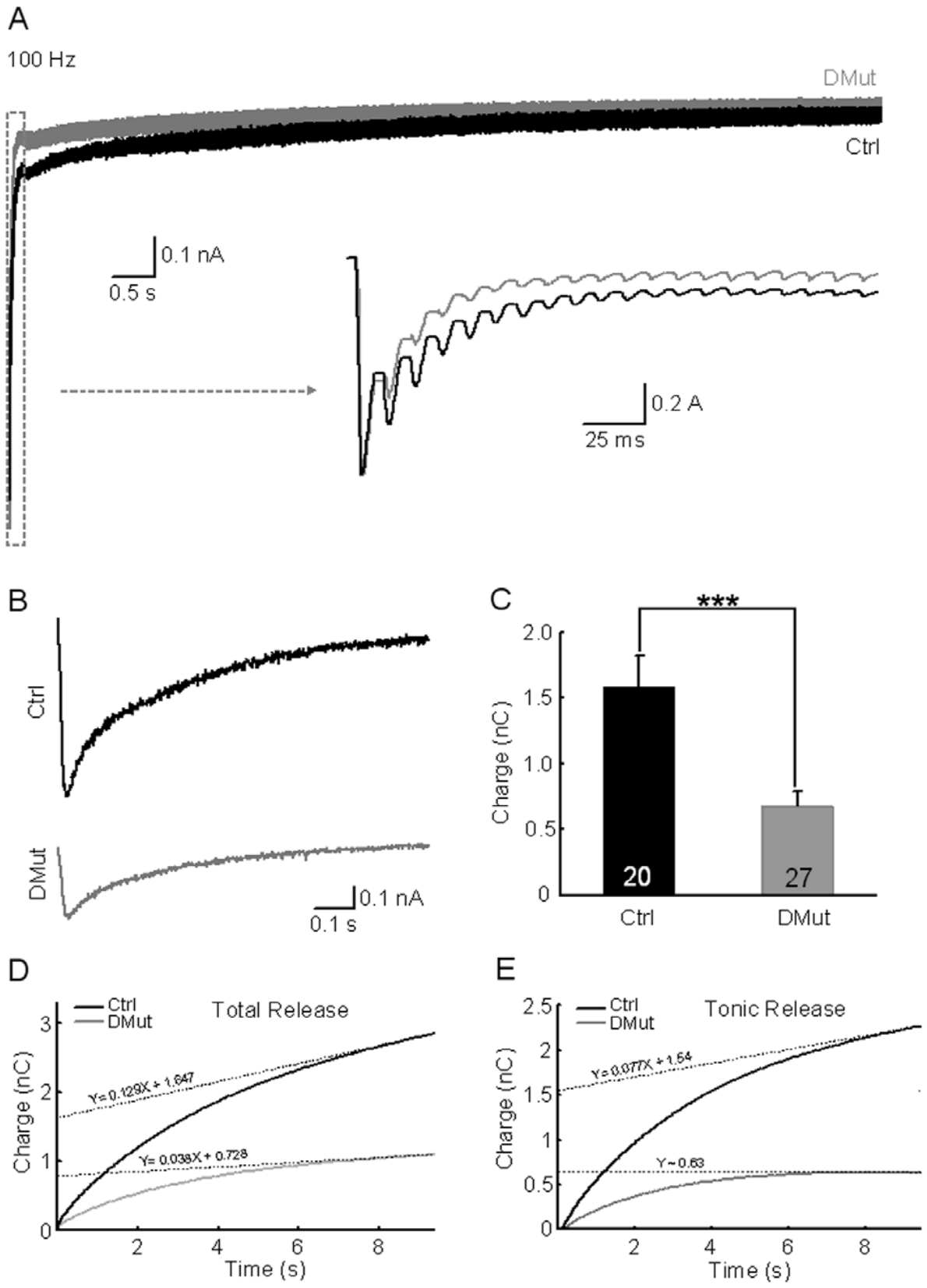

Figure 25 **Strong Reduction in Tonic Neurotransmitter Release during 100 Hz Stimulation in Double Mutant Neurons.** Neurotransmitter release was monitored during 900 stimuli at 100 Hz. Double mutant neurons showed a drastic reduction in total release, which was mainly

accounted for by an underlying strong reduction in the tonic release component. (A) Normalized average of continuous EPSC traces during 100 Hz stimulation from double mutant (grey) and control (black) neurons are shown. Stimulation artefacts were removed. The inset shows a magnification of the marked section (white box) from the cumulative traces. (B) Cumulative tonic release traces, calculated by subtraction of the phasic component from total cumulative traces shown in (A). Stimulation artefacts after subtraction of phasic release were removed from the traces by interpolation. (C) Total charge transfer for tonic release shown in (B). (D) Integral of the total synaptic charge being transferred during the 100 Hz stimulation train. (E) Integral of the "tonic" synaptic charge being transferred during the 100 Hz stimulation train. Numbers in the bars indicate the number of cells. Error bars indicate standard error of the mean. Stars above two bars indicate a statistically significant difference.

The major contribution to total release at 100 Hz arises from the tonic component, which in control neurons accounts for ~90% of the total release (Fig. 25A). That is, the great majority of primed vesicles were released tonically during the train. Therefore I separately quantified tonic release by subtracting the phasic component from the total cumulative traces (Fig. 25B). The quantification shows that in double mutant neurons tonic release triggered by 900 stimuli at 100 Hz is ~60% smaller than in controls (Fig. 25C-E). However, the timing of tonic release was not changed (rise time, Ctrl = 130.6 ms; DMut = 127.7 ms; time-to-peak, Ctrl = 250 ms; DMut = 210 ms; decay time constant, Ctrl = 3.52 s; DMut = 3.50 s. n Ctrl = 20; n DMut = 27). These data indicate that the "pool" of primed vesicles which are tonically released during a stimulation train is ~60% reduced in double mutant neurons.

3.4.3.6 Overexpression of α- and β-SNAP in Wild-type Hippocampal Neurons has no Effect on Glutamatergic Synaptic Transmission

A number of contradictory data have been accumulated over recent years concerning the effects of increasing α-SNAP levels in cells on neurotransmitter and catecholamine release.

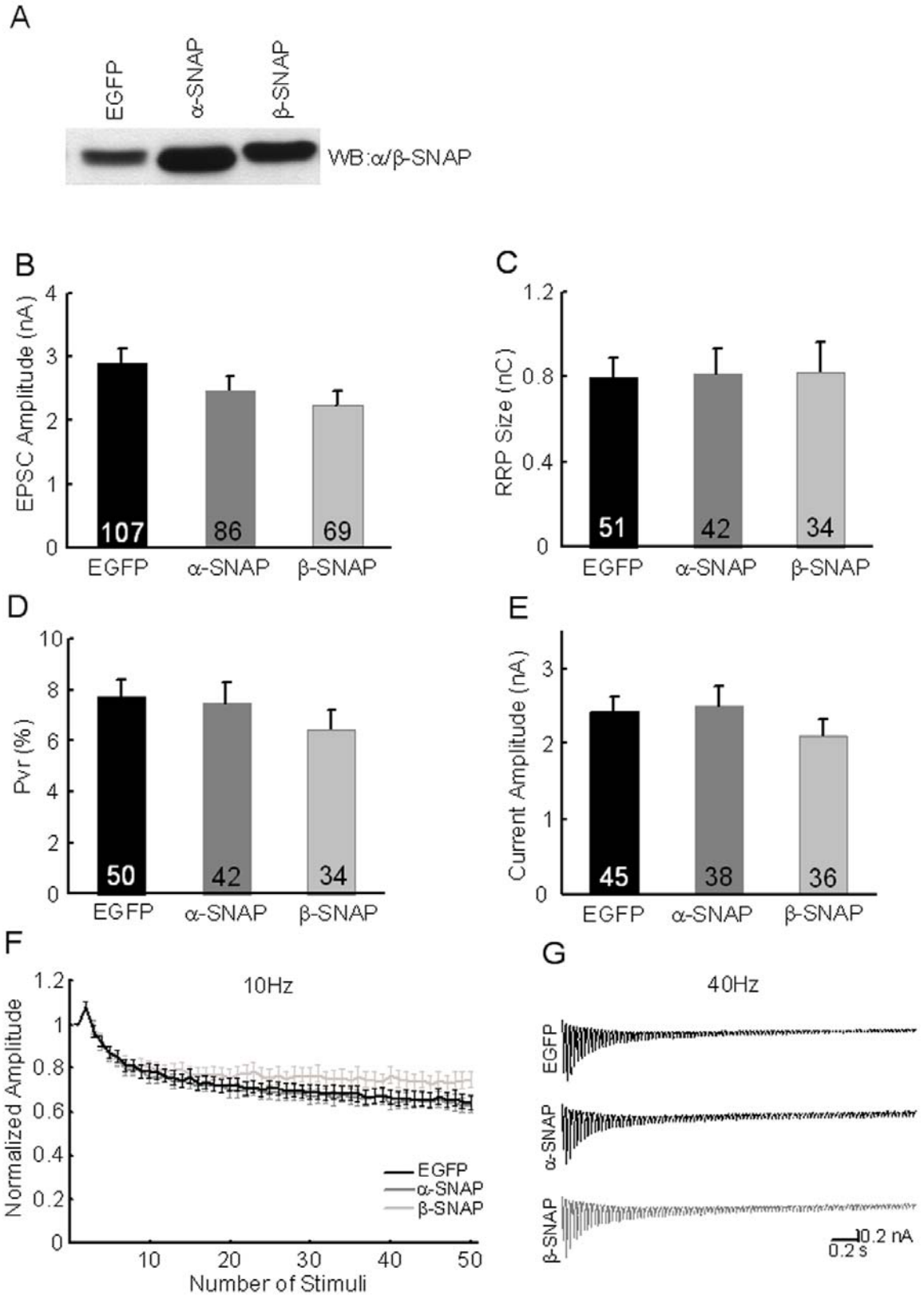

Figure 26 **Overexpression of α- and β-SNAP in Wild-Type Hippocampal Neurons has no Effect on Glutamatergic Synaptic Transmission.** α- and β-SNAP were overexpressed in autaptic hippocampal neurons using Semliki Forest Viruses. (A) Representative Western blot with anti-α/β-SNAP antibody on continental hippocampal cultures 12 hours after

infection. EGFP-, α-SNAP and β-SNAP overexpressing cells were analysed. Glutamatergic synaptic transmission was analysed, and none of the tested parameters were found to be statistically different between control EGFP, α- and β-SNAP overexpressing neurons. The following parameters were analysed. (B) Mean EPSC amplitudes in EGFP (black), α-SNAP (dark grey) and β-SNAP (light grey) overexpressing cells. (C) Mean RRP size estimated by the charge integral measured after release induced by application of 0.5 M sucrose solution. (D) P_{vr}, calculated by dividing the charge transfer during single EPSCs by the charge transfer measured during RRP release. (E) Similar current amplitude in response to 10 μM kainate application, indicating that the total pool of surface expressed glutamate (kainate and AMPA) receptors is very similar in the different neurons. (F) Normalised EPSC depression during 10 Hz stimulation (EGFP, n = 88; α-SNAP, n = 72; β-SNAP, n = 57). (G) Normalized average of continuous EPSC traces during 40 Hz stimulation (EGFP, n = 68; α-SNAP, n = 60; β-SNAP, n = 48). Numbers in the bars indicate the number of cells tested. Error bars indicate standard error of the mean.

The majority of these studies indicated that increasing α-SNAP levels results in an increase in release, while some proposed that high α-SNAP levels could inhibit fusion (1.10.280). These studies thus proposed contradictory models for the role of α-SNAP in the regulation of exocytosis. So far however, the effect of SNAP overexpression at central mammalian synapses has not been investigated. Furthermore, all previous studies concentrated on the α-SNAP isoform, and a comparative analysis of both α- and β-SNAP has not been performed. Therefore, I took advantage of the Semliki Forest Virus mediated overexpression system and analysed excitatory synaptic transmission in α- and β-SNAP overexpressing autaptic hippocampal neurons.

With the Semliki Forest Virus system, already 12 hours after infection I could detect a strong increase in α- and β-SNAP levels, as shown by the representative Western blots in Fig. 26A. The electrophysiological analysis showed that overexpression of α- and β-SNAP in wild-type neurons had no effect on glutamatergic synaptic transmission (Fig. 25). Basic release parameters (EPSC amplitude, sucrose-mediated release, P_{vr}) and short-term plasticity of synaptic transmission were not statistically different between control EGFP, and α- or β-SNAP overexpressing neurons. In the past, a single study reported a differential effect of α- and β-SNAP on the surface expression of AMPA receptors (Hanley et al., 2002). However, I found that the current amplitude induced by kainate application was not

changed between α- and β-SNAP overexpressing neurons (Fig. 26D), indicating that the total pool of surface expressed kainate and AMPA receptors is also not changed by altered SNAP levels.

3.4.3.7 Rescue of the Electrophysiological Phenotype by Overexpression of α- and β-SNAP in Double Mutant Neurons

One caveat of deletion mutant studies is the possibility that the changes observed do not reflect the primary consequence of the deletion but are a secondary consequence. Therefore, rescue of a knock-out phenotype by reintroduction of the deletion protein is a necessary criterion to prove that the mutant phenotype is directly linked to the removal of the protein itself.

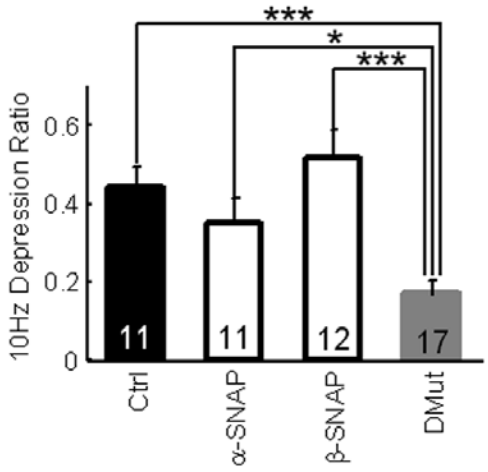

Figure 27 Rescue of the Electrophysiological Phenotype by Overexpression of α- and β-SNAP in Double Mutant Neurons. α- and β-SNAP were overexpressed in double mutant neurons via Semliki Forest Virus, and short-term synaptic depression during 10 Hz was monitored. Both isoforms were able to restore 10 Hz depression to control levels. .Neurons were stimulated with 50 stimuli at 10 Hz and the 10 Hz depression ratio was calculated as the ratio of the last to the first response of the 10 Hz train. Numbers in the bars indicate the number of cells tested. Error bars indicate standard error of the mean. Stars above two bars indicate a statistically significant difference.

To address this issue, I overexpressed α- and β-SNAP in double mutant neurons and tested if short-term synaptic plasticity was restored to control levels. Overrexpression of both α- and β-SNAP restored the depression of EPSCs during 10 Hz stimulation (Fig. 27). As shown in Fig. 27, the 10 Hz depression ratio (last EPSC

amplitude of the 10 Hz train divided by the first) was restored to control levels in α- and β-SNAP overexpressing cells. This result indicates that the electrophysiological phenotype I observed in double mutant neurons is due to the loss of SNAPs, and that α- and β-SNAP are functionally equivalent, since overexpression of either isoform alone can rescue the phenotype of double mutant cells.

3.5 The HYH Mutation does not Disrupt the Interaction of α-SNAP with its Putative Interaction Partners, and Overexpression of HYH α-SNAP Mutant in Wild-Type Hippocampal Neurons has no Effect on Glutamatergic Synaptic Transmission

HYH mice bear a point mutation in the NAPA gene, leading to an amino acid exchange in the α-SNAP protein. It was shown previously that the mutation does not alter protein folding, and *in vitro* disassembly of the SNARE core complex is comparable in the presence of HYH mutant or wild-type α-SNAP (Chae et al., 2004). Based on these data it was concluded that HYH is a hypomorphic mutation which results in low levels of protein and does not affect protein function *per se*. There is however still the possibility that the HYH mutant could be less efficient or even dominant negative in processes that were not directly tested in the present or previous studies. To exclude the possibility that the point mutation could disrupt the interaction of HYH α-SNAP with its interaction partners, I first tested by yeast two hybrid assays its interactions with previously identified α-SNAP interaction partners (Martin et al., 2006). As shown in Fig. 28, both HYH mutant and wild-type α-SNAP interacted equally well with all tested interactors, indicating that the HYH point mutation does not disrupt these interactions.

In order to exclude possible dominant-negative effects of the HYH mutation on synaptic function, I overexpressed the HYH α-SNAP mutant in autaptic hippocampal wild-type neurons and analysed glutamatergic synaptic transmission (Fig. 28). Neither the measured basic release parameters (EPSC amplitude, sucrose-mediated release, P_{vr}) nor the time course of EPSC depression during high-frequency stimulations (10 Hz-40 Hz) were different between EGFP and HYH α-SNAP mutant overexpressing neurons (Fig. 28B-F). One can therefore conclude that the HYH mutation has no dominant-negative effect on glutamatergic synaptic transmission.

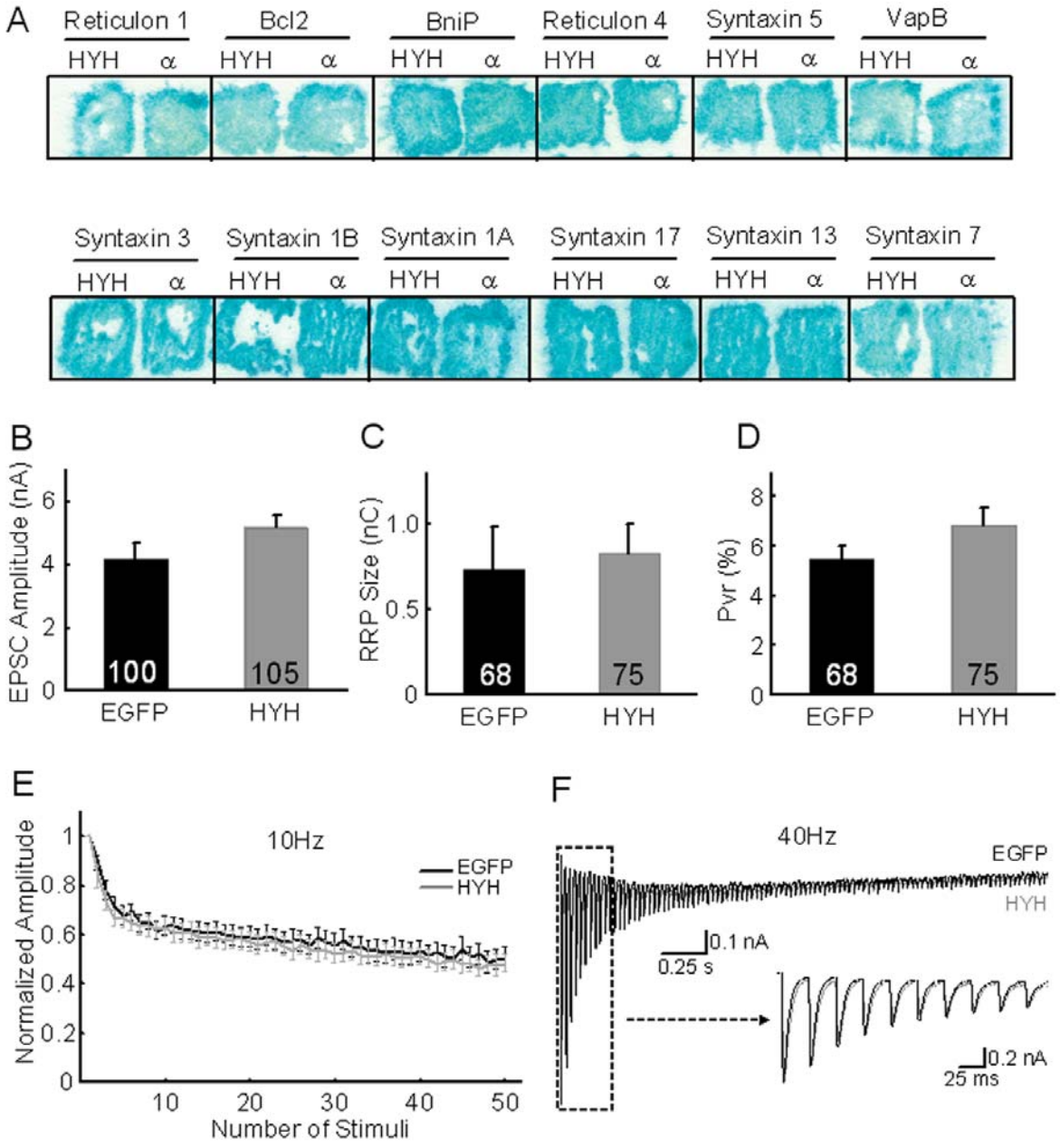

Figure 28 **The HYH Mutation does not Disrupt Interactions of α-SNAP with Putative Interaction Partners, and Overexpression of HYH α-SNAP Mutant has no Effect on Glutamatergic Synaptic Transmission.** HYH mutant and wild-type α-SNAP interacted equally well in the yeast two-hybrid system with putative α-SNAP interaction partners, indicating that the point mutation does not disrupt these interactions. (A) β-galactosidase activity of yeast cells co-transformed with either α-SNAP (α) or the HYH mutant (HYH), and the indicated putative binding binding partners. The HYH mutant of α-SNAP was overexpressed in wild-type neurons by Semliki Forest Virus, and glutamatergic synaptic transmission was analysed. None of the tested parameters were found to be statistically different between control EGFP and HYH overexpressing neurons. The following parameters were analysed. (B)

Mean EPSC amplitudes in EGFP (black) and HYH (grey) overexpressing cells. (C) Mean RRP size estimated by the charge integral measured after release induced by application of 0.5 M sucrose solution. (D) P_{vr} calculated by dividing the charge transfer during single EPSC by the charge transfer measured during RRP release. (E) Normalised EPSC depression during 10 Hz stimulation (WT, n = 54; HYH, n = 63). (F) Normalized average of continuous EPSC traces during 40 Hz stimulation (WT, n = 49; HYH, n = 52). Numbers in the bars indicate the number of cells. Error bars indicate standard error of the mean.

4 Discussion

4.1 β-SNAP, Synaptic Transmission and Epilepsy

β-SNAP deficient mice suffer from an epileptic syndrome, characterised by recurrent generalised seizures. In general terms, epilepsy arises from an imbalance of the excitation/inhibition ratio in the brain. Possible substrates for such an imbalance are highly diverse and include alterations of neuronal excitability, synaptic transmission, and neuronal network architecture. Apart from exogenous traumata, many molecular alterations of the brain have been reported to perturb the excitation/inhibition equilibrium in the brain, and to lead to seizure activity. Indeed, numerous genetic causes for epilepsy in human patients have been described in the past (see Abad et al., 2007, for a recent review). Similarly, database searches reveal that more than 290 spontaneous or targeted genetic mutations in rodents lead to spontaneous seizure activity, and that more than twice as many mutations increase the susceptibility to seizure induction (MGI Database, The Jackson Laboratory, Maine, USA). Among these are mutations of ion channels (Brill et al., 2004; Smart et al., 1998; Ogiwara et al., 2007), post-synaptic receptors (Brusa et al., 1995; Gassmann et al., 2004; Masugi et al., 1999), cell-adhesion molecules (Fuerst et al., 2008), metabolic enzymes (Lei et al., 1996; Enquist et al., 2007; Li et al., 1995), transcription factors (Barndt et al., 2000), and SV associated proteins (Rosahl et al., 1995; Krowder et al., 1999). Interestingly, some of these mutations were shown to alter synapse strength, which may be linked directly to the aberrant electrical activity of brain circuits in the corresponding epileptic brains.

β-SNAP (but not α-SNAP) expression is developmentally regulated. It commences around birth and reaches its maximum level around the second to third week of postnatal life, i.e. during the period of synapse formation in the mouse brain. Thus, at a time when the majority of synapses are established and mature in the mouse brain, β-SNAP mutant mice start to manifest the epileptic syndrome. The overlap of the epileptic phenotype onset with the period of synapse formation may therefore be indicative of a synaptic dysfunction in β-SNAP deficient brains that underlies its epileptic activity. Strikingly, in cultured hippocampal β-SNAP deficient neurons I did not detect any alteration of glutamatergic transmission, but it remains unknown if a similar situation holds true for glutamatergic transmission in general or

for inhibitory neurons. Inhibitory neurons, although less abundant than excitatory neurons in the brain, shape network responses and are primary determinants of circuit outputs and their dynamic behaviour. In particular, many inhibitory neuron subtypes belonging to the class of “fast-spiking” cells have been shown to fire at much higher frequencies *in vivo* than excitatory neurons, and may therefore be more susceptible to changes in SNARE complex disassembly activity (Yuste, 2005; Bartos et al., 2007). This raises the interesting possibility of a differential dependence of excitatory and inhibitory synapses on SNARE complex disassembly.

The present study focussed on the synaptic functional consequences of the β-SNAP deficiency and was not aimed at elucidating the cause of the epileptic phenotype of β-SNAP deletion mutant mice. This strategic decision was based on two arguments. First, epilepsies represent a highly diverse and heterogeneous group of diseases, particularly with regard to possible molecular and genetic causes. Therefore, the detailed analysis of yet another genetically induced form of epilepsy in rodents was considered to be of secondary importance. Second, most previous attempts to explain the epileptic phenotype of mutant mice lacking certain functional presynaptic proteins in the context of a network dysfunction have failed. Experimental approaches where brain connectivity is preserved at least to a certain extent, like *in vivo* recordings from intact brains or *ex vivo* brain slice preparations are typically used to gain insights into electrophysiological alterations of epileptic brains (Gloveli et al., 1998; Stief et al., 2007), and may therefore be helpful for future investigations of the effects of the β-SNAP deletion on brain network physiology.

4.2 α-SNAP, Cell Polarity and Development

My data indicate that cultured HYH mutant hippocampal neurons are morphologically indistinguishable from wild type control neurons, and that glutamatergic synaptic transmission of cultured autaptic hippocampal neurons is not affected by the HYH mutation. These findings were rather unexpected, especially in view of the fact that Chae et al. (2004) proposed a role for α-SNAP in regulating neuronal cell fate by controlling polarized protein transport in neural progenitor cells. These authors demonstrated a drastic defect of apical protein trafficking in neuroepithelial cells of HYH mutants *in vivo*, which resulted in marked abnormalities of the normally polarized structure of the ventricular zone. Although I did not directly test apical

protein trafficking in HYH mutant neurons, my data do not support the notion of a general trafficking defect in HYH neurons. Rather, they indicate that apical trafficking, and in fact general neuronal protein trafficking to axons, dendrites, and other compartments is normal to the extent that it guarantees normal basal synaptic transmission. At least three explanations for this discrepancy are conceivable. First, the phenotypic analysis of the HYH mutant cortex performed by Chae et al. (2004) was performed at day 3 of postnatal development (P3), a time at which neurogenesis is complete. I, on the other hand, obtained hippocampal neurons from newborn animals (P0), and cultured them for about 15-16 days *in vitro* on artificial astrocyte islands. Thus, neuronal development and differentiation may not have been fully recapitulated in the *in vitro* system used for the present study. Secondly, and most likely, the disruption of the normally polarized structure of the ventricular zone reported by Chae at al. (2004) might not represent a cell autonomous defect in apical trafficking, as was postulated, but might rather arise from a dysfunction in cell-to-cell and cell-to-matrix signaling, which takes place in more the complex *in vivo* environment but not in my culture system. Indeed, my electrophysiological data (Fig. 13) on cultured isolated hippocampal neurons would provide evidence for the absence of a cell autonomous defect in apical trafficking as a consequence of the HYH mutation. Finally, the data described by Chae et al. (2004) concern only neuropithelial cells, which are a subtype of stem cells lining the surface of the ventricular zone. The defect in this cell type may be a cell specific consequence of the HYH mutation and therefore not be present in postmitotic neurons, which were in the focus of the present analysis.

4.3 Normal Morphology and Development of Cultured SNAP Double Mutant Neurons

In neurons, the NSF/SNAP machinery does not only operate at synapses. Rather, its constitutive activity is essential for the function of the secretory pathway throughout the development and lifetime of the cell, by maintaining all SNAREs, and not only the neuronal ones, in their active state, thereby controlling almost all cellular membrane fusion reactions (Jahn and Scheller, 2006; Martin et al., 2006). It is therefore surprising that synaptic transmission is rather specifically and selectively impaired by genetic impairment SNAPs, while other membrane reactions in SNAP double mutant

neurons seem to proceed normally. Indeed, I found in fact that neither the surface-expressed pool of AMPA and Kainate-type glutamate receptors, nor the size of neuronal cell bodies, dendrite extension and branching, or synapse numbers were altered by the mutation. These observations indicate that double mutant neurons develop normally in culture, and that none of the membrane transport events that support neuron growth and development are significantly impaired by the SNAP double mutation. Interestingly, dendrites are more strictly dependent on constitutive membrane supply than axons as mutations that impair the secretory pathway have drastic effects on dendrites but only moderately affect axonal morphology and extension (Zhang et al., 2007). Thus, alone the fact that dendritic branching and extension are normal in SNAP double mutant neurons already indicates that the constitutive secretory pathway is not sensibly impaired in double mutant neurons.

The finding that a ~70% reduction of SNAP levels has no impact on the majority of membrane trafficking events of the secretory pathway in the neuron, except for regulated SV exocytosis, indicates that high levels of SNARE complex disassembly activity are specifically needed to support synaptic transmission. This is intuitively plausible as neurons are highly specialised for Ca^{2+} regulated neurotransmitter release, and may therefore have a higher demand for free neuronal SNAREs at synapses than in other membrane fusion reactions, which are likely to happen at a much lower rate as compared to SV exocytosis.

4.4 Basic Synaptic Transmission and RRP Dynamics in SNAP Double Mutant Neurons

The present data show that basic synaptic transmission is moderately affected by genetic impairment of the SNARE complex disassembly machinery (Fig. 17). Release evoked by single APs is remarkably similar between double mutant and control neurons. However, the sucrose sensitive RRP is slightly reduced (25%) in double mutant neurons as compared to controls. Therefore, the P_{vr}, which represents the fraction of the RRP being released by single AP stimulation, is slightly higher in double mutant neurons. This increase in P_{vr} is also confirmed by stronger paired-pulse depression in double mutant neurons at both 10 and 40 Hz stimulation frequencies (Fig. 19). The increase in P_{vr} in double mutant neurons is very interesting, as it is indicative of an effect of the SNAP double mutation on the

neurotransmitter release process itself. However, it is unclear how SNAPs, either directly or indirectly, may regulate the average probability of a single vesicle to be released upon stimulation. It has been shown *in vitro* that SNAPs compete with Complexins and Synaptotagmin-1 for binding to SNARE complexes (McMahon et al., 1995; Kee and Scheller, 1996). Therefore, one possibility is that a reduction in SNAP levels may favour the association of late regulatory proteins with *trans*-SNARE complexes, thereby enhancing the stabilisation of SVs in their highly fusogenic state. On the othe hand, the P_{vr} increase we observed in double mutant cells, although highly significant, is very mild. SNAPs are therefore not major determinants of P_{vr}, but rather act as fine-modulators of the release machinery. Even slight changes in initial P_{vr}, however, can have strong effects on short-term synaptic plasticity (Zucker and Regher, 2002; Schlueter et al., 2006), and the physiological impact of subtle P_{vr} modulations on synaptic transmission can be highly significant during fast and repetitive information transfer. Correspondingly, SNAP double mutant neurons display faster and stronger EPSC depression during high-frequency stimulations (Fig. 19). As expected, though, based on the fact that the increased P_{vr} is paralleled by a concomitant decrease in RRP size in SNAP double mutant cells, the observed alterations of basic synaptic transmission parameters have no impact on the synaptic release probability P_r (Fig. 20), which is proportional to the product of both RRP size and P_{vr} ($P_r \propto$ RRP * P_{vr}; Rosenmund et al., 1993)

In view of the short-term plasticity changes seen in SNAP double mutant neurons, it is surprising that basal RRP dynamics are not affected by the mutations. After being exocytosed, SVs recycle back into the RRP. Fast and slow recycling pathways have been described for this process, with corresponding rate constant estimates in the minute range (3.4.3.3.1). Synaptic vesicle re-use, as assessed by monitoring synaptic responses to consecutive hypertonic sucrose applications over several minutes, is not impaired in double mutant neurons (Fig. 21), which indicates that under resting conditions SV endocytosis and recycling of primed RRP vesicles are not affected by the SNAP deficiency. In addition, RRP refilling after RRP depletion using hypertonic sucrose is not altered at basal or increased Ca^{2+} levels (Fig. 21-22). RRP refilling processes are know to be faster in the presence of increased intracellular Ca^{2+} concentrations (Dittmann and Regher, 1998; Stevens and Wesseling, 1998; Wang and Kaczmarek, 1998). In the corresponding experiments described here, I used a 10 Hz stimulation protocol to load Ca^{2+} into presynaptic

terminals. Under these stimulation conditions and in the presence of standard Ca^{2+}/Mg^{2+} concentrations (4 mM each) release is predominantly phasic with insignificant contribution of tonic release (data not shown). Both in the presence and in the absence of stimulation, and after depletion of the sucrose-sensitive pool, SVs are recruited and primed into the RRP with similar kinetics in double mutant and control neurons, indicating that SVs can be recruited and primed efficiently into the RRP and the mutation does not alter the kinetics of this process.

The NSF/SNAP machinery is required to maintain a pool of SNAREs in their active state. Strong reductions in SNAP levels are likely to result in a reduction of the free SNAREs available for fusion, due to an accumulation of SNARE complexes. Since priming is known to depend on the formation of *trans*-SNARE complexes, mutations that limit the availability of SNAREs would be expected to limit SV priming. However I did not detect an impairment in RRP refilling kinetics after pool depletion in the experiments discussed so far. This indicates that the remaining α-SNAP activity is sufficient to maintain a pool of active SNAREs that is large enough to support SV cycling and RRP refilling in the conditions tested. Thus, under resting conditions and during moderate stimulation, the RRP seems to have a rather low requirement for the SNARE complex disassembly activity, as a strong reduction in SNAP levels by ~70% only moderately affects its size and has no impact on its refilling after depletion and SVs cycling.

4.5 Different Forms of Asynchronous Neurotransmitter Release

Traditionally, four types of asynchronous release have been described: (1) Asynchronous release evoked by single APs, (2) tonic release, (3) delayed release, and (4) spontaneous release. By definition, these release forms are termed “asynchronous” because they are not synchronously coupled to the stimulation or occur even in the absence of stimulation, as is the case for spontaneous release. To date, it is common use to refer to these distinct forms of release simply as “asynchronous”. In fact, early observations seemed to indicate that all these forms of release exhibit similar properties (e.g similar Ca^{2+} dependence), which led to the assumption that they are simply different manifestations of the heterogeneous nature of the same releasable SV pool. However, recent evidence indicates that this may not be the case. Indeed, these forms of release seem to be differentially regulated,

and may therefore represent unique mechanistic forms of release. Recent functional studies, particularly on Synaptotagmins and CAPS proteins, provided an excellent framework to determine the nature of these forms of neurotransmitter release.

Synaptotagmin-1 deficient neurons, although displaying normal single AP-evoked asynchronous release and tonic release, show a selective augmentation of spontaneous and delayed release (Maximov and Südhof, 2005). Similarly, a selective increase in mEPSC frequency was found in Synaptotagmin-2 knock-out mice at the calyx of Held synapse, where this Synaptotagmin isoform is believed to be the sensor for fast synchronous release (Pang et al., 2006). On the other hand, overexpression studies employing Synaptotagmin-12, an isoform that differs from classical Synaptotagmins in that it does not bind Ca^{2+}, induced a drastic and selective increase in spontaneous release in hippocampal neurons, while AP evoked release was not affected (Maximov et al., 2007).

Recently, CAPS-1 and -2 double knock-out neurons were analysed. Their phenotype is striking in that mutant neurons that display no evoked release at all (and therefore no AP-evoked synchronous or asynchronous release) and completely lack an RRP as assessed by hypertonic sucrose stimulation, show normal tonic release during high-frequency stimulation (Jockusch et al., 2007).

In summary, various different genetic and molecular manipulations can cause a selective impairment of either delayed, spontaneous or AP-evoked asynchronous release, indicating that these release forms indeed represent mechanicistically different variants of neurotransmitter release that are independently regulated. Interestingly, none of the genetic modifications reported so far was shown to cause a selective impairment of tonic release. As a consequence, the source of tonic release and its molecular components remain to be identified. As will be outlined below, it is in this context that the phenotype of SNAP mutant neurons provides novel and very useful information.

4.6 SNAP Double Mutant Neurons Show a Drastic Reduction in Bulk Ca^{2+}-Induced Neurotransmitter Exocytosis

A striking phenotype of SNAP double mutant neurons is that the sucrose-sensitive RRP pool is only slightly reduced by ~25% as compared to control cells (Fig. 17), while the total amount of neurotransmitter that can be released during a 100 Hz train

is much more strongly decreased (Fig. 25). So far, no stimulation protocols that can cause complete exhaustion of neurotransmitter release from hippocampal synapses have been reported (Hagler and Goda, 2001; Cliachko and Stevens, 2006; Pyott and Rosenmund, 2002). Indeed, even though 10-50 Hz stimulus trains of sufficient duration would probably suffice to deplete the sucrose-sensitive RRP in these neurons (Stevens and Williams, 2007; Moulder and Mennerick, 2005), they are not sufficient to deplete the tonic component of release, which is still present and prominent even after 100 stimuli at 40 Hz (Fig. 19). However, because SVs supporting tonic release are drawn from a depletable source (Otsu et al., 2004), very strong high-frequency stimulation trains may exhaust the tonic release component.

In order to compare the total amount of neurotransmitter that can be released from hippocampal autapses in SNAP deficient and wild-type neurons, I applied an intense stimulation protocol consisting of 900 stimuli given at 100 Hz. Surprisingly, double mutant neurons showed a drastic reduction in the total charge being transferred in response to the stimulation train. To characterise this phenomenon in more detail, I separately analysed the phasic and tonic release components. Several previously published studies reported that at higher stimulation frequencies release becomes predominantly tonic, with only a small phasic component (Alturi and Regher, 1998; Maximov and Südhof, 2005; Hefft and Jonas, 2005; Lu and Trussell, 2000). Consistent with this, tonic release was the major component of release in control neurons during the 100 Hz stimulation train, accounting for more than 80% of the total release (Fig. 25). While in these experiments phasic release was only moderately decreased in double mutant neurons, which is consistent with the observed slight reduction of RRP in mutant neurons, the tonic release component was strongly reduced. This allows for the conclusion that the strong reduction of total release observed in double mutant neurons during long 100 Hz stimulation trains mainly arises from a selective reduction in the tonic release component.

Another way of quantifying total synaptic neurotransmitter release takes advantage of the Ca^{2+} ionophore Calcymicin, which leads to fast and complete exhaustion of neurotransmitter release from presynaptic sites (Reim et al., 2001; Fernandez-Chacon et al., 2001; Jockusch et al., 2007). I observed a strong reduction of release induced by Calcimycin in double mutant neurons (Fig. 24), which is remarkably similar to the reduction I observed during the long 100 Hz stimulation. Calcimycin in fact mimics the effects of high-frequency stimulation, since both

stimulations lead to strong and prolonged increases in intracellular Ca^{2+} concentrations. Based on these findings, one can conclude that double mutant neurons show a strong reduction in total release elicited by bulk Ca^{2+} (either via electrical stimulation or via Ca^{2+} ionophores) and that this reduction selectively arises from changes in the tonic release component.

Tonic release has been shown to be dependent on increases in intracellular Ca^{2+} concentrations. Therefore, a possible explanation for the selective reduction of tonic release in double mutant neurons could be that Ca^{2+} channel density, localisation and/or function are impaired, thus causing reduced Ca^{2+} transients during AP trains. However, a strong reduction in neurotransmitter release is still detected when Ca^{2+} channels are bypassed by Calcimycin, indicating that alterations of Ca^{2+}channels density, localisation and/or function do not contribute to the phenotipic alteration of double mutant neurons. Furthermore, basal synaptic release properties are not altered in mutant cells (Fig. 20B), indicating that Ca^{2+} transients and Ca^{2+} handling by the presynaptic apparatus are not significantly affected by the mutation.

Taken together, my results showing that in double mutant neurons the sucrose sensitive pool is only slightly reduced while the total amount of neurotransmitter released by Ca^{2+} is drastically decreased, indicate that Ca^{2+} has access to a larger releasable SV pool than hypertonic sucrose. This would represent the first evidence for the existence of a pool of releasable SVs that can undergo Ca^{2+} regulated exocytosis but are insensitive to hypertonic sucrose stimulation. Based on to the data presented here, I propose that this Ca^{2+}-accessible SV pool supports tonic release.

4.7 Tonic Release Arises From a Separate SV Pool

Somewhat unexpectedly, my study on SNAP deficient neurons yielded interesting and unique data on the specific nature of tonic release. To date, three possible hypotheses have been formulated concerning the nature of tonic release: (1) Tonic release may arise from the summation of single-AP elicited “asynchronous” release during the train; (2) tonic release may reflect a continuous release process during the stimulation train, arising from fusion of primed SVs that enter into the RRP from an unprimed state, and are then immediately released in the presence of elevated intracellular Ca^{2+} - according to this hyopthesis, slow tonic release represents the desynchronization of the fusion of SVs that newly enter the RRP and immediately

fuse due to the residual Ca^{2+} accumulated in the terminal; or (3) tonic release may arise from a releasable pool of SVs that is distinct from the RRP.

The first hypothesis cannot account for the data described here, because the amount of asynchronous release elicited by single APs is very similar in mutant and control neurons, as indicated by the very similar shape of evoked EPSCs (Fig. 17A), but tonic release is strongly reduced in mutant cells. Thus, “asynchronous” release after single AP stimulation and tonic release seem to represent different mechanicistic forms of neurotransmitter release. Likewise, the second of the hypotheses described above fails to account for the data described in the present study, since I found that the kinetics of RRP refilling after depletion was unchanged in mutant cells at resting and elevated Ca^{2+} concentrations (Fig. 21-22). Therefore, the strong reduction in tonic release in double mutant neurons does not arise from slower basal or Ca^{2+}-stimulated priming rates of SVs into the RRP. Furthermore, phorbol ester dependent stimulation of neurotransmitter release, which in our experimental system is absolutely dependent on Munc13-mediated priming (Rhee et al 2002), was very similar in control and double mutant neurons, indicating that Munc13-dependent priming processes are not affected by the SNAP deficiency. Therefore, tonic release is unlikely to originate from release of SVs that continuously refill the RRP from an unprimed pool.

On the other hand, I found that the strong reduction of tonic release in double mutant cells was paralleled by a similar decrease in neurotransmitter release directly elicited by massive Ca^{2+} influx (Fig. 24). Since release induced by hypertonic sucrose showed only a comparatively moderate reduction in double mutant neurons (~25%), these data point towards the existence of an alternative pool of SVs, which is distinct from the sucrose-sensitive RRP, supports tonic release, and is accessible for release upon strong increases in Ca^{2+}-concentrations. The strongest support for this notion is provided by a recent study on CAPS-1 and -2 double deficient neurons (Jockusch et al., 2007). CAPS deletion selectively abolishes phasic release, while leaving the tonic component unaltered. The majority of CAPS double knock-out (DKO) neurons do not respond to hypertonic sucrose stimulation or single AP stimulation, although the expression level of Munc13 priming factors is normal. These findings can be taken as evidence for the existence of a pool of SVs that are selectively supporting tonic release, in addition to the sucrose-sensitive pool (RRP), which supports phasic release.

4.8 Two Sequential SV Pools Support Tonic and Phasic Release

The data discussed so far indicate that tonic release arises from a releasable SV pool that is distinct from the RRP. These two pools may represent sequential maturation or primed SV states, as it was previously suggested based on the analysis of CAPS-1 and 2 double knock-out neurons (Juckusch et al., 2007). If RRP vesicles are indeed derived from the tonic release pool by further modification or maturation, the present data on SNAP double mutant neurons would indicate that a ~60% reduction of the tonic release pool size is still able to maintain RRP refilling to control levels (Fig. 21-22). However, further reductions of the tonic pool size should eventually limit RRP recovery. To test this prediction, I analysed RRP recovery of double mutant and control neurons after 40 Hz stimulation. The 40 Hz train, in addition to completely depleting the RRP, also reduces the tonic release pool size by releasing SVs from this pool (Fig. 19C). Furthermore, this stimulation is expected to empty the pool in double mutant neurons to a greater extent than in controls, since their tonic release pool is already strongly reduced. Thus, if a further reduced tonic pool becomes limiting for RRP recovery, one would expect RRP recovery after 40 Hz stimulation to be more strongly affected in double mutant neurons because of their smaller residual tonic pool at the end of the 40 Hz train.

As expected, RRP recovery rates in mutant neurons are markedly slower than in controls after electrical discharge of the RRP by a 40 Hz stimulation. Since I showed that the RRP refilling rate itself is not changed at resting Ca^{2+} concentrations or in the presence of high Ca^{2+} concentrations (Fig. 21-22), these data indicate that RRP refilling after 40 Hz stimulation is slower in double mutant neurons as a consequence of the further reduced tonic release pool, which has become a limiting factor for RRP recovery (Fig. 29).

I measured RRP refilling rates after hypertonic sucrose depletion of the RRP in the presence of continuous 10 Hz stimulation (Fig. 22), and after electrical discharge of the RRP via 100 stimuli at 40 Hz (Fig. 23). These two experimental approaches have been used before as a readout for Ca^{2+}-dependent refilling kinetics of the RRP, since in both, Ca^{2+} concentrations are increased as a consequence of activity (Dittmar and Regher, 1998; Stevens and Wesseling, 1998; Sakaba and Neher, 2001). Intriguingly, I obtained opposing results with the two protocols as the first indicated no change in RRP refilling kinetics in SNAP double mutant animals while

the latter did. Based on the currently accepted interpretation of the two experimental approaches, it is thus not possible to conclude if Ca^{+2} dependent RRP refilling is impaired in double mutant neurons or not. However, two major differences between the two experiments must be considered. First, while continuous 10 Hz stimulation allows the exact measurement of Ca^{2+}-dependent RRP refilling rates since Ca^{2+} is maintained at high levels by continuous stimulation, in the 40 Hz experiment Ca^{2+} is increased only during the RRP depletion and EPSC recovery is then monitored up to 30 seconds after the stimulation, a time long enough for Ca^{2+} concentrations to decay to basal levels. In fact, estimates of the slow decay time constant of AP evoked Ca^{2+} transients are in the order of a few hundred milliseconds (Helmchen et al., 1997; Mueller et al., 2007). The 40 Hz experiment therefore cannot be taken as readout for Ca^{2+} dependent refilling kinetics of the RRP. Second, 40 Hz stimulation trains can elicit prominent tonic release, while hypertonic sucrose has been shown to leave the tonic release component largely unaffected (Otsu et al., 2004), even in the presence of 10 Hz stimulation. This major difference between the two stimuli employed to deplete the RRP is expected to have strong impact on RRP recovery, especially if tonic and phasic release are supported by sequential SV primed states (Jockusch et al., 2007; see below). Therefore, EPSC recovery after electrical discharge of the RRP cannot be taken as a direct measure of Ca^{2+} dependent refilling rates. Rather, it provides a readout for RRP recovery in which several factors come into play, including Ca^{2+} transient kinetics and tonic release pool size. In the light of above considerations, my data indicate that Ca^{2+}-dependent and -independent RRP refilling rates are not changed in double mutant neurons, but that RRP recovers more slowly after 40 Hz stimulation as a consequence of the profound reduction of the tonic release pool.

My data thus support a model according to which tonic release represents a first intermediate priming step before the establishment of the RRP. Interestingly, similar interdependent two-pool models were recently proposed to describe neurotransmitter release at central synapses. It was suggested that the tonic release pool and the RRP may correspond to sequential maturation steps of SVs (Jockusch et al., 2007), with Munc13s first generating a primed pool of SVs that can support tonic release, which then matures via CAPS action into the RRP that supports phasic release. In addition, at the calyx of Held synapse it was beautifully shown that the recovery of fast-releasing vesicles is retarded when the recovery of the slowly-releasing vesicles

is slowed down (Sakaba and Neher, 2003). These and other more recent observations (Sakaba, 2006) led to the working hypothesis that the two SV pools are kinetically interdependent, with slow-releasing vesicles supporting recovery of fast-releasing ones.

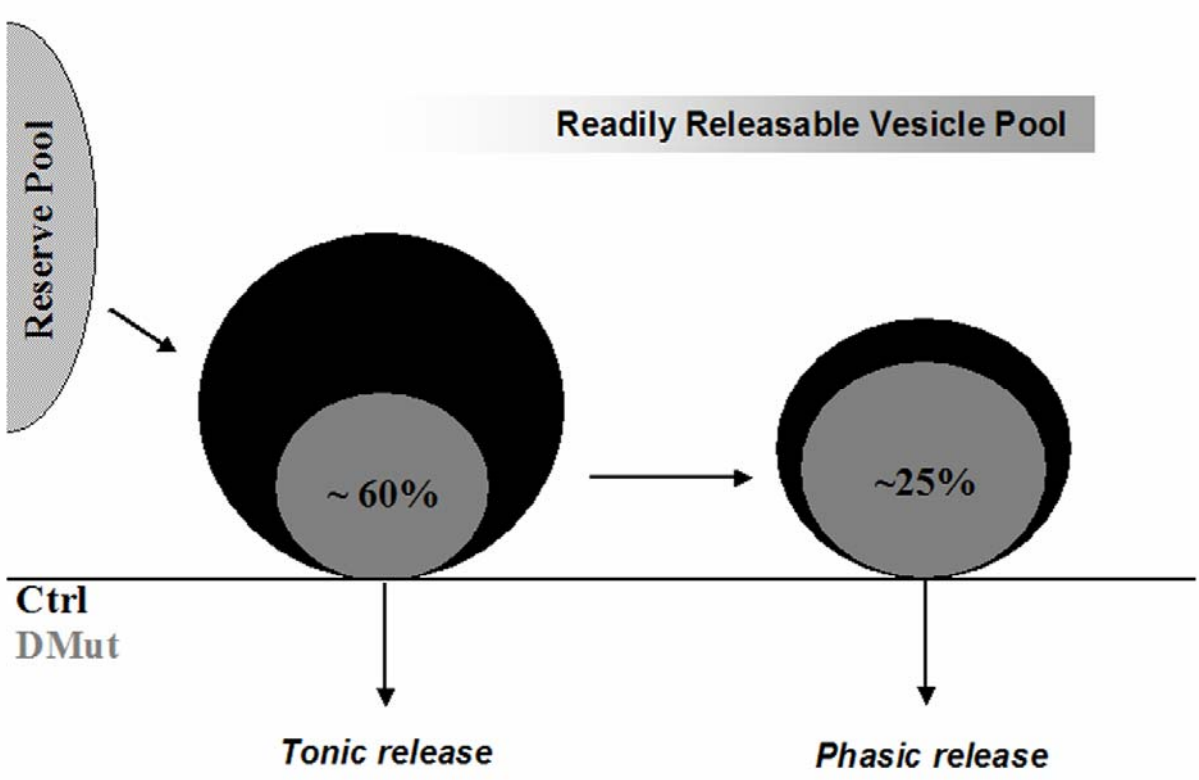

Figure 29 **Neurotransmitter Release During High-Frequency Stimulation in SNAP Double Mutant and Control Neurons.** The model describes the impairment of neurotransmitter release in SNAP double mutant neurons as observed during high-frequency stimulation trains. Double mutant neurons (grey) display a strong reduction in the tonic component of release as compared to controls (black), while phasic release (which probably arises from the sucrose sensitive pool, the RRP) is only moderately decreased.

In summary, I showed that RRP recovery rates are not changed in SNAP mutant cells when tonic release is not elicited. Since I estimated the tonic release pool to be reduced by ~60% in mutant neurons as compared to controls, one can conclude that a ~60% reduction of the tonic release pool can still support RRP refilling to control levels. However, when the tonic release pool is further reduced (e.g. via a 40 Hz stimulation train) it cannot support RRP refilling to control levels any more, and a

slower RRP recovery becomes apparent. These data support a sequential two-pool model to describe neurotransmitter release at hippocampal synapses during high-frequency stimulation, with slow-releasing SVs (primed for tonic release) and fast-releasing SVs (primed for phasic release) corresponding to sequential primed states.

Despite the argumentation developed above, it could be argued that when a higher stimulation frequency is employed, refilling processes of the RRP become slower in double mutant neurons - the stronger the stimulation challenge to the synapse, the slower the RRP recovery. This simple interpretation could in principle explain why double mutant neurons recover more slowly after 40 Hz stimulation but not in the presence of an ongoing 10 Hz stimulation. To exclude this possibility, I monitored RRP recovery after 900 stimuli delivered at 100 Hz. I showed before that this stimulation can almost completely deplete neurotransmitter release from presynaptic terminals, by inducing massive SV exocytosis from presynaptic terminals (Fig. 25). If stronger stimulation challenges were really causing a slower RRP recovery, one would predict RRP recovery of double mutant neurons to be more drastically impaired upon 100 Hz stimulation than after the previous 40 Hz stimulation train. However, this was not the case, since, relative to controls, double mutant neurons recovered even faster from 100 Hz stimulation than in the experiment employing 40 Hz stimulation. Therefore, it can be concluded that the strength of the stimulation itself cannot account for the slower RRP recovery observed in double mutant neurons after 40 Hz trains, and it is likely that this phenomenon is directly correlated to the size of the tonic release “feeding-pool” (Fig. 29).

A model of rapid re-use of SNARE complexes at synapses that would maintain synaptic transmission, as suggested by Kawasaki et al. (1998) based on work on Comatose mutant neuromuscular junctions (Kawasaki et al., 1998), is also not consistent with our data. This model implies that accumulation of *cis*-SNARE complexes as a result of SV fusion becomes limiting for RRP recovery. This process is expected to be strictly dependent on the amount of exocytosis elicited, since the more SVs are exocytosed, the more *cis*-SNARE complexes are forming. It is however important to point out that, in absolute terms, the number of SVs undergoing fusion during the 10Hz-10Hz/Sucrose stimulation protocol (Fig. 22A) is actually higher than during the 40 Hz train employed (Fig. 23). Therefore, if post-fusion accumulation of SNARE complexes becomes limiting for subsequent rounds of fusion, a slower RRP recovery in double mutant neurons would be expected after the 10 Hz protocol, and

not vice versa. It could, of course, be argued that at 10 Hz (one stimulus every 100 ms), even though more *cis*-SNARE complexes are formed than during 40 Hz trains, they do not accumulate in double mutant neurons because they are readily disassembled during inter-stimulus intervals. On the other hand, at 40 Hz (one stimulus every 25 ms), less *cis*-complexes are formed, but they might accumulate because their disassembly is not fast enough to happen in the inter-stimulus intervals, and hence RRP recovery of double mutant neurons might become slower after the train. However, I would argue that this explanation is not likely, since even 100 ms appear to be too short for a complex biochemical reaction to take place, that consists of a sequence of at least three events, i.e. binding of SNAP molecules, recruitment and activation of NSF, and several rounds of catalytic ATP-dependent activity, which are necessary to completely disassemble the SNARE complex (Hanson and Whiteheart, 2005). Another argument against the notion that altered rapid re-use of SNAREs is causally involved in the phenotype of SNAP deficient neurons is provided by the paired hypertonic sucrose stimulation experiments, which were used to monitor RRP refilling under basal conditions (Fig. 21). Here, already 200 ms after the RRP had been depleted, no difference between double mutant and control neurons was evident with regard to the fraction of the releasable pool that had recovered. Essentially, I would conclude based on the above arguments that different phenotypic alterations would be expected in SNAP double mutant neurons if alterations in rapid SNARE complex disassembly and reuse were the basis of the mutant phenotype.

4.9 Molecular Model to Describe Synaptic Neurotransmitter Release During High-Frequency Stimulation

The present and recently published data (Jockusch et al., 2007; Sakaba and Neher, 2003; Sakaba, 2006) are consistent with a two-pool model of neurotransmitter release at synapses during high-frequency stimulations, with one SV pool supporting tonic release, and a sucrose-sensitive pool, functionally defined as the RRP, supporting fast, phasic release (Fig. 30). Interestingly, the existence of two molecularly distinct SV pools differing in the state of the *trans*-SNARE complex has been postulated for chromaffin cells - one pool of vesicles, whose *trans*-SNARE complexes are in a “loose” configuration, contributing to the slow component of the

release burst, and a second pool of vesicles whose *trans*-SNARE complexes are in a in a “tight” state that allows for the fast phase of release (Xu et al., 1999). Assembly of *trans*-SNARE complexes was proposed to proceed sequentially from the “loose” to the “tight” configuration. Analogously, at synapses the SV priming reaction may consist of two sequential steps (Fig. 30). First, SVs approaching the active zone initially undergo formation of *trans*-SNARE complexes in the “loose” configuration. In this configuration, SVs are primed for slow, tonic release. Subsequently late regulatory proteins like Complexins, CAPS, and Synaptotagmin-1 would regulate the transition from “loose” to “tight” *trans*-SNARE configuration. In this highly-fusogenic metastable “tight” state, SVs are primed for fast, phasic release.

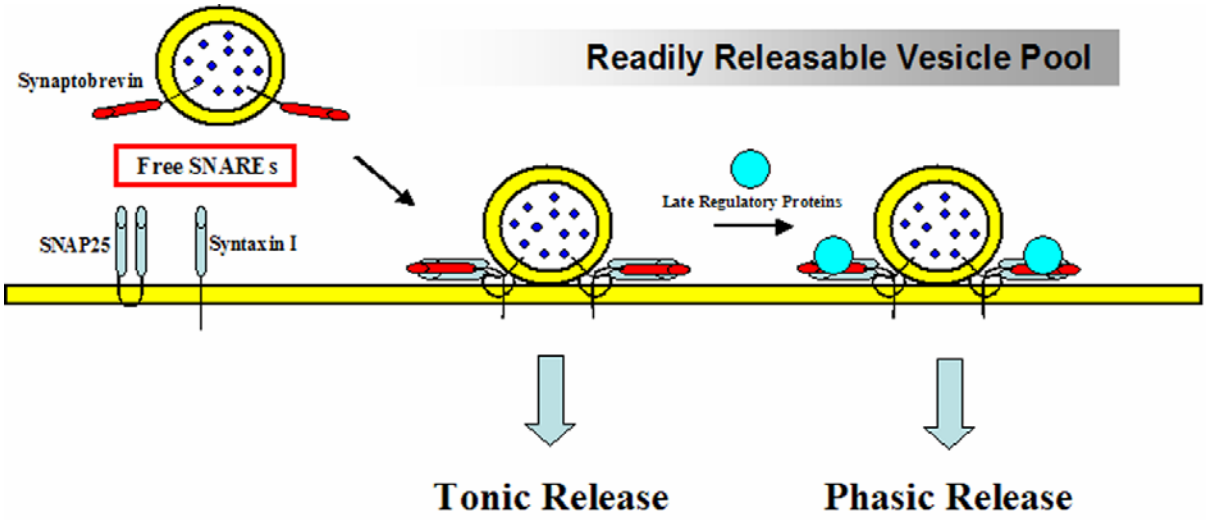

Figure 30 **Molecular Model of Neurotransmitter Release During High-Frequency Stimulation.** A sequential two-pool model can describe neurotransmitter release during high-frequency stimulation. From the molecular point of view, the SV priming reaction may consist of two sequential steps. First, SVs undergo formation of *trans*-SNARE complexes in the “loose” configuration, and are thus first primed for slow, tonic release. Subsequently, late regulatory proteins mediate the transition from “loose” to “tight” *trans*-SNARE complex configuration. In this highly-fusogenic metastable “tight” state, SVs are primed for fast, phasic release.

The present study indicates that genetic impairment of the SNARE complex disassembly machinery, which is likely to result in a reduction of free “active” neuronal SNAREs, leads to a strong reduction of the tonic release pool. The above model predicts this pool, but not the RRP, to be dependent on the amount of free

SNAREs available for priming, because priming into the RRP for fast release has been designated a virtually irreversible “locking” step due to the fact that its de-priming kinetics are very slow (Nagy et al., 2004; Heidelberger and Mattews, 2004; Heidelberger et al., 2002). These predictions are consistent with the present data, which show that, despite a strong reduction of the tonic release pool in SNAP double mutant neurons, the limited RRP “slots” are almost fully occupied by SVs locked in the primed state for phasic release (Fig. 29).

4.10 The SNAP Double Mutant Phenotype is Due to a Decrease in SNAP Dosage

A number of findings indicate that the aberrant synaptic phenotype observed in SNAP double mutant neurons is specifically due to a decrease in SNAP levels and not to changes that are secondary to the mutation. First, while single mutant mice are alive at birth, double mutant mice die perinatally, indicating a cumulative gene-dosage effect of the SNAP mutations. Second, glutamatergic synaptic transmission is selectively impaired in double mutant neurons, while no evidence of impairment was found in single mutant cells, again indicating a gene-dosage effect. Third, and most importantly, I showed that the double mutant phenotype can be rescued by reintroducing high levels of SNAP proteins, with α- and β-SNAP being equally efficient in this rescue.

Double mutant neurons express only low levels of a mutated form of α-SNAP, the HYH mutant. It can therefore be argued that the phenotype observed in double mutant neurons might be due to a dominant negative effect of the point mutant α-SNAP, which is the only SNAP isoform expressed. However, this is unlikely because HYH neurons showed no detectable alteration of synaptic transmission, because overexpression of HYH in wild-type neurons did not affect synaptic transmission, and because the HYH mutation did not disrupt the *in vitro* interaction of α-SNAP with previously identified putative interaction partners. Based on these arguments, one can safely conclude that the observed synaptic phenotype in SNAP double mutant neurons is primarily due to a decrease in SNAP levels, which in glutamatergic neurons becomes limiting for SVs exocytosis.

It is interesting to note in this context that SNAP levels seem to be super-saturating in glutamatergic hippocampal neurons *in vivo* - SNAP overexpression in

wild-type neurons had no effect (Fig. 26), and only a strong reduction of SNAP levels interferes glutamatergic synaptic transmission (Fig. 17). Indeed, SNAPs are very abundant in the brain (McMahon et al., 1995). These very high SNAP levels are probably responsible for the high efficiency of the SNARE complex disassembly machinery, which, under physiological conditions, is able to maintain the great majority of SNAREs in their uncomplexed state, as suggested by the fact that only very low levels of complexes can be detected *in vivo* under normal conditions (Fig. 10-16; Sanjal et al., 2001). However, the fact that β-SNAP mutant mice suffer from profound epilepsy indicates that other neuron types are more susceptible to reductions in SNAP levels, probably because their normal SNAP levels are lower than those of the neurons tested in the present study.

4.11 Analogies Between SNAP Double Mutant and *Drosophila* Comatose Mutant Synaptic Phenotypes

Basic neurotransmitter release is remarkably similar in SNAP double mutant synapses and *Drosophila* Comatose (i.e. NSF-mutant) neuromuscular synapses. For the latter, Kawasaki et al. (1998) reported that repetitive stimulation causes a stronger depression of evoked responses in Comatose mutants as compared to wild-type controls, while neurotransmitter release evoked by single stimulations was not impaired. This is remarkably similar to the present results, which show that in SNAP double mutant neurons EPSCs evoked by single APs were normal, while glutamate release was strongly depressed during high-frequency stimulation trains (Fig. 25). As NSF and SNAPs are components of the same SNARE complex disassembly machinery, the striking similarities between SNAP double mutant and Comatose mutant synapses indicate that indeed an impairment of SNARE complex disassembly is the underlying cause of the two phenotypes.

Kawasaki et al. (1998) attributed the activity-dependent depression of evoked responses in the Comatose neuromuscular junction to a parallel decrease in RRP size. Consequently, NSF-mediated SNARE complex disassembly was proposed to function in SV priming by maintaining the size of the primed SV pool under high-frequency stimulation protocols. However, the neuromuscular junction preparation that was used by these authors to study Ca^{2+}-regulated neurotransmitter exocytosis is not optimally accessible for detailed measurements of release parameters such as

RRP or P_{vr}. Kawasaki et al. (1998) only measured evoked postsynaptic potentials elicited by direct stimulation of axons innervating dorsal longitudinal flight muscles but did not directly measure RRP size or P_{vr}. Particularly information on the latter would have been important for the interpretation of the Comatose phenotype because the very fast onset of the activity-dependent phenotype, requiring less than 1 sec (Kawasaki et al., 1998), may be indicative of altered vesicular release probability in Comatose mutants.

The autaptic culture system used here has proven to be extremely useful for the detailed characterisation of the neurotransmitter release process under conditions of genetic impairment of SNARE complex disassembly. In particular, it allowed me to extend the initial observations made by Kawasaki et al. (1998) to central mammalian synapses. Moreover, using this system, I was able to elucidate the reasons for the apparent RRP "instability" during high-frequency stimulation, that Kawasaki et al. (1998) interpreted as a defect in SV recruitment. Based the present data, I propose an alternative model according to which SNARE complex disassembly is a key determinant for the generation of the SV pool that supports tonic release.

4.12 Impact of the SNAP Mutation on Synaptic Physiology

The genetic impairment of the SNARE complex disassembly machinery has severe consequences for the physiology of synaptic transmission. Although single-AP evoked neurotransmitter release is remarkably similar between SNAP double mutant and control neurons, short-term synaptic plasticity is drastically impaired. Mutant synapses show stronger and faster depression of evoked responses during trains of activity (Fig. 19). The more rapid decay of phasic release induced by high frequency stimulation trains is predicted to have profound effects on neuronal network information processing in double mutant brains, since phasic release is the main determinant of the temporal and spatial precision of information transfer in nerve cell communication (Hull and Scanziani, 2007; Gabernet et al., 2005).

In vivo, neurons do not typically fire single APs that are widely separated in time. More typically, firing patterns are often characterized by bursts at tens of Hz or even higher frequency trains (Alturi and Regher, 1998). During very high frequency trains, the temporal precision of the stimulation pattern is lost very rapidly, and a continuous tonic current is elicited in the postsynaptic cell long after the phasic component has

decayed. Even though tonic release seems to be a physiological and prominent mode of synaptic information transfer in the brain, its significance has been poorly investigated. SNAP double mutant neurons display a strong decrease in the tonic component of release elicited during high-frequency stimulation trains. Therefore, in addition to an impairment of fast phasic information processing, mutant neurons would also respond aberrantly to long-lasting trains of activity in the brain. It is therefore not surprising that SNAP double mutant mice die perinatally. In mice, brain networks controlling basic body functions that are necessary to support life are mature and completely functional at birth (Varoqueaux et al., 2006; Schuelter et al., 2004). The present data indicate that these basic network functions may not be correctly supported by double mutant neurons, whose synaptic transmission is considerably "weaker" than normal, thus leading to perinatal death.

4.13 α- and β-SNAP are Functionally Equivalent

An additional major conclusion from the present study is that α- and β-SNAP appear to be functionally equivalent isoforms. Several lines of evidence support this conclusion. First of all, I demonstrated a genetic interaction between the α- and β-SNAP mutation. While single mutant mice are alive at birth and display no sign of impairment of glutamatergic transmission, double mutants die perinatally and show strong impairment of presynaptic glutamate release. Second, α- and β-SNAP display very similar biochemical properties *in vitro*. Both isoforms can be incorporated into the 20S complex and mediate its disassembly via NSF and ATP-hydrolysis. Third, and most importantly, both α- and β-SNAP rescue the phenotype of double mutant neurons.

However, if α- and β-SNAP are functionally equivalent, one might expect single mutant mice to have similar phenotypes. This is obviously not the case as the hypomorphic HYH mutation of α-SNAP causes progressive hydrocephalus and strong developmental abnormalities of the brain, while β-SNAP deletion has no impact on brain structure but leads to severe seizures. This apparent contradiction can be explained by taking into account the expression pattern of the two isoforms. Only α-SNAP is expressed during embryonic development, and the decrease of α-SNAP levels observed in HYH brains cannot be complemented by the β-SNAP isoform, which first appears around birth, once the developmental defects of HYH

mutants are already apparent. In β-SNAP deletion mutant mice, on the other hand, brain development occurs normally, and the lack of the β-SNAP isoform in glutamatergic neurons is probably compensated by α-SNAP, which alone seems to be sufficient to support normal glutamatergic transmission.

Therefore, SNAP isoforms are important for both brain development and synaptic function. During embryonic life, α-SNAP alone is necessary to support normal brain development, which is apparently very sensitive to a decrease in SNAP levels. Starting from birth, increased SNAP levels are necessary to support normal brain function. This additional need for SNAP in the period of synapse formation and function indicates a role of SNAPS in tuning and shaping network activity in the brain.

5. Summary and Conclusions

In summary, the two aims of my study were successfully accomplished. First, I provided a description of the **role of SNARE recycling** in SV exocytosis at central synapses. My data indicate that tonic release is strongly decreased as a result of genetic impairment of the SNARE complex disassembly machinery. On the other hand, phasic release is only mildly affected by the SNAP mutations. The present is the first report on a mutant mouse phenotype that shows a rather selective impairment of the tonic component of neurotransmitter release. This surprising finding sheds light on the mechanistic and molecular nature of this form of release. The present data indicate that tonic release arises from a subpool of releasable SVs that is distinct from the RRP. This tonically releasable pool is accessible for release triggered by Ca^{2+} but not for hypertonic sucrose stimulation. My data also indicate that the tonic release pool and the RRP may represent sequential maturation and/or allosteric states of primed SVs, the first being highly dependent on the level of available free SNAREs, and the latter being stabilised by late regulatory proteins (e.g. CAPS) for fast, phasic release. Second, I showed that **α- and β-SNAP are functionally equivalent** isoforms, at least in the context of glutamatergic synaptic transmission. Furthermore, unlike other neurosecretory systems or synapses (1.10.2) where SNAP overexpression was shown to have a modulatory effect on exocytosis, SNAP levels in mammalian glutamatergic synapses seem to be saturating, since SNAP overexpression has no effect on synaptic transmission and only a strong reduction of SNAP levels is limiting SV exocytosis.

6 Bibliography

Aravanis, A. M., J. L. Pyle, et al. (2003). "Single synaptic vesicles fusing transiently and successively without loss of identity." Nature **423**(6940): 643-7.

Abad, R. S., F. X. Vilaplana, et al. (2007). "Genetic causes of epilepsy." Neurologist **13** (6 suppl 1), S47-51

Atluri, P. P. and W. G. Regehr (1998). "Delayed release of neurotransmitter from cerebellar granule cells." J Neurosci **18**(20): 8214-27.

Atwood, H. L. and S. Karunanithi (2002). "Diversification of synaptic strength: presynaptic elements." Nat Rev Neurosci **3**(7): 497-516.

Augustin, I., C. Rosenmund, et al. (1999). "Munc13-1 is essential for fusion competence of glutamatergic synaptic vesicles." Nature **400**(6743): 457-61.

Bai, J. and E. R. Chapman (2004). "The C2 domains of synaptotagmin--partners in exocytosis." Trends Biochem Sci **29**(3): 143-51.

Banerjee, A., V. A. Barry, et al. (1996). "N-Ethylmaleimide-sensitive factor acts at a prefusion ATP-dependent step in Ca2+-activated exocytosis." J Biol Chem **271**(34): 20223-6.

Barndt, R. J., M. Dai, et al. (2000). "Functions of E2A-HEB heterodimers in T-cell development revealed by a dominant negative mutation of HEB." Mol Cell Biol **20**(18): 6677-85.

Barrett, E. F. and C. F. Stevens (1972). "The kinetics of transmitter release at the frog neuromuscular junction." J Physiol **227**(3): 691-708.

Barry, M. A., S. Haglund, et al. (2001). "Association of extracellular acetylcholinesterase with gustatory nerve terminal fibers in the nucleus of the solitary tract." Brain Res **921**(1-2): 12-20.

Bartos, M., I. Vida, et al. (2007). "Synaptic mechanisms of synchronized gamma oscillations in inhibitory interneuron networks." Nat Rev Neurosci **8**(1): 45-56.

Batiz, L. F., P. Paez, et al. (2006). "Heterogeneous expression of hydrocephalic phenotype in the hyh mice carrying a point mutation in alpha-SNAP." Neurobiol Dis **23**(1): 152-68.

Bekkers, J. M. and C. F. Stevens (1991). "Excitatory and inhibitory autaptic currents in isolated hippocampal neurons maintained in cell culture." Proc Natl Acad Sci U S A **88**(17): 7834-8.

Bergmann, M., G. Lahr, et al. (1991). "Expression of synaptophysin during the prenatal development of the rat spinal cord: correlation with basic differentiation processes of neurons." Neuroscience **42**(2): 569-82.

Betz, A., P. Thakur, et al. (2001). "Functional interaction of the active zone proteins Munc13-1 and RIM1 in synaptic vesicle priming." Neuron **30**(1): 183-96.

Bhalla, A., M. C. Chicka, et al. (2006). "Ca(2+)-synaptotagmin directly regulates t-SNARE function during reconstituted membrane fusion." Nat Struct Mol Biol **13**(4): 323-30.

Bittner, M. A. and R. W. Holz (1992). "Kinetic analysis of secretion from permeabilized adrenal chromaffin cells reveals distinct components." J Biol Chem **267**(23): 16219-25.

Borst, J. G. and B. Sakmann (1996). "Calcium influx and transmitter release in a fast CNS synapse." Nature **383**(6599): 431-4.

Brill, J., R. Klocke, et al. (2004). "entla, a novel epileptic and ataxic Cacna2d2 mutant of the mouse." J Biol Chem **279**(8): 7322-30.

Brose, N., K. Hofmann, et al. (1995). "Mammalian homologues of Caenorhabditis elegans unc-13 gene define novel family of C2-domain proteins." J Biol Chem **270**(42): 25273-80.

Brose, N., A. G. Petrenko, et al. (1992). "Synaptotagmin: a calcium sensor on the synaptic vesicle surface." Science **256**(5059): 1021-5.

Brusa, R., F. Zimmermann, et al. (1995). "Early-onset epilepsy and postnatal lethality associated with an editing-deficient GluR-B allele in mice." Science **270**(5242): 1677-80.

Catsicas, S., D. Larhammar, et al. (1991). "Expression of a conserved cell-type-specific protein in nerve terminals coincides with synaptogenesis." Proc Natl Acad Sci U S A **88**(3): 785-9.

Chae, T. H., S. Kim, et al. (2004). "The hyh mutation uncovers roles for alpha Snap in apical protein localization and control of neural cell fate." Nat Genet **36**(3): 264-70.

Chandra, S., G. Gallardo, et al. (2005). "Alpha-synuclein cooperates with CSPalpha in preventing neurodegeneration." Cell **123**(3): 383-96.

Chen, X., D. R. Tomchick, et al. (2002). "Three-dimensional structure of the complexin/SNARE complex." Neuron **33**(3): 397-409.

Chen, Y. A. and R. H. Scheller (2001). "SNARE-mediated membrane fusion." Nat Rev Mol Cell Biol **2**(2): 98-106.

Cheung, Z. H. and N. Y. Ip (2007). "The roles of cyclin-dependent kinase 5 in dendrite and synapse development." Biotechnol J **2**(8): 949-57.

Chitwood, R. A., A. Hubbard, et al. (1999). "Passive electrotonic properties of rat hippocampal CA3 interneurones." J Physiol **515 (Pt 3)**: 743-56.

Collins, R. L. and J. L. Fuller (1968). "Audiogenic seizure prone (asp): a gene affecting behavior in linkage group 8 of the mouse." Science **162**(858): 1137-9.

Crowder, K. M., J. M. Gunther, et al. (1999). "Abnormal neurotransmission in mice lacking synaptic vesicle protein 2A (SV2A)." Proc Natl Acad Sci U S A **96**(26): 15268-73.

Cummings, D. D., K. S. Wilcox, et al. (1996). "Calcium-dependent paired-pulse facilitation of miniature EPSC frequency accompanies depression of EPSCs at hippocampal synapses in culture." J Neurosci **16**(17): 5312-23.

Daly, C. and E. B. Ziff (1997). "Post-transcriptional regulation of synaptic vesicle protein expression and the developmental control of synaptic vesicle formation." J Neurosci **17**(7): 2365-75.

Danzer, S. C., K. R. Crooks, et al. (2002). "Increased expression of brain-derived neurotrophic factor induces formation of basal dendrites and axonal branching in dentate granule cells in hippocampal explant cultures." J Neurosci **22**(22): 9754-63.

Davis, A. F., J. Bai, et al. (1999). "Kinetics of synaptotagmin responses to Ca2+ and assembly with the core SNARE complex onto membranes." Neuron **24**(2): 363-76.

Deak, F., S. Schoch, et al. (2004). "Synaptobrevin is essential for fast synaptic-vesicle endocytosis." Nat Cell Biol **6**(11): 1102-8.

DeBello, W. M., V. O'Connor, et al. (1995). "SNAP-mediated protein-protein interactions essential for neurotransmitter release." Nature **373**(6515): 626-30.

Deitcher, D. L., A. Ueda, et al. (1998). "Distinct requirements for evoked and spontaneous release of neurotransmitter are revealed by mutations in the Drosophila gene neuronal-synaptobrevin." J Neurosci **18**(6): 2028-39.

Dittman, J. S. and W. G. Regehr (1998). "Calcium dependence and recovery kinetics of presynaptic depression at the climbing fiber to Purkinje cell synapse." J Neurosci **18**(16): 6147-62.

Elmqvist, D. and D. M. Quastel (1965). "A quantitative study of end-plate potentials in isolated human muscle." J Physiol **178**(3): 505-29.

Enquist, I. B., C. Lo Bianco, et al. (2007). "Murine models of acute neuronopathic Gaucher disease." Proc Natl Acad Sci U S A **104**(44): 17483-8.

Farsad, K. and P. De Camilli (2002). "Neurotransmission and the synaptic vesicle cycle." Yale J Biol Med **75**(5-6): 261-84.

Fasshauer, D., W. Antonin, et al. (1999). "Mixed and non-cognate SNARE complexes. Characterization of assembly and biophysical properties." J Biol Chem **274**(22): 15440-6.

Fasshauer, D., W. K. Eliason, et al. (1998). "Identification of a minimal core of the synaptic SNARE complex sufficient for reversible assembly and disassembly." Biochemistry **37**(29): 10354-62.

Fernandez-Chacon, R., A. Konigstorfer, et al. (2001). "Synaptotagmin I functions as a calcium regulator of release probability." Nature **410**(6824): 41-9.

Frankel, W. N., B. A. Taylor, et al. (1994). "Genetic epilepsy model derived from common inbred mouse strains." Genetics **138**(2): 481-9.

Fuerst, P. G., A. Koizumi, et al. (2008). "Neurite arborization and mosaic spacing in the mouse retina require DSCAM." Nature **451**(7177): 470-4.

Furshpan, E. J. (1989). "A cell-culture approach to the study of seizure activity." Q J Exp Physiol **74**(7): 975-85.

Gabernet, L., S. P. Jadhav, et al. (2005). "Somatosensory integration controlled by dynamic thalamocortical feed-forward inhibition." Neuron **48**(2): 315-27.

Gandhi, S. P. and C. F. Stevens (2003). "Three modes of synaptic vesicular recycling revealed by single-vesicle imaging." Nature **423**(6940): 607-13.

Gassmann, M., H. Shaban, et al. (2004). "Redistribution of GABAB(1) protein and atypical GABAB responses in GABAB(2)-deficient mice." J Neurosci **24**(27): 6086-97.

Geppert, M., B. T. Archer, 3rd, et al. (1991). "Synaptotagmin II. A novel differentially distributed form of synaptotagmin." J Biol Chem **266**(21): 13548-52.

Gerber, S. H. and T. C. Sudhof (2002). "Molecular determinants of regulated exocytosis." Diabetes **51 Suppl 1**: S3-11.

Goda, Y. and C. F. Stevens (1994). "Two components of transmitter release at a central synapse." Proc Natl Acad Sci U S A **91**(26): 12942-6.

Gracheva, E. O., A. O. Burdina, et al. (2006). "Tomosyn inhibits synaptic vesicle priming in Caenorhabditis elegans." PLoS Biol **4**(8): e261.

Hagler, D. J., Jr. and Y. Goda (2001). "Properties of synchronous and asynchronous release during pulse train depression in cultured hippocampal neurons." J Neurophysiol **85**(6): 2324-34.

Hanley, J. G., L. Khatri, et al. (2002). "NSF ATPase and alpha-/beta-SNAPs disassemble the AMPA receptor-PICK1 complex." Neuron **34**(1): 53-67.

Hanson, P. I., H. Otto, et al. (1995). "The N-ethylmaleimide-sensitive fusion protein and alpha-SNAP induce a conformational change in syntaxin." J Biol Chem **270**(28): 16955-61.

Hanson, P. I. and S. W. Whiteheart (2005). "AAA+ proteins: have engine, will work." Nat Rev Mol Cell Biol **6**(7): 519-29.

Hayashi, T., H. McMahon, et al. (1994). "Synaptic vesicle membrane fusion complex: action of clostridial neurotoxins on assembly." Embo J **13**(21): 5051-61.

Hayashi, T., S. Yamasaki, et al. (1995). "Disassembly of the reconstituted synaptic vesicle membrane fusion complex in vitro." Embo J **14**(10): 2317-25.

Hefft, S. and P. Jonas (2005). "Asynchronous GABA release generates long-lasting inhibition at a hippocampal interneuron-principal neuron synapse." Nat Neurosci **8**(10): 1319-28.

Heidelberger, R. and G. Matthews (2004). "Vesicle priming and depriming: a SNAP decision." Neuron **41**(3): 311-3.

Heidelberger, R., P. Sterling, et al. (2002). "Roles of ATP in depletion and replenishment of the releasable pool of synaptic vesicles." J Neurophysiol **88**(1): 98-106.

Helmchen, F., J. G. Borst, et al. (1997). "Calcium dynamics associated with a single action potential in a CNS presynaptic terminal." Biophys J **72**(3): 1458-71.

Hong, H. K., A. Chakravarti, et al. (2004). "The gene for soluble N-ethylmaleimide sensitive factor attachment protein alpha is mutated in hydrocephaly with hop gait (hyh) mice." Proc Natl Acad Sci U S A **101**(6): 1748-53.

Hull, C. and M. Scanziani (2007). "It's about time for thalamocortical circuits." Nat Neurosci **10**(4): 400-2.

Jahn, R., T. Lang, et al. (2003). "Membrane fusion." Cell **112**(4): 519-33.

Jahn, R. and R. H. Scheller (2006). "SNAREs--engines for membrane fusion." Nat Rev Mol Cell Biol **7**(9): 631-43.

Jockusch, W. J., D. Speidel, et al. (2007). "CAPS-1 and CAPS-2 are essential synaptic vesicle priming proteins." Cell **131**(4): 796-808.

Jonas, P., J. Bischofberger, et al. (2004). "Interneuron Diversity series: Fast in, fast out--temporal and spatial signal processing in hippocampal interneurons." Trends Neurosci **27**(1): 30-40.

Junge, H. J., J. S. Rhee, et al. (2004). "Calmodulin and Munc13 form a Ca2+ sensor/effector complex that controls short-term synaptic plasticity." Cell **118**(3): 389-401.

Kandel, E. R., Schwartz, J. H., Jessell, T. M., (2000). „Principles of neural science.“ McGraw-Hill Companies, fourth edition

Katz, B. and R. Miledi (1968). "The role of calcium in neuromuscular facilitation." J Physiol **195**(2): 481-92.

Katz, B. and R. Miledi (1969). "Spontaneous and evoked activity of motor nerve endings in calcium Ringer." J Physiol **203**(3): 689-706.

Kawasaki, F., A. M. Mattiuz, et al. (1998). "Synaptic physiology and ultrastructure in comatose mutants define an in vivo role for NSF in neurotransmitter release." J Neurosci **18**(24): 10241-9.

Kee, Y. and R. H. Scheller (1996). "Localization of synaptotagmin-binding domains on syntaxin." J Neurosci **16**(6): 1975-81.

Klingauf, J., E. T. Kavalali, et al. (1998). "Kinetics and regulation of fast endocytosis at hippocampal synapses." Nature **394**(6693): 581-5.

Lang, T., M. Margittai, et al. (2002). "SNAREs in native plasma membranes are active and readily form core complexes with endogenous and exogenous SNAREs." J Cell Biol **158**(4): 751-60.

Lee, S. H., L. Liu, et al. (2002). "Clathrin adaptor AP2 and NSF interact with overlapping sites of GluR2 and play distinct roles in AMPA receptor trafficking and hippocampal LTD." Neuron **36**(4): 661-74.

Lei, K. J., H. Chen, et al. (1996). "Glucose-6-phosphatase dependent substrate transport in the glycogen storage disease type-1a mouse." Nat Genet **13**(2): 203-9.

Li, Y., T. T. Huang, et al. (1995). "Dilated cardiomyopathy and neonatal lethality in mutant mice lacking manganese superoxide dismutase." Nat Genet **11**(4): 376-81.

Liley, A. W. and K. A. North (1953). "An electrical investigation of effects of repetitive stimulation on mammalian neuromuscular junction." J Neurophysiol **16**(5): 509-27.

Lu, T. and L. O. Trussell (2000). "Inhibitory transmission mediated by asynchronous transmitter release." Neuron **26**(3): 683-94.

Madison, J. M., S. Nurrish, et al. (2005). "UNC-13 interaction with syntaxin is required for synaptic transmission." Curr Biol **15**(24): 2236-42.

Malenka, R. C. and M. F. Bear (2004). "LTP and LTD: an embarrassment of riches." Neuron **44**(1): 5-21.

Martin, H. G., J. M. Henley, et al. (2006). "Novel putative targets of N-ethylmaleimide sensitive fusion protein (NSF) and alpha/beta soluble NSF attachment proteins (SNAPs) include the Pak-binding nucleotide exchange factor betaPIX." J Cell Biochem **99**(4): 1203-15.

Masugi, M., M. Yokoi, et al. (1999). "Metabotropic glutamate receptor subtype 7 ablation causes deficit in fear response and conditioned taste aversion." J Neurosci **19**(3): 955-63.

Maximov, A., O. H. Shin, et al. (2007). "Synaptotagmin-12, a synaptic vesicle phosphoprotein that modulates spontaneous neurotransmitter release." J Cell Biol **176**(1): 113-24.

Maximov, A. and T. C. Sudhof (2005). "Autonomous function of synaptotagmin 1 in triggering synchronous release independent of asynchronous release." Neuron **48**(4): 547-54.

McMahon, H. T., M. Missler, et al. (1995). "Complexins: cytosolic proteins that regulate SNAP receptor function." Cell **83**(1): 111-9.

Moulder, K. L. and S. Mennerick (2005). "Reluctant vesicles contribute to the total readily releasable pool in glutamatergic hippocampal neurons." J Neurosci **25**(15): 3842-50.

Nagy, G., K. Reim, et al. (2004). "Regulation of releasable vesicle pool sizes by protein kinase A-dependent phosphorylation of SNAP-25." Neuron **41**(3): 417-29.

Neher, E. (2006). "A comparison between exocytic control mechanisms in adrenal chromaffin cells and a glutamatergic synapse." Pflugers Arch **453**(3): 261-8.

Neher, E. and R. S. Zucker (1993). "Multiple calcium-dependent processes related to secretion in bovine chromaffin cells." Neuron **10**(1): 21-30.

Neumann, P. E. and R. L. Collins (1991). "Genetic dissection of susceptibility to audiogenic seizures in inbred mice." Proc Natl Acad Sci U S A **88**(12): 5408-12.

Nishiki, T., I. Nihonmatsu, et al. (2001). "Distribution of soluble N-ethylmaleimide fusion protein attachment proteins (SNAPs) in the rat nervous system." Neuroscience **107**(3): 363-71.

Noel, J., G. S. Ralph, et al. (1999). "Surface expression of AMPA receptors in hippocampal neurons is regulated by an NSF-dependent mechanism." Neuron **23**(2): 365-76.

Novick, P., C. Field, et al. (1980). "Identification of 23 complementation groups required for post-translational events in the yeast secretory pathway." Cell **21**(1): 205-15.

Ogiwara, I., H. Miyamoto, et al. (2007). "Na(v)1.1 localizes to axons of parvalbumin-positive inhibitory interneurons: a circuit basis for epileptic seizures in mice carrying an Scn1a gene mutation." J Neurosci **27**(22): 5903-14.

Otsu, Y. and T. H. Murphy (2003). "Miniature transmitter release: accident of nature or careful design?" Sci STKE **2003**(211): pe54.

Otto, H., P. I. Hanson, et al. (1997). "Assembly and disassembly of a ternary complex of synaptobrevin, syntaxin, and SNAP-25 in the membrane of synaptic vesicles." Proc Natl Acad Sci U S A **94**(12): 6197-201.

Pabst, S., M. Margittai, et al. (2002). "Rapid and selective binding to the synaptic SNARE complex suggests a modulatory role of complexins in neuroexocytosis." J Biol Chem **277**(10): 7838-48.

Pallanck, L., R. W. Ordway, et al. (1995). "Distinct roles for N-ethylmaleimide-sensitive fusion protein (NSF) suggested by the identification of a second Drosophila NSF homolog." J Biol Chem **270**(32): 18742-4.

Pang, Z. P., E. Melicoff, et al. (2006). "Synaptotagmin-2 is essential for survival and contributes to Ca2+ triggering of neurotransmitter release in central and neuromuscular synapses." J Neurosci **26**(52): 13493-504.

Parnas, I., G. Rashkovan, et al. (2006). "Role of NSF in neurotransmitter release: a peptide microinjection study at the crayfish neuromuscular junction." J Neurophysiol **96**(3): 1053-60.

Perin, M. S., V. A. Fried, et al. (1990). "Phospholipid binding by a synaptic vesicle protein homologous to the regulatory region of protein kinase C." Nature **345**(6272): 260-3.

Peter, F., S. H. Wong, et al. (1998). "Alpha-SNAP but not gamma-SNAP is required for ER-Golgi transport after vesicle budding and the Rab1-requiring step but before the EGTA-sensitive step." J Cell Sci **111 (Pt 17)**: 2625-33.

Piano, F., A. J. Schetter, et al. (2000). "RNAi analysis of genes expressed in the ovary of Caenorhabditis elegans." Curr Biol **10**(24): 1619-22.

Poirier, M. A., W. Xiao, et al. (1998). "The synaptic SNARE complex is a parallel four-stranded helical bundle." Nat Struct Biol **5**(9): 765-9.

Puschel, A. W., V. O'Connor, et al. (1994). "The N-ethylmaleimide-sensitive fusion protein (NSF) is preferentially expressed in the nervous system." FEBS Lett **347**(1): 55-8.

Pyle, J. L., E. T. Kavalali, et al. (2000). "Rapid reuse of readily releasable pool vesicles at hippocampal synapses." Neuron **28**(1): 221-31.

Pyott, S. J. and C. Rosenmund (2002). "The effects of temperature on vesicular supply and release in autaptic cultures of rat and mouse hippocampal neurons." J Physiol **539**(Pt 2): 523-35.

Reim, K., M. Mansour, et al. (2001). "Complexins regulate a late step in Ca2+-dependent neurotransmitter release." Cell **104**(1): 71-81.

Rhee, J. S., A. Betz, et al. (2002). "Beta phorbol ester- and diacylglycerol-induced augmentation of transmitter release is mediated by Munc13s and not by PKCs." Cell **108**(1): 121-33.

Richmond, J. E., R. M. Weimer, et al. (2001). "An open form of syntaxin bypasses the requirement for UNC-13 in vesicle priming." Nature **412**(6844): 338-41.

Rorsman, P., L. Eliasson, et al. (2000). "The Cell Physiology of Biphasic Insulin Secretion." News Physiol Sci **15**: 72-77.

Rosahl, T. W., D. Spillane, et al. (1995). "Essential functions of synapsins I and II in synaptic vesicle regulation." Nature **375**(6531): 488-93.

Rosenmund, C., J. D. Clements, et al. (1993). "Nonuniform probability of glutamate release at a hippocampal synapse." Science **262**(5134): 754-7.

Rosenmund, C., J. Rettig, et al. (2003). "Molecular mechanisms of active zone function." Curr Opin Neurobiol **13**(5): 509-19.

Rosenmund, C. and C. F. Stevens (1996). "Definition of the readily releasable pool of vesicles at hippocampal synapses." Neuron **16**(6): 1197-207.

Sabatini, B. L. and W. G. Regehr (1996). "Timing of neurotransmission at fast synapses in the mammalian brain." Nature **384**(6605): 170-2.

Sagane, K., K. Hayakawa, et al. (2005). "Ataxia and peripheral nerve hypomyelination in ADAM22-deficient mice." BMC Neurosci **6**(1): 33.

Sakaba, T. (2006). "Roles of the fast-releasing and the slowly releasing vesicles in synaptic transmission at the calyx of held." J Neurosci **26**(22): 5863-71.

Sakaba, T. and E. Neher (2001a). "Calmodulin mediates rapid recruitment of fast-releasing synaptic vesicles at a calyx-type synapse." Neuron **32**(6): 1119-31.

Sakaba, T. and E. Neher (2001b). "Preferential potentiation of fast-releasing synaptic vesicles by cAMP at the calyx of Held." Proc Natl Acad Sci U S A **98**(1): 331-6.

Sakaba, T. and E. Neher (2001c). "Quantitative relationship between transmitter release and calcium current at the calyx of held synapse." J Neurosci **21**(2): 462-76.

Sakaba, T., R. Schneggenburger, et al. (2002). "Estimation of quantal parameters at the calyx of Held synapse." Neurosci Res **44**(4): 343-56.

Sakaba, T., A. Stein, et al. (2005). "Distinct kinetic changes in neurotransmitter release after SNARE protein cleavage." Science **309**(5733): 491-4.

Sanyal, S., L. A. Tolar, et al. (2001). "Genetic interaction between shibire and comatose mutations in Drosophila suggest a role for snap-receptor complex assembly and disassembly for maintenance of synaptic vesicle cycling." Neurosci Lett **311**(1): 21-4.

Sara, Y., M. G. Mozhayeva, et al. (2002). "Fast vesicle recycling supports neurotransmission during sustained stimulation at hippocampal synapses." J Neurosci **22**(5): 1608-17.

Schluter, O. M., J. Basu, et al. (2006). "Rab3 superprimes synaptic vesicles for release: implications for short-term synaptic plasticity." J Neurosci **26**(4): 1239-46.

Schluter, O. M., F. Schmitz, et al. (2004). "A complete genetic analysis of neuronal Rab3 function." J Neurosci **24**(29): 6629-37.

Schneggenburger, R. and I. D. Forsythe (2006). "The calyx of Held." Cell Tissue Res **326**(2): 311-37.

Schneggenburger, R. and E. Neher (2000). "Intracellular calcium dependence of transmitter release rates at a fast central synapse." Nature **406**(6798): 889-93.

Schneggenburger, R. and E. Neher (2005). "Presynaptic calcium and control of vesicle fusion." Curr Opin Neurobiol **15**(3): 266-74.

Schneggenburger, R., T. Sakaba, et al. (2002). "Vesicle pools and short-term synaptic depression: lessons from a large synapse." Trends Neurosci **25**(4): 206-12.

Schoch, S., et al. (2001). „SNARE function analysed in synaptobrevin/VAMP knockout mice.“ Science **294**, 1117-1122

Schweizer, F. E., T. Dresbach, et al. (1998). "Regulation of neurotransmitter release kinetics by NSF." Science **279**(5354): 1203-6.

Seyfried, T. N., R. K. Yu, et al. (1980). "Genetic analysis of audiogenic seizure susceptibility in C57BL/6J X DBA/2J recombinant inbred strains of mice." Genetics **94**(3): 701-18.

Siddiqi, O. and S. Benzer (1976). "Neurophysiological defects in temperature-sensitive paralytic mutants of Drosophila melanogaster." Proc Natl Acad Sci U S A **73**(9): 3253-7.

Silver, R. A., A. Momiyama, et al. (1998). "Locus of frequency-dependent depression identified with multiple-probability fluctuation analysis at rat climbing fibre-Purkinje cell synapses." J Physiol **510 (Pt 3)**: 881-902.

Smart, S. L., V. Lopantsev, et al. (1998). "Deletion of the K(V)1.1 potassium channel causes epilepsy in mice." Neuron **20**(4): 809-19.

Sollner, T., M. K. Bennett, et al. (1993a). "A protein assembly-disassembly pathway in vitro that may correspond to sequential steps of synaptic vesicle docking, activation, and fusion." Cell **75**(3): 409-18.

Sollner, T., S. W. Whiteheart, et al. (1993). "SNAP receptors implicated in vesicle targeting and fusion." Nature **362**(6418): 318-24.

Sorensen, J. B. (2004). "Formation, stabilisation and fusion of the readily releasable pool of secretory vesicles." Pflugers Arch **448**(4): 347-62.

Stevens, C. F. and T. Tsujimoto (1995). "Estimates for the pool size of releasable quanta at a single central synapse and for the time required to refill the pool." Proc Natl Acad Sci U S A **92**(3): 846-9.

Stevens, C. F. and J. F. Wesseling (1998). "Activity-dependent modulation of the rate at which synaptic vesicles become available to undergo exocytosis." Neuron **21**(2): 415-24.

Stevens, C. F. and J. H. Williams (2000). ""Kiss and run" exocytosis at hippocampal synapses." Proc Natl Acad Sci U S A **97**(23): 12828-33.

Stevens, D. R., Z. X. Wu, et al. (2005). "Identification of the minimal protein domain required for priming activity of Munc13-1." Curr Biol **15**(24): 2243-8.

Sudhof, T. C. (1995). "The synaptic vesicle cycle: a cascade of protein-protein interactions." Nature **375**(6533): 645-53.

Sudhof, T. C. (2002). "Synaptotagmins: why so many?" J Biol Chem **277**(10): 7629-32.

Sudhof, T. C. (2004). "The synaptic vesicle cycle." Annu Rev Neurosci **27**: 509-47.

Sudlow, A. W., B. W. McFerran, et al. (1996). "Similar effects of alpha- and beta-SNAP on Ca(2+)-regulated exocytosis." FEBS Lett **393**(2-3): 185-8.

Sun, J., Z. P. Pang, et al. (2007). "A dual-Ca2+-sensor model for neurotransmitter release in a central synapse." Nature **450**(7170): 676-82.

Sun, J. Y., X. S. Wu, et al. (2002). "Single and multiple vesicle fusion induce different rates of endocytosis at a central synapse." Nature **417**(6888): 555-9.

Sutton, R. B., D. Fasshauer, et al. (1998). "Crystal structure of a SNARE complex involved in synaptic exocytosis at 2.4 A resolution." Nature **395**(6700): 347-53.

Tang, J., A. Maximov, et al. (2006). "A complexin/synaptotagmin 1 switch controls fast synaptic vesicle exocytosis." Cell **126**(6): 1175-87.

Thomas, P., J. G. Wong, et al. (1993). "Millisecond studies of secretion in single rat pituitary cells stimulated by flash photolysis of caged Ca2+." Embo J **12**(1): 303-6.

Varoqueaux, F., G. Aramuni, et al. (2006). "Neuroligins determine synapse maturation and function." Neuron **51**(6): 741-54.

Varoqueaux, F., A. Sigler, et al. (2002). "Total arrest of spontaneous and evoked synaptic transmission but normal synaptogenesis in the absence of Munc13-mediated vesicle priming." Proc Natl Acad Sci U S A **99**(13): 9037-42.

Verhage, M., A. S. Maia, et al. (2000). "Synaptic assembly of the brain in the absence of neurotransmitter secretion." Science **287**(5454): 864-9.

von Ruden, L. and E. Neher (1993). "A Ca-dependent early step in the release of catecholamines from adrenal chromaffin cells." Science **262**(5136): 1061-5.

Wainer, B. H., H. J. Lee, et al. (1991). "In vitro cell cultures as a model of the basal forebrain." Adv Exp Med Biol **295**: 415-37.

Wang, L. Y. and L. K. Kaczmarek (1998). "High-frequency firing helps replenish the readily releasable pool of synaptic vesicles." Nature **394**(6691): 384-8.

Washbourne, P., et al., (2002). "Genetic ablation of the t-SNARE SNAP-25 distinguishes mechanisms of neuroexocytosis."Nature Neuroscience **5**, 19-26

Weimer, R. M., J. E. Richmond, et al. (2003). "Defects in synaptic vesicle docking in unc-18 mutants." Nat Neurosci **6**(10): 1023-30.

Whiteheart, S. W., M. Brunner, et al. (1992). "Soluble N-ethylmaleimide-sensitive fusion attachment proteins (SNAPs) bind to a multi-SNAP receptor complex in Golgi membranes." J Biol Chem **267**(17): 12239-43.

Whiteheart, S. W., I. C. Griff, et al. (1993). "SNAP family of NSF attachment proteins includes a brain-specific isoform." Nature **362**(6418): 353-5.

Whiteheart, S. W. and E. A. Matveeva (2004). "Multiple binding proteins suggest diverse functions for the N-ethylmaleimide sensitive factor." J Struct Biol **146**(1-2): 32-43.

Williams, A., Warwick, R., et al. (1989). "Gray's anatomy". 37th Edition, pp 859-919, Edimbrough, Livingstone

Wilson, D. W., S. W. Whiteheart, et al. (1992). "A multisubunit particle implicated in membrane fusion." J Cell Biol **117**(3): 531-8.

Wimmer, C., T. M. Hohl, et al. (2001). "Molecular mass, stoichiometry, and assembly of 20 S particles." J Biol Chem **276**(31): 29091-7.

Wojcik, S. M. and N. Brose (2007). "Regulation of membrane fusion in synaptic excitation-secretion coupling: speed and accuracy matter." Neuron **55**(1): 11-24.

Xingjian, L. and Bixby, J. (1993). "Coordinate and noncoordinate regulation in synaptic vesicle protein genes during embryonic development." Developmental Biology, **159**: 327-337

Xu, J., Y. Xu, et al. (2002). "Differential regulation of exocytosis by alpha- and beta-SNAPs." J Neurosci **22**(1): 53-61.

Xu, T. and S. M. Bajjalieh (2001). "SV2 modulates the size of the readily releasable pool of secretory vesicles." Nat Cell Biol **3**(8): 691-8.

Xu, T., B. Rammner, et al. (1999). "Inhibition of SNARE complex assembly differentially affects kinetic components of exocytosis." Cell **99**(7): 713-22.

Xu-Friedman, M. A. and W. G. Regehr (1999). "Presynaptic strontium dynamics and synaptic transmission." Biophys J **76**(4): 2029-42.

Xu-Friedman, M. A. and W. G. Regehr (2000). "Probing fundamental aspects of synaptic transmission with strontium." J Neurosci **20**(12): 4414-22.

Yang, B., L. Gonzalez, Jr., et al. (1999). "SNARE interactions are not selective. Implications for membrane fusion specificity." J Biol Chem **274**(9): 5649-53.

Yuste, R. (2005). "Origin and classification of neocortical interneurons." Neuron **48**(4): 524-7.

Zhao, C., J. T. Slevin, et al. (2007). "Cellular functions of NSF: not just SNAPs and SNAREs." FEBS Lett **581**(11): 2140-9.

Zilly, F. E., J. B. Sorensen, et al. (2006). "Munc18-bound syntaxin readily forms SNARE complexes with synaptobrevin in native plasma membranes." PLoS Biol **4**(10): e330.

Zucker, R. S. (1996). "Exocytosis: a molecular and physiological perspective." Neuron **17**(6): 1049-55.

Zucker, R. S. (2005). "Minis: whence and wherefore?" Neuron **45**(4): 482-4.

Zucker, R. S. and W. G. Regehr (2002). "Short-term synaptic plasticity." Annu Rev Physiol **64**: 355-405.

7 *Curriculum Vitae*

Scientific Education

October 1997 - July 2003: University of Perugia (Italy)
Course of Biological Molecular Sciences
Faculty of Mathematical, Physical and Natural Sciences
Final grade: 110/110 cum Laude

May 2003 - July 2003: Research project: "Mutational analysis of the human MANB gene in patients affected by α-mannosidosis"
Dept. of Biochemisty and Molecular Biology (Prof. Beccari)
University of Perugia

Sept 2003 - Aug 2004: Selection and admission to Molecular Biology International PhD Program, University of Göttingen
http://www.gpmolbio.uni-goettingen.de/
First year master's Examination
Final grade: 1.15

Sept 2004 Selection and admission to Neuroscience Early Stage Research Training (NEUREST) Program
Marie-Curie Actions
http://www.neurest.mpg.de/

Oct 2004 - March 2008 PhD in the Department of Molecular Neurobiology (Prof. Nils Brose), Max-Planck Institute for Experimental Medicine, Göttingen

Advanced Method Courses

Methods for studying secretion: Patch-Clamp, Amperometry, TIRFM
(Klingauf, Sorensen, Prof. Neher)
MPI Biophysical Chemistry, Göttingen

Patch-clamp measurements of synaptic transmission in cultured hippocampal neurons
(Sorensen, Prof. Neher)
MPI Biophysical Chemistry, Göttingen

Posttranslational modification with ubiquitin-related protein SUMO
(Prof. Melchior)
Institute of Biochemistry I, University of Göttingen

European Synapse Summer School
PENS Training Center
Bordeaux (France)